

# **POWER SYSTEM OPERATION WITH WIND ENERGY INTEGRATIONS**

**BY**

**JIABIN SHEN, B.E.**

A thesis submitted to the School of Graduate Studies in  
partial fulfillment of the requirements for the  
degree of Master of Engineering

Faculty of Engineering and Applied Science  
Memorial University of Newfoundland

May 2017

St John's

Newfoundland

Canada

# ABSTRACT

Wind energy with its low environmental impacts and sustainability has taken up a large share of the electricity generation market and it is expected to grow. The original power systems are primarily dominated by synchronous generators while wind generators utilize asynchronous induction machine to convert wind energy into electricity. Moreover, wind speed is not controllable. The integrations of wind energy into power systems have a great impact on power system operation. The influences brought by wind generators should be understood for maintaining secure and reliable operation of power systems.

The inclusion of power electronic devices enables the variable speed operation of the wind generators. It largely facilitates the integrations of wind energy. This thesis considers doubly fed induction generators (DFIGs) type of wind generators. The appropriate modelling of wind generators for power system analysis is discussed. Three aspects of power system operations are considered in this thesis, which are steady state, small signal stability and transient stability analysis. The effects of wind energy integrations on these three aspects of power systems are investigated in detail.

Different cases studies are provided throughout the thesis to illustrate effects brought by wind energy and arrive at the conclusions.

# ACKNOWLEDGEMENTS

I would like to thank my supervisor Dr. Benjamin Jeyasurya for his constant guidance and helps during all stages of this thesis.

I would also like to thank my parents and my loving girlfriend Yuanyuan for their love and supports. Without them, this work would never have come to existence.

Special thanks and appreciation are given to Natural Sciences and Engineering Research Council of Canada and to Memorial University of Newfoundland for the financial support, which made this research possible. Thanks are also given to the Faculty of Engineering of Memorial University for providing the resources to carry out this research.

# LIST OF ABBREVIATIONS

DFIG	Doubly Fed Induction Generator
SMIB	Single Machine Infinite Bus
DAE	Differential Algebraic Equation
TLR	Transmission Loading Relief
WTLR	Weighted Transmission Loading Relief
ETLR	Equivalent Transmission Loading Relief
IEC	Island Electric Company
PSAT	Power System Analysis Toolbox

# CONTENTS

<b>ABSTRACT</b> .....	i
<b>ACKNOWLEDGEMENTS</b> .....	ii
<b>LIST OF ABBREVIATIONS</b> .....	iii
<b>CONTENTS</b> .....	iv
<b>LIST OF FIGURES</b> .....	x
<b>LIST OF TABLES</b> .....	xviii
<b>Chapter 1 Introduction</b> .....	1
1.1 Objectives of the Research.....	1
1.2 Organization of Thesis .....	2
<b>Chapter 2 Wind Energy Development and Doubly Fed Induction Generator</b> .....	4
2.0 Introduction .....	4
2.1 Wind Energy Developments in the World.....	4
2.2 Wind Energy Developments in Canada.....	7

2.3 Wind Generators.....	10
2.4 Basic Operation of Induction Generators.....	12
2.5 Introduction to Doubly Fed Induction Generators.....	13
2.6 Modeling of Doubly Fed Induction Generators.....	15
2.6.1 Modeling for Steady State Analysis.....	15
2.6.2 Modeling for dynamic analysis.....	16
2.7 Summary.....	24

**Chapter 3 Power System Steady State Operation with Wind Energy Integrations**

.....	25
3.0 Introduction.....	25
3.1 Different Wind Farm Types.....	25
3.1.1 Case Study: Different Wind Farm Types.....	26
3.2 Wind Farm Planning.....	31
3.2.1 Weighted Transmission Loading Relief.....	32
3.2.2 Case Study: Wind Farm Planning in a Large system.....	36
3.3 Wind Farm Temporal Intermittency.....	43
3.3.1 Case Study: Wind Farm Temporal Intermittency.....	43
3.4 Summary.....	50

<b>Chapter 4 Conventional Small Signal Stability Analysis .....</b>	<b>51</b>
4.0 Introduction .....	51
4.1 Power System Stability .....	51
4.2.1 Swing Equation.....	52
4.2.2 Synchronous and Damping Torques .....	54
4.2.3 Power System Oscillation.....	54
4.2 Analysis Methods for Small Signal Stability .....	56
4.2.1 Time Domain Simulation.....	56
4.2.2 Eigenvalue Analysis.....	60
4.3 Small Signal Stability of a Large System.....	68
4.3.1 Case Study: Small Signal Stability Analysis of New England Power System .....	69
4.4 Summary .....	73
 <b>Chapter 5 Power System Small Signal Stability Analysis with Wind Energy Integrations.....</b>	 <b>74</b>
5.0 Introduction .....	74
5.1 Small Signal Stability Analysis of SMIB Systems.....	74
5.1.1 Small Signal Stability Analysis of a SMIB System with a Synchronous	

Generator.....	75
5.1.2 Small Signal Stability Analysis of a SMIB System with a DFIG.....	82
5.2 Small Signal Stability Analysis with Wind Energy Integrations using PSAT....	90
5.2.1 Small Signal Stability Analysis of Two Area Power System with Wind Energy Integrations.....	91
5.2.2 Small Signal Stability Analysis of New England Power System with Wind Energy Integrations.....	97
5.4 Summary .....	100
<b>Chapter 6 Conventional Transient Stability Analysis.....</b>	<b>102</b>
6.0 Introduction .....	102
6.1 Power System Transient Stability Analysis Method .....	102
6.1.1 Equal Area Criterion .....	103
6.1.2 Case Study: Equal Area Criterion.....	105
6.2 Transient Stability Analysis using PowerWorld.....	110
6.2.1 Case Study: Transient Stability Analysis of Five-Bus Two-Machine Power System.....	110
6.2.2 Case Study: Transient Stability Analysis of New England Power System	112
6.3 Summary .....	116

## **Chapter 7 Power System Transient Stability Analysis with Wind Energy**

<b>Integrations.....</b>	<b>117</b>
7.0 Introduction .....	117
7.1 Time Domain Simulation for Transient Stability Analysis .....	118
7.2 Time Domain Simulation Application on Synchronous Generators .....	119
7.2.1 Time Domain Simulation of Classical Model of Synchronous Generators .....	120
7.2.2 Time Domain Simulation of Two-Axis Model of Synchronous Generators .....	123
7.3 Analysis and Simulation of DFIGs.....	127
7.3.1 Comparison of 5 <sup>th</sup> and 3 <sup>rd</sup> Order DFIG Models.....	128
7.3.2 Simulation and Analysis of A DFIG based Wind Generation System and its Transient Behaviors .....	133
7.4 Transient Stability Analysis with Wind Energy Integrations using PowerWorld .....	143
7.4.1 Transient Stability Evaluation Index.....	144
7.4.2 Case Study: Transient Stability Analysis of 9 Bus Power System with Wind Energy Integrations .....	145
7.4.3 Case Study: Transient Stability Analysis of New England Power System	153
7.5 Summary .....	157

<b>Chapter 8 Conclusions and Future Work</b> .....	160
8.1 Conclusions .....	160
8.2 Future Work.....	162
<b>References</b> .....	164
<b>Appendix A: 7 Bus Power System Data</b> .....	169
<b>Appendix B: IEC Power System Data</b> .....	171
<b>Appendix C: Two Area System</b> .....	173
<b>Appendix D: New England Power System</b> .....	174
<b>Appendix E: Single Machine Infinite Bus System with A Synchronous Generator</b> .....	175
<b>Appendix F: Single Machine Infinite Bus System with A DFIG</b> .....	177
<b>Appendix G: Eigenvalues Comparison of Two Area Power System</b> .....	177
<b>Appendix H: Five-Bus Two-Machine Power System</b> .....	177
<b>Appendix L: 9 Bus Power System</b> .....	179

# LIST OF FIGURES

Figure 2.1: Annually Installed Global Wind Energy Capacities 2000- 2015.....	6
Figure 2.2: Newly Installed Capacities in Different Countries in 2015.....	7
Figure 2.3: Installed Capacity of Wind Generation in Different Provinces of Canada as of December 2015.....	8
Figure 2.4: Wind Diesel System in Ramea.....	9
Figure 2.5: Type A Configuration.....	10
Figure 2.6: Type B Configuration.....	10
Figure 2.7: Type C Configuration.....	11
Figure 2.8: Type D Configuration.....	11
Figure 2.9: Structure of An Induction Generator.....	13
Figure 2.10: Diagram of A Doubly Fed Induction Generator.....	14
Figure 3.1: One Line Diagram of 7 Bus Power System with Wind Farm.....	27
Figure 3.2: Connection of Bus 4 with A Type One Wind Farm .....	28
Figure 3.3: Contingency Condition of A Type One Wind Farm .....	28

Figure 3.4: Connection of Bus 4 with A Type Two Wind Farm.....	30
Figure 3.5: Contingency Condition of A Type Two Wind Farm.....	30
Figure 3.6: Weak Element Visualization.....	34
Figure 3.7: WTLR Sensitivity Visualization.....	35
Figure 3.8: One Line Diagram of Island Electric Company (IEC) Power System.....	37
Figure 3.9: Bus Voltage Magnitude Variations of IEC Power System Base Case.....	38
Figure 3.10: Bus Voltage Magnitude Variations of IEC Power System with Synchronous Generator Disconnection .....	39
Figure 3.11: Aggregated MVA Overload of Different Connection Schemes at 100 MW Output.....	42
Figure 3.12: Varying Scaled Load Demand and Wind Farm Output.....	45
Figure 3.13: Bus Voltage Magnitude Variations of 7 Bus System over 24 Hours.....	47
Figure 3.14: Synchronous Generator Output Variations of 7 Bus System over 24 Hours.....	48
Figure 3.15: System Aggregated MVA Overload Variations of 7 Bus System over 24 Hours.....	49
Figure 4.1: Illustration of Power System Oscillation.....	55

Figure 4.2: One Line Diagram of Two Area Power System.....	57
Figure 4.3: Responses of Rotor Angles When Load Increase Applied (Scenario One).....	58
Figure 4.4: Responses of Rotor Speeds When Load Increase Applied (Scenario One).....	58
Figure 4.5: Responses of Rotor Angles When Load Increase Applied (Scenario Two).....	59
Figure 4.6: Responses of Rotor Speeds When Load Increase Applied (Scenario Two).....	59
Figure 4.7: Eigenvalues on Complex Plane of Two Area Power System (Scenario One).....	63
Figure 4.8: Eigenvalues on Complex Plane of Two Area Power System (Scenario Two).....	66
Figure 4.9: One Line Diagram of New England Power System.....	69
Figure 4.10: Eigenvalues on Complex Plane of New England Power System.....	70
Figure 4.11: Rotor Speed of New England Power System.....	72
Figure 4.12: Rotor Angle of New England Power System.....	73

Figure 5.1: SMIB System with A Synchronous Generator Connected to An Infinite Bus. ....	76
Figure 5.2: Eigenvalues on Complex Plane of SMIB System with A Synchronous Generator.....	80
Figure 5.3: Eigenvalues of SMIB System with A Synchronous Generator Corresponding to Different $X_t$ .....	82
Figure 5.4: SMIB System with A DFIG connected to An Infinite Bus.....	83
Figure 5.5: Eigenvalues on Complex Plane of SMIB System with A DFIG.....	87
Figure 5.6: Eigenvalues of SMIB System with A DFIG Corresponding to Different $X_t$ .....	89
Figure 5.7: Comparisons of Two Area System without Wind Energy Integrations and with DFIG connected to Bus 1.....	92
Figure 5.8: Effects of Different Wind Farm Locations on Two Area Power System.....	93
Figure 5.9: Comparisons of Two Area Power System with AVRs and PSSs with DFIGs connected to Different Locations. ....	95
Figure 5.10: Comparisons of the Lowest Damping of Two Area System with AVR and PSS.....	96

Figure 5.11: Comparisons of New England Power System without Wind Energy Integrations and with DFIGs connected to Bus 32.....	98
Figure 5.12: Rotor Speed of New England Power System with Wind Energy.....	99
Figure 5.13: Rotor Angle of New England Power System with Wind Energy.....	100
Figure 6.1: Relationship of Power Transfer Curve and Energy.....	104
Figure 6.2: Simplified System.....	106
Figure 6.3: Simplified System Equivalent Circuit during Fault.....	107
Figure 6.4: Generator Rotor Angle when Fault Clearing Time is 0.34 seconds.....	109
Figure 6.5: Generator Rotor Angle when Fault Clearing Time is 0.4 seconds.....	109
Figure 6.6: Five-Bus Two-Machine Power System.....	111
Figure 6.7: Generator Rotor Angles when Fault Clearing Time is 0.05 seconds of Five-Bus Two-Machine System.....	112
Figure 6.8: Generator Rotor Angles when Fault Clearing Time is 2.5 seconds Five-Bus Two-Machine System.....	113
Figure 6.9: Generator Rotor Angle at Bus 30 of New England Power System.....	114
Figure 6.10: Generator Rotor Angle at Bus 34 of New England Power System.....	115
Figure 6.11: Generator Rotor Angle at Bus 30 of New England Power System	

(Increased Fault Clearing Time).....	116
Figure 6.11: Generator Rotor Angle at Bus 34 of New England Power System (Increased Fault Clearing Time).....	116
Figure 7.1: Comparisons of Rotor Angles from Matlab and PowerWorld of Classical Model. ....	123
Figure 7.2: Comparisons of Generator Speeds from Matlab and PowerWorld of Classical Model.....	123
Figure 7.3: Comparisons of Rotor Angles from Matlab and PowerWorld of Two-Axis Model.. ....	126
Figure 7.4: Comparisons of Generator Speeds from Matlab and PowerWorld of Two-Axis Model.....	126
Figure 7.5: Comparisons of Internal Voltage $E'_q$ from Matlab and PowerWorld of Two-Axis Model.....	127
Figure 7.6: Comparison of Internal Voltage $E'_d$ from Matlab and PowerWorld of Two-Axis Model.....	127
Figure 7.7: Comparisons of Electromagnetic Torques of 5 <sup>th</sup> Order and 3 <sup>rd</sup> Order Models of A DFIG.....	131
Figure 7.8: Comparisons of Generator Terminal Voltages of 5 <sup>th</sup> Order and 3 <sup>rd</sup> Order	

Models of A DFIG.....	131
Figure 7.9: Comparisons of Generator Inner Voltages of 5 <sup>th</sup> Order and 3 <sup>rd</sup> Order Models of A DFIG ( $E'_d$ ).....	132
Figure 7.10: Comparisons of Generator Stator Currents of 5 <sup>th</sup> Order and 3 <sup>rd</sup> Order Models of A DFIG ( $I_{ds}$ ).....	132
Figure 7.11: DFIG based Wind Generation System Block Diagram.....	134
Figure 7.12: Model Implemented in Simulink .....	134
Figure 7.13: Mechanical Torque vs Turbine Speed.....	136
Figure 7.14: Torque Controller for Rotor Side Converter.....	136
Figure 7.15: Reactive Power Controller for Rotor Side Converter.....	137
Figure 7.16: Mechanical Torque Response of the DFIG System.....	138
Figure 7.17: Rotor Speed Response of the DFIG System.....	139
Figure 7.18: Turbine Speed Response of the DFIG System.....	139
Figure 7.19: Reference Torque Response of the DFIG System.....	140
Figure 7.20: Electromagnetic Torque Response of the DFIG System.....	140
Figure 7.21: Active Power Response of the DFIG System.....	141
Figure 7.22: Reactive Power Response of the DFIG System.....	141
Figure 7.23: $I_{dr}$ Response of the DFIG System.....	142

Figure 7.24: $I_{qr}$ Response of the DFIG System.....	142
Figure 7.25: One Line Diagram of 9 Bus Power System.....	145
Figure 7.26: Rotor Angle Responses of Generator at Bus 1 (Fault at Bus 6).....	147
Figure 7.27: Rotor Angle Responses of Generator at Bus 2 (Fault at Bus 6).....	148
Figure 7.28: Comparison of Bus 3 Voltage (Fault at Bus 6).....	149
Figure 7.29: Comparison of Reactive Power Output (Fault at Bus 6).....	149
Figure 7.30: Rotor Angle Responses of Generator at Bus 1 (Fault at Bus 8).....	150
Figure 7.31: Rotor Angle Responses of Generator at Bus 2 (Fault at Bus 8).....	151
Figure 7.32: Rotor Angle Responses of Base Case System.....	151
Figure 7.33: Rotor Responses of Wind Energy Case.....	152
Figure 7.34: Generator 31 Rotor Angle Responses of New England Power System.....	154
Figure 7.35: Generator 34 Rotor Angle Responses of New England Power System.....	154
Figure 7.36: Reactive Power Output Comparison at Bus 32 of New England Power System.....	155
Figure 7.37: Bus Voltage Comparison at Bus 32 of New England Power System.....	155

# LIST OF TABLES

Table 3.1: Results of Contingency Analysis with A Type One Wind Farm.....	29
Table 3.2: Results of Contingency Analysis with A Type Two Wind Farm.....	31
Table 3.3: System Aggregated MVA Overload for A Wind Farm connecting at Bus 5 and 3.....	35
Table 3.4: Available Approaches for Construction.....	40
Table 3.5: NewWind Substation Connection Schemes.....	41
Table 3.6: Varying Actual and Scaled Data of Load Demand and Wind Farm Output.....	44
Table 4.1: Instable Modes of Two Area Power System (Scenario One).....	64
Table 4.2: Oscillation Modes of Two Area Power System (Scenario One).....	65
Table 4.3: Oscillation Modes of Two Area Power System (Scenario Two).....	67
Table 4.4: Oscillation Modes Of New England Power System.....	70
Table 5.1: Eigenvalues of SMIB System with A Synchronous Generator.....	80

Table 5.2: Participation Factors of SMIB System with A Synchronous Generator.....	81
Table 5.3: Eigenvalues of SMIB System with A DFIG.....	88
Table 5.4: Participation Factors of SMIB System with A DFIG.....	88
Table 5.5: Eigenvalues of SMIB System with A DFIG Corresponding to Different $X_t$ .....	90
Table 5.6: Comparisons of Two Area System without Wind Energy Integrations and with DFIG connected to Bus 1.....	93
Table 5.7: Comparisons of Damping of Different Wind Farm Locations in Two Area Power System.....	94
Table 5.9 Comparisons of the Lowest Damping of Two Area System with AVR and PSS.....	96
Table 5.10: Comparisons of the Lowest Damping of New England Power System without Wind Energy Integration and with DFIG connected to Bus 32.....	98
Table 7.1: Models Used in PowerWorld for Generator at Bus 3.....	146
Table 7.2: Critical Fault Clearing Time Comparison.....	146
Table A.1: Generation Schedule and Generator Limits of 7 Bus Power System.....	167

Table A.2: Load Demand of 7 Bus Power System.....	168
Table B.1: Generation Schedule and Generator Limits of IEC Power System.....	169
Table B.2: Load Demand of IEC Power System.....	169
Table C.1: Steady State Data of Two Area Power System.....	171
Table C.2: Dynamic Data of Two Area Power System.....	171
Table D.1: Steady State Data of New England Power System.....	172
Table D.2: Dynamic Data of New England Power System .....	174
Table G.1: Eigenvalues of Two Area Power System without AVR and PSSs.....	177
Table G.2: Eigenvalues of Two Area Power System with AVR and PSSs .....	177
Table H.1: Steady State Data of Five-Bus Two-Machine Power System.....	178
Table L.1: Generation Schedule and Generator Limits of 9 Bus Power System.....	179
Table L.2: Load Demand of 9 Bus Power System.....	179

# Chapter 1

## Introduction

### 1.1 Objectives of the Research

The demand for clean and renewable energy in electricity generation has been increasing around the world. Wind energy has received significant attentions. The power quality and energy efficiency of a single wind generator are greatly improved due to the development of power electronic devices. However, with the integration scales of wind energy increase in power systems, its impacts on power systems have raised concerns. This thesis addresses the problem of large scale integrations of wind energy in power systems.

The main goals of this research are listed as following.

- To recognize the wind energy development and available wind generation technologies.
- To study doubly fed induction generators (DFIGs) and the modeling of DFIGs for power system analysis.
- To implement models of DFIGs for steady state and dynamic analysis.

- To discuss the power system steady state, small signal stability and transient stability analysis and the impacts brought by large scale integrations of DFIG based wind farms.
- To use suitable case studies to present the impacts and draw conclusions.

## **1.2 Organization of Thesis**

Chapter 2 presents the developments of the wind energy in the world and in Canada. Different types of wind generators are introduced. To study the impacts of DFIG-based wind farms on power system operations, the modeling of DFIGs is also given in this chapter. The models of DFIG for both steady state analysis and dynamic analysis are presented and the simplifications for power system analysis are discussed. The impacts of wind energy on power system steady state operation are presented in Chapter 3. This chapter mainly comprises three case studies to discuss the features of different types of wind generators, the impacts of the wind farm locations and connection schemes, and the impacts of varying power output of wind farms in steady state operation.

In Chapter 4, the conventional power system small signal stability analysis without wind energy integration is presented. An overview of small signal stability and its analysis methods are given. Both time domain simulation and eigenvalue analysis are used and compared using case studies. The purpose of this chapter is to give an overview of power system small signal stability analysis.

The impacts of wind energy integrations on power system small signal stability are given in Chapter 5. Dynamic models of a synchronous generator and a DFIG for small signal stability analysis are compared and implemented to give insights to the differences between a synchronous generator and a DFIG. Two case studies are used to investigate the influences of the DFIG base wind farms on power system small signal stability.

In Chapter 6, the conventional power system transient stability analysis without wind energy integration is presented. Equal area criterion is introduced to determine the critical fault clearing time. Time domain simulation for transient stability analysis is introduced and cases studies are given in this chapter. It aims to give an overview of power system transient stability analysis.

Chapter 7 presents the impacts of wind energy integrations on power system transient stability analysis. Time domain simulation is first applied to the single machine infinite bus (SMIB) systems with a synchronous generator. Different models for DFIGs are compared and a DFIG-based wind generation system is implemented to investigate its transient behaviors. This gives the insights of dynamic performance of a synchronous generator and a DFIG in power system transient stability analysis. Two case studies are implemented to investigate the influences of integrations of DFIG-based wind farms on power system transient stability.

Chapter 8 gives the conclusions of the thesis and suggestions for future works.

## **Chapter 2**

# **Wind Energy Development and the Doubly-Fed Induction Generator**

### **2.0 Introduction**

This chapter presents an overview of wind energy developments and basic knowledge on wind generators. The operation and modeling of a doubly-fed induction generator (DFIG) is explained in detail. Section 2.1 and 2.2 provide information on the developments of wind energy in the world and in Canada respectively. Four types of wind generators are introduced in section 2.3. The basic features of induction generators are given in section 2.4. Then, the DFIG and its modeling are discussed in section 2.5 and 2.6. Section 2.7 summarizes this chapter.

### **2.1 Wind Energy Developments in the World**

Electrical power systems are of great significance in modern society. They have been growing into the world's biggest energy sources for individual households and

industries due to their fast and economic transmission capability. However, traditional fossil fuels consumed for electricity generation have caused serious environmental problems. Various researches have been conducted on using renewable energy as an alternative primary energy source for electricity generations.

Among all renewable energies, wind energy is the most promising one. It has the least impact on the surrounding ecosystem. Besides, wind energy is an unlimited source for providing electricity to the grid.

Under the above circumstances, many countries have dedicated to develop wind power generation technologies, especially countries like Denmark and Germany. Other governments have also issued policies to promote the development of wind energy. In the recent two decades, the installed capacities of wind farms have increased rapidly with annual installations reaching 60 GW in 2015, as shown in Figure 2.1. The wind power installed capacity was only 3,760 MW in 2000, and has grown to 63,013 MW in 2015 [1].

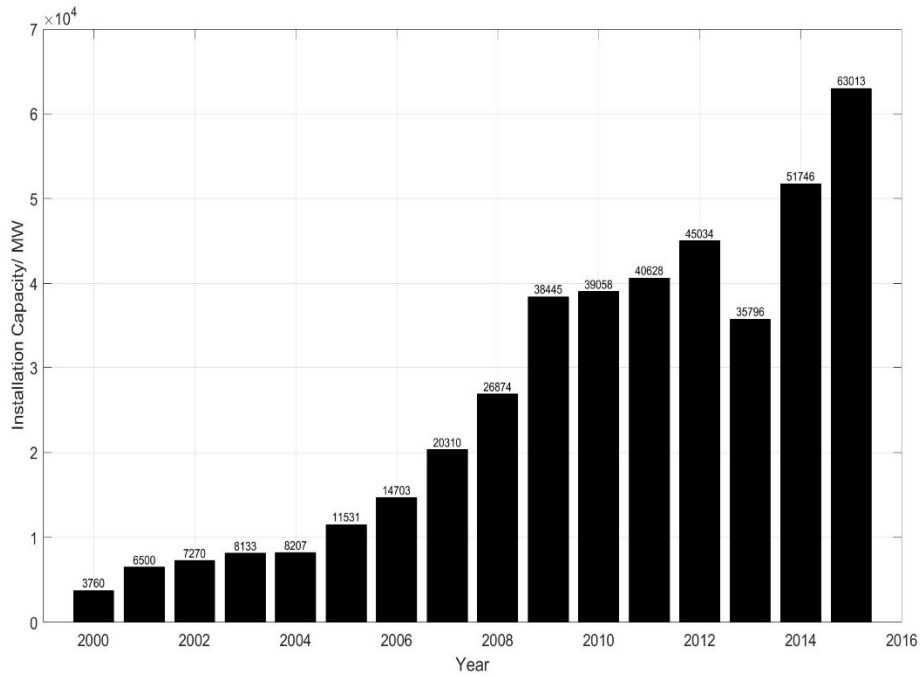


*Figure 2.1 Annually Installed Global Wind Energy Capacities 2000- 2015 [1]*

Figure 2.2 presents the newly installed capacities in different countries during 2015. It is illustrated in Figure 2.2 that China has the largest wind energy installation capacity in 2015, followed by Germany, USA and India [1].

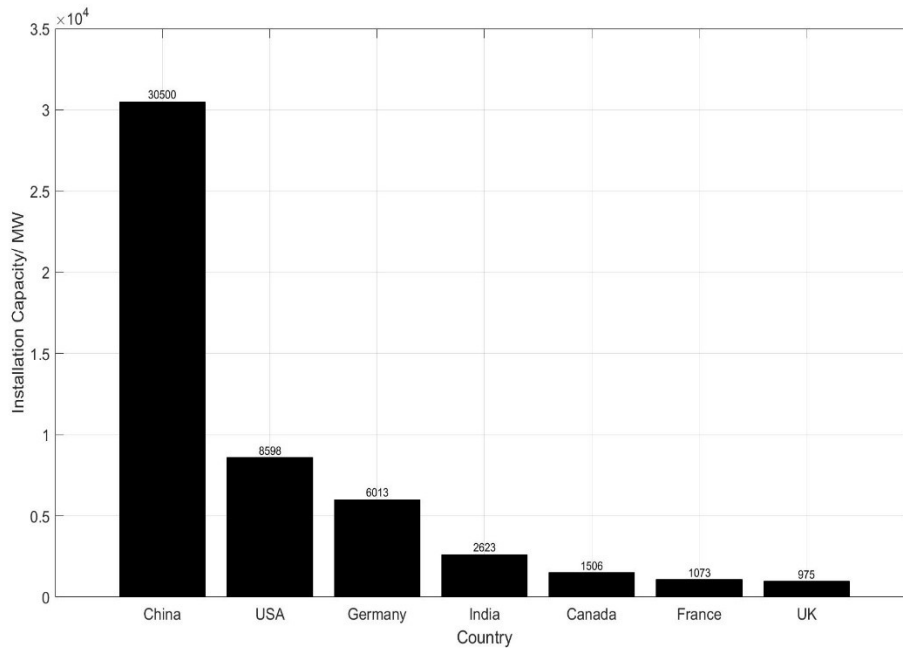


*Figure 2.2 Newly Installed Capacities in Different Countries in 2015 [1]*

Wind energy has shown great potentials for future electricity generation and has been appreciated by many countries across the world. It can be anticipated that the total installed capacity of wind energy will keep increasing.

## **2.2 Wind Energy Developments in Canada**

While the development of wind and other renewable energies in Canada has lagged somewhat behind other parts of the world, the recent growth and plans for future development are promising [2].

The development of wind energy for electricity generation in Canada is noticeable and Canada is one of the seven countries that surpass the 10,000 MW installation

threshold. As reported in [3], Canada finished 2015 with over 11, 000 MW of total installed capacity. The total newly installed capacity was 1, 506 MW during 2015.

The installed capacity status in different provinces of Canada in 2015 is shown in Figure 2.3. The installed capacity status in Ontario and Quebec are noticeable, which are 4,361 MW and 3,262 MW respectively [3]. Compared to these two provinces, other provinces have lower installed capacities of wind energy.

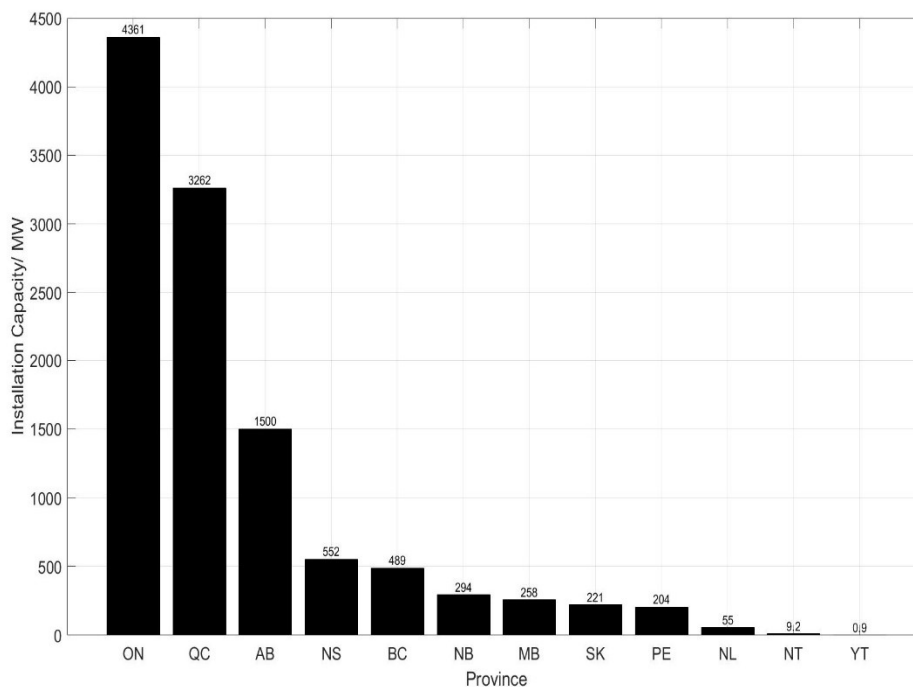


*Figure 2.3 Installed Capacities of Wind Generation in Different Provinces of Canada as of December 2015 [3]*

Ramea, as a remote community in Newfoundland and Labrador, has developed its own way for accepting wind energy into the local power system. Since 2004, Frontier Power Systems started to construct a wind farm for Ramea [2, 4]. A wind-diesel

hybrid solution has been developed in Ramea, as shown in Figure 2.4, with wind energy accounting for a large amount of electricity demands of the local community. It is expected to cover electricity demands in Ramea totally by green energy, using diesel as backup generators. The excess electricity generated from the wind farm will be stored as hydrogen, obtained from water electrolysis. In case the wind generators power output cannot meet the load demand, stored hydrogen can be used to generate electricity to the grid. This provides a good practice for tackling the intermittent and unpredictable characteristics of wind energy.

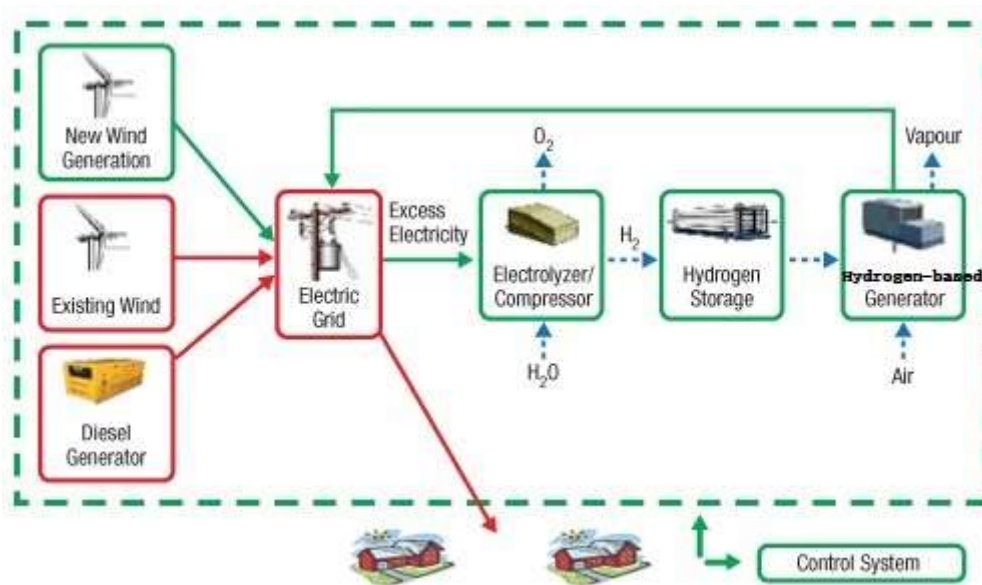


Figure 2.4 Wind Diesel System in Ramea [4]

## 2.3 Wind Generators

Over the past periods of development, many concepts of converting wind energy into electrical power have been proposed. They can be generally classified into fixed speed and variable speed wind power generators. Four types of wind generation configurations are commonly used and presented in Figure 2.5-2.8 [5].

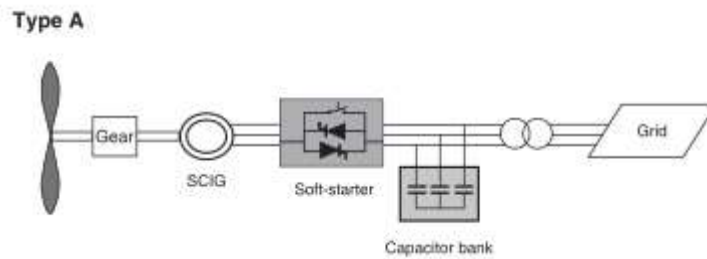


Figure 2.5 Type A Configuration [5]

In the Type A configuration, a squirrel cage induction generator (SCIG) is connected to the grid directly and a capacitor bank is used for supplying reactive power, which is one type of the fixed speed wind generators. This configuration can only operate in a limited range of speed resulting in low efficiency as the wind speed is variable with time.

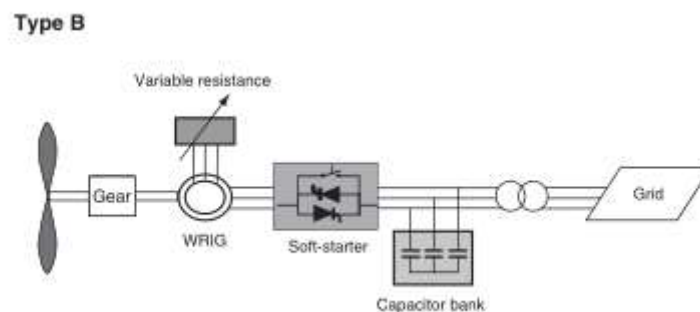


Figure 2.6 Type B Configuration [5]

The Type B configuration can operate on limited variable speed by adding a variable resistance to the rotor, which can provide limited variable speed operation. This configuration can operate at different speeds by adjusting the variable resistance.

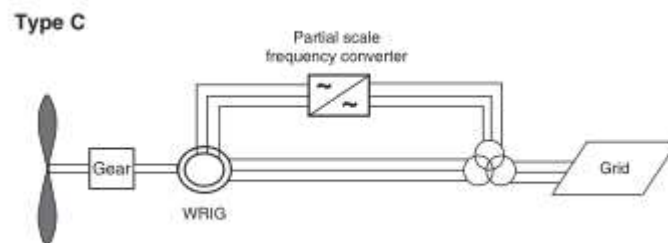


Figure 2.7 Type C Configuration [5]

Type C is commonly referred to as doubly fed induction generator (DFIG). The rotor of the induction machine is connected to an AC-DC-AC power electronic converter. The rotor speed can be adjusted by the rotor side converter. This type of wind generator is attracting increasing attention due to its energy and cost effectiveness compared to other configurations. This is one type of the variable speed wind generators. The detailed descriptions of this type are illustrated in section 2.5 and 2.6.

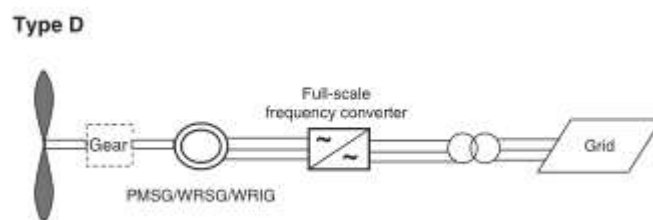


Figure 2.8 Type D Configuration [5]

Permanent magnet synchronous generator (PMSG) (wound rotor synchronous generator (WMSG) or wound rotor induction generator (WRIG)) with full-scale converter is the type D configuration as shown in Figure 2.8, which is one type of

variable speed wind generators. The generator is connected to the grid through an AC-DC-AC power electronic converter.

The detailed descriptions of wind energy conversion systems are available in [5]. Due to the popularity and high demand for DFIGs, this thesis will focus on DFIGs [5].

## **2.4 Basic Operation of Induction Generators**

To better understand the operation of a doubly fed induction generator, it is necessary to first review the basic operation of induction generators. When the induction machine is running as a motor, the stator is connected to a three-phase power supply, which produces a rotating magnetic field. The rotating magnetic field ‘pulls’ the rotor to run behind it. To work as a generator, a primary mover should be applied to the rotor to accelerate rotor speed. When the speed of the rotor surpasses the rotating magnetic field, the stator will provide active power to the power source. However, as the induction generator is not a self-excited machine, it still requires reactive power supplied from the external power source for generating the rotating magnetic field. The reactive power can be supplied by the implementation of capacitor banks, as shown in the Type A configuration in Figure 2.3. A demonstration of the components of an induction generator is shown in Figure 2.9. The stator and rotor are the main components of an induction machine. The stator is connected to a power supply, through which it can obtain or provide electrical power, and produce a rotating

magnetic field. The rotor is short circuited for a normal induction machine, where it can receive or provide mechanical power.

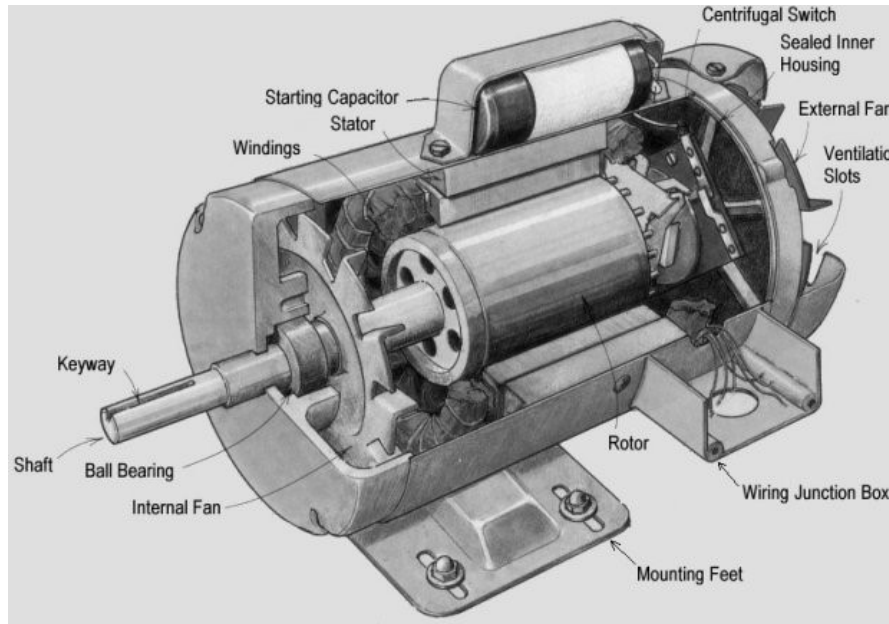


*Figure 2.9 Structure of An Induction Generator [6]*

## **2.5 Introduction to Doubly Fed Induction Generators**

There are many types of wind energy generators available, among which, DFIGs are the most popular ones, due to their high efficiency and flexible control [5, 7]. A DFIG is essentially a wound rotor induction generator with its rotor connected to a back-to-back power electronic converter, which delivers approximately 30% of the rated power, while the stator is connected to the grid directly or through a transformer. A structure of the wind energy system with DFIG is provided in Figure 2.10 [7].

Control systems are applied for controlling pitch angle and back-to-back converter,

which renders more control flexibilities to DFIGs. Under the rated wind speed, the rotor side converter is used to control the rotor speed to extract the maximum power from the wind. Above the rated wind speed, the pitch angle control is activated to limit the rotor speed and provide constant power output. The purpose of the grid side converter is to provide a path for exchanging power between the rotor and grid, which is normally operated at unity power factor, and keep the capacitor voltage constant.

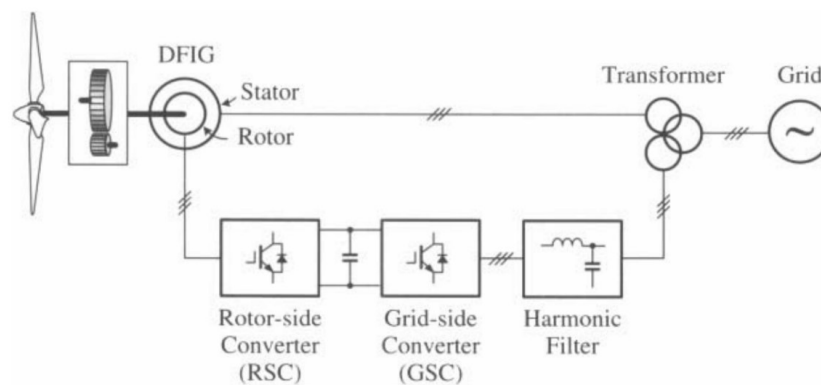


*Figure 2.10 Diagram of A Doubly Fed Induction Generator [7]*

Compared with Type A and Type B configurations, the DFIG can operate at variable speed and supply limited reactive power to the grid without the requirement of external capacitor. Compared with Type D configuration, where full scale of power is conveyed through power electronic devices, only 30% of the rated power passes through power electronic devices in DFIGs. This reduces the cost of implementing the back-to-back converter.

## **2.6 Modeling of Doubly Fed Induction Generators**

For analyzing the impact of wind energy on power system operations, appropriate wind generator models should be developed. For this thesis, the focus is the DFIGs. Detailed models of DFIGs which include details of the power electronic devices are time consuming and unnecessary for power system analysis studies. Assumptions could be made that the performances of the power electronic converters are satisfactory and its switching dynamics are neglected. These assumptions are reasonable when the purpose is to observe the effect of wind energy penetration on the external network rather than within the wind farm [8].

The modeling of DFIGs can be divided into models for steady state analysis and models for dynamic analysis.

### **2.6.1 Modeling for Steady State Analysis**

Although the power outputs of wind generators within a wind farm may vary, they all connect to the same bus within the power system. DFIGs have reactive power capability, which makes them behave more like synchronous generators. Under steady state analysis, buses with DFIGs can be represented as voltage controlled (PV) buses with appropriate reactive power (VAR) limits [9]. The investigation on power system steady state operation with DFIG based wind farms is provided in Chapter 3.

## 2.6.2 Modeling for dynamic analysis

In dynamic analysis, a DFIG based wind farm can be modeled as a single equivalent machine. For power system stability studies, a simplified model of DFIG is normally adopted to reduce the computational burdens as a large power system may contain more than several hundreds of states. A simplified model is presented below for both understanding the model that is commonly used in stability analysis and illustrating the operational characteristics of a DFIG. The model is used in Chapter 5 and Chapter 7 for small signal and transient stability analysis. The DFIG system model can be divided into wind turbine model, rotor model, generator model and converter model [10, 11].

### 2.6.2.1 Wind Turbine Model

The mechanical power extracted from wind can be represented by (2.1) [12].

$$P_m = \frac{\rho}{2} C_p(\lambda, \theta) A_r V_w^3 \quad (2.1)$$

Where

$\rho$  represents air density,  $C_p$  represents power coefficient,  $A_r$  represents the area swept by the rotor and  $V_w$  represents wind speed.

The power coefficient  $C_p$  depends on tip speed ratio  $\lambda$  and pitch angle  $\theta$  and they are the only controllable quantities in the equation (2.1). The tip speed ratio  $\lambda$  is defined in (2.2).

$$\lambda = \frac{\omega_r R}{V_w} \quad (2.2)$$

Where

$R$  represents rotor radius and  $\omega_r$  is the rotor speed.

The characteristic of  $C_p$  is typically provided by wind turbine manufactures and it varies from manufacture to manufacture. Here, the  $C_p(\lambda, \theta)$  is approximated as (2.3) [12].

$$C_p = 0.5 \left( \frac{116}{\lambda_i} - 0.4\theta - 5 \right) e^{-\frac{21}{\lambda_i}} \quad (2.3)$$

With

$$\frac{1}{\lambda_i} = \frac{1}{\lambda + 0.08\theta} - \frac{0.035}{\theta^3 + 1} \quad (2.4)$$

Under the rated wind speed, the rotor side converter adjusts the electromagnetic torque to adjust the rotor speed  $\omega_r$ , which controls the tip speed ratio  $\lambda$ , as shown in (2.2), to obtain the maximum power from the wind. The pitch angle is governed by pitch angle controller. Above rated wind speed, the pitch angle controller adjusts  $\theta$  to keep power constant. Combining the controlling methods for  $\lambda$  and  $\theta$ , the optimal mechanical power extracted from wind is obtained under different conditions.

To simplify the studies, the mechanical power from the wind turbine can be considered constant during stability analysis.

### 2.6.2.2 Rotor Model

The rotor speed results from the balance between the mechanical torque  $T_m$  and the generator electromagnetic torque  $T_e$ . Two-mass model and one-mass model are used for representing the rotor model of a DFIG.

The two-mass model is given in (2.5)- (2.7).

$$2H_t \frac{d\omega_t}{dt} = T_m - [K\theta_{tw} + D(\omega_t - \omega_r)] \quad (2.5)$$

$$\frac{d\theta_{tw}}{dt} = \omega_t - \omega_r \quad (2.6)$$

$$2H_g \frac{d\omega_r}{dt} = [K\theta_{tw} + D(\omega_t - \omega_r)] \quad (2.7)$$

Where

$T_m$  is the mechanical torque,  $T_e$  is the electromagnetic torque,  $\omega_t$  is the turbine speed,  $\theta_{tw}$  is the shaft twist angle,  $K$  is the shaft stiffness coefficient,  $D$  is the damping coefficient and  $H_t$  and  $H_g$  are turbine and generator inertia constants.

It is also practical to use the one mass rotor model when the oscillations of electrical components are the research focus, which is shown in (2.8).

$$\frac{d\omega_r}{dt} = \frac{\omega_s}{2H} (T_m - T_e) \quad (2.8)$$

Where

$H$  is the generator inertia.

### 2.6.2.3 Generator Model

The dynamic generator model of DFIG is the model of an induction generator with the rotor not short-circuited. The basic equations for a DFIG in d-q frame are given in equation (2.9)- (2.16) [13].

$$V_{ds} = R_s I_{ds} - \omega_s \psi_{qs} + p\psi_{ds} \quad (2.9)$$

$$V_{qs} = R_s I_{qs} + \omega_s \psi_{ds} + p\psi_{qs} \quad (2.10)$$

$$V_{dr} = R_r I_{dr} - (\omega_s - \omega_r) \psi_{qr} + p\psi_{dr} \quad (2.11)$$

$$V_{qr} = R_r I_{qr} + (\omega_s - \omega_r) \psi_{dr} + p\psi_{qr} \quad (2.12)$$

$$\psi_{ds} = L_{ss} I_{ds} + L_m I_{dr} \quad (2.13)$$

$$\psi_{qs} = L_{ss} I_{qs} + L_m I_{qr} \quad (2.14)$$

$$\psi_{dr} = L_m I_{ds} + L_{rr} I_{dr} \quad (2.15)$$

$$\psi_{qr} = L_m I_{qs} + L_{rr} I_{qr} \quad (2.16)$$

Where

$V$  represents the voltage,  $I$  represents the current,  $R$  represents the resistance,  $\omega_s$  represents the synchronous rotating speed,  $\psi$  represents the magnetic flux and  $L$  represents inductance. The subscript of  $q$  or  $d$  means it is a quantity of quadrature axis or direct axis, the subscript  $s$  or  $r$  means it is a quantity of stator or rotor.

The rotor fluxes in the basic equations can be converted into generator internal voltages using (2.17) and (2.18).

$$E'_d = -\frac{\omega_s L_m}{L_{rr}} \psi_{qr} \quad (2.17)$$

$$E'_q = \frac{\omega_s L_m}{L_{rr}} \psi_{dr} \quad (2.18)$$

From the above basic equations, the following dynamic model can be derived.

$$\frac{X'_s}{\omega_s} \frac{dI_{ds}}{dt} = V_{ds} - \left( R_s + \frac{X_s - X'_s}{T'_0} \right) I_{ds} - \frac{\omega_r}{\omega_s} E'_d - \frac{L_m}{L_{rr}} V_{dr} + \frac{1}{T'_0} E'_q + X'_s I_{qs} \quad (2.19)$$

$$\frac{X'_s}{\omega_s} \frac{dI_{qs}}{dt} = V_{qs} - \left( R_s + \frac{X_s - X'_s}{T'_0} \right) I_{qs} - \frac{\omega_r}{\omega_s} E'_q - \frac{L_m}{L_{rr}} V_{qr} - \frac{1}{T'_0} E'_d - X'_s I_{ds} \quad (2.20)$$

$$\frac{dE'_d}{dt} = (\omega_s - \omega_r) E'_q - \frac{\omega_s L_m}{L_{rr}} V_{qr} - \frac{\omega_s}{T'_0} [E'_d - (X_s - X'_s) I_{qs}] \quad (2.21)$$

$$\frac{dE'_q}{dt} = -(\omega_s - \omega_r) E'_d + \frac{\omega_s L_m}{L_{rr}} V_{dr} - \frac{\omega_s}{T'_0} [E'_q + (X_s - X'_s) I_{ds}] \quad (2.22)$$

Where

$\theta_{tw}$  is the shaft twist angle,  $I_{qs}$  and  $I_{ds}$  are stator current in d-q frame,  $E'_q$  and  $E'_d$  are equivalent voltage source,  $X_s$  is the steady-state reactance,  $X'_s$  is the transient reactance,  $T'_0$  is the transient time constant,  $L_m$  is the mutual inductance and  $L_{rr}$  is the rotor inductance.

Combining (2.19)- (2.22) with (2.8) gives the 5<sup>th</sup> order model for DFIGs. In stability analysis, it is common to neglect the stator transient term [20]. Then, the differential equations for the stator currents (2.19) and (2.20) are eliminated and a reduced order model is derived.

The active and reactive power generated can be calculated by (2.23) and (2.24).

$$P = V_{ds} I_{ds} + V_{qs} I_{qs} + V_{dr} I_{dr} + V_{qr} I_{qr} \quad (2.23)$$

$$Q = V_{qs}I_{ds} - V_{ds}I_{qs} + V_{qr}I_{dr} - V_{dr}I_{qr} \quad (2.24)$$

The electromagnetic torque  $T_e$  developed on the rotor is shown in equation (2.25).

$$T_e = \psi_{ds}I_{qs} - \psi_{qs}I_{ds} = E'_dI_{ds} + E'_qI_{qs} \quad (2.25)$$

#### 2.6.2.4 Converter Model

In some studies, when the focus is on the internal converter dynamic performance, a detailed power electronic converter model is required. In this thesis, the research focus is on the impact of DFIG based wind farms on the external power systems. The converter can be modeled as a controlled voltage source, assuming the converter can reach a new set point quickly. This assumption is mostly possible in practice, as the modern power electronic devices equipped with high switching frequencies and advanced controllers can provide a desirable dynamic performance [10, 11].

The rotor side converter controls the voltage and current applied to the rotor, which can be used to control the stator active and reactive power and electromagnetic torque.

The common control method for rotor side converter of a DFIG is the decoupled control [14], which can provide separate controls over stator active and reactive power.

The stator active power and reactive power are shown in (2.26) and (2.27).

$$P_s = V_{ds}I_{ds} + V_{qs}I_{qs} \quad (2.26)$$

$$Q_s = V_{qs}I_{ds} - V_{ds}I_{qs} \quad (2.27)$$

In decoupled active and reactive power control, the stator flux is oriented to align the stator flux vector position with d-axis, giving (2.28) and (2.29) [14].

$$\psi_{ds} = \psi_s \quad (2.28)$$

$$\psi_{qs} = 0 \quad (2.29)$$

Neglecting the stator resistor in (2.9) and (2.10) gives (2.30) and (2.31).

$$V_{ds} = -\omega_s \psi_{qs} + p\psi_{ds} = \frac{d\psi_s}{dt} = 0 \quad (2.30)$$

$$V_{qs} = \omega_s \psi_{ds} + p\psi_{qs} = \omega_s \psi_s = E_t \quad (2.31)$$

Where

$E_t$  is the terminal voltage.

From the basic equations (2.13) and (2.14), (2.32) and (2.33) can be derived.

$$I_{ds} = \frac{\psi_s - L_m I_{dr}}{L_{ss}} = \frac{E_t}{\omega_s L_{ss}} - \frac{L_m}{L_{ss}} I_{dr} \quad (2.32)$$

$$I_{qs} = -\frac{L_m}{L_{ss}} I_{qr} \quad (2.33)$$

Substituting (2.30) - (2.33) into (2.26) and (2.27) gives (2.34) and (2.35).

$$P_s = E_t I_{qs} = -\frac{L_m E_t}{L_{ss}} I_{qr} \quad (2.34)$$

$$Q_s = V_t I_{ds} = \frac{E_t^2}{\omega_s L_{ss}} - \frac{E_t L_m}{L_{ss}} I_{dr} \quad (2.35)$$

From (2.34) and (2.35), it is shown that stator active and reactive power outputs are controlled by rotor currents  $I_{qr}$  and  $I_{dr}$  separately. For the desired active and reactive power, the rotor currents are determined. Then, the rotor voltages from rotor

side converter are determined.

Mostly, the electromagnetic torque is controlled to force the rotor to operate at the optimal speed. The rotor speed is determined by the balancing between the mechanical torque and electromagnetic torque. The equation for electromagnetic torque is derived in (2.25), which is related to (2.26). The torque controller is used to replace the active power controller. The electromagnetic torque can be controlled by rotor current  $I_{qr}$  independently, as given in (2.36).

$$T_e = L_m I_{qs} I_{dr} - L_m I_{ds} I_{qr} = -\frac{L_m V_t}{\omega_s L_{ss}} I_{qr} \quad (2.36)$$

The aim of the grid side converter is to keep the capacitor DC voltage constant and provide a path for power exchange. It can be assumed that the grid side converter is ideal and operated at unity power factor. The reactive power supplied by the converter to the grid is zero. Thus, it makes the reactive power supplied to the grid equal to the reactive power from the stator.

## **2.7 Summary**

In this chapter, the general wind power development and wind generators are introduced. The demands and the installed capacities of wind energy in the world and the wind energy development in Canada are presented. Then, different types of wind generation configurations are introduced. As the focus of this thesis is on DFIGs, the features and modeling techniques of DFIGs are discussed in detail. The steady state model of DFIG will be used in Chapter 3 while the dynamic model will be used in Chapters 5 and 7 for small signal and transient stability analysis. This chapter sets a foundation for the following chapters.

## **Chapter 3**

# **Power System Steady State Operation with Wind Energy Integrations**

### **3.0 Introduction**

This chapter introduces the steady state characteristics of wind farms by performing power flow and contingency analysis. In section 3.1, 3.2 and 3.3, three aspects of the wind farm characteristics are considered and related case studies are presented. The first aspect is the effects of different wind farm types on the power system operation, with or without reactive power capabilities. The second aspect is planning the locations and connection schemes of a wind farm considering power system steady state operation. The last aspect focuses on the temporal intermittency of a wind farm and its impact on the power system operation. A summary is given in section 3.4.

### **3.1 Different Wind Farm Types**

In power system steady state operation, wind farms can be aggregated as voltage

controlled (PV) or real and reactive power specified (PQ) bus generators with their own features. Different types of wind generators can be divided into two groups. One group is those absorbing reactive power from the grid, which are Type A and Type B configurations. The other group is those with capabilities of providing reactive power, which are Type C and Type D configurations. Wind farms without reactive power capabilities cannot contribute to the voltage regulation and therefore modeled as PQ bus generators. They are commonly controlled as generators with fixed real power output and constant power factors (absorbing reactive power). This group will be referred to as Type one wind farm in the following sections. Wind farms with reactive power capabilities can contribute to voltage regulation and they are modeled as PV buses. They are commonly controlled as generators with fixed real power output and limited variable reactive power outputs [9]. This group will be referred to as Type two wind farm in the following sections.

### **3.1.1 Case Study: Different Types of Wind Farm**

This case study compares the power system steady state operations of two groups of wind generation units. The simulation software used for this case study and the following cases is the PowerWorld simulator [14]. In PowerWorld, the first group wind farm is represented as a generator with fixed real power (100 MW) and constant power factor (absorbs 48.43 Mvar). The second group wind farm is represented as a generator with fixed real power (100 MW) and limited reactive power (-50 Mvar ~ 50

Mvar). As this case aims to study the characteristics of a specific wind farm, a small 7 Bus power system is used to give a clear illustration. Both types of wind farms are connected to Bus 4 in a 7 Bus power system and both power flow and contingency analysis are performed to assess and compare their features and impacts.

Figure 3.1 shows the 7 Bus power system used for this case study. The wind farm is connected to Bus 4 and a capacitor is connected only when the Type one wind farm is connected. The system data are given in Appendix A.

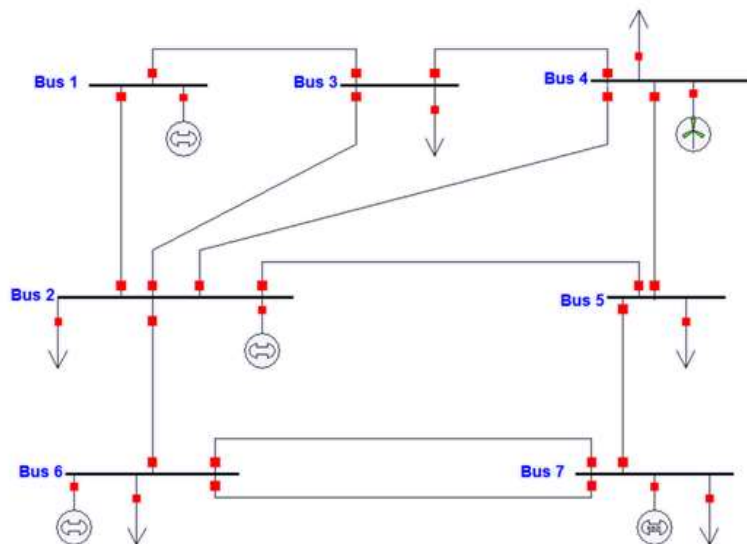


*Figure 3.1 One Line Diagram of the 7 Bus Power System with Wind Farm*

Figure 3.2 shows the connection diagram of Bus 4 with the Type one wind farm and the result of power flow analysis. Bus 4 is modeled as PQ bus and the wind farm connected to it requires reactive power from the grid. A capacitor is also connected to Bus 4 for bus voltage regulation. It shows that after conducting the power flow analysis, the wind farm provides 100 MW of real power and absorbs 48 Mvar of reactive power and the capacitor provides 65.94 Mvar for maintaining the bus voltage

at 1 pu.

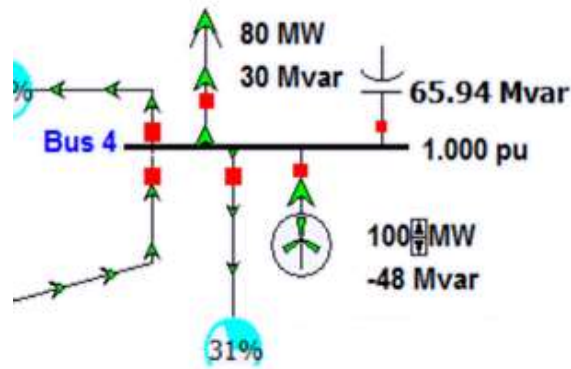


Figure 3.2 Connection of Bus 4 with a Type One Wind Farm

Figure 3.3 shows the condition of Bus 4 with Type one wind farm after opening Line 2-4. The voltage magnitude at Bus 4 is 'pulled' down, from 1 pu to 0.973 pu, due to the loss of power from Bus 2.

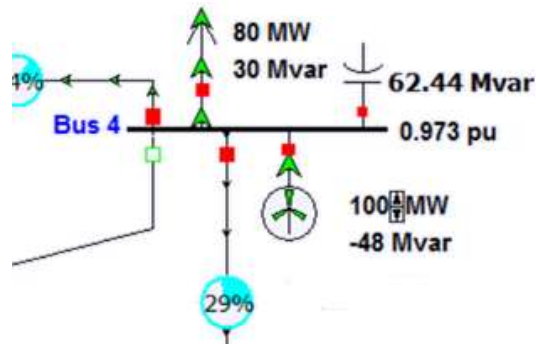


Figure 3.3 Contingency Condition of a Type One Wind Farm

An N-1 contingency analysis is performed for the Type one wind farm condition. The line overload violations are shown in Table 3.1.

Table 3.1 Results of Contingency Analysis with a Type One Wind Farm

Contingency Definitions	Contingencies	Percent Overload	MVA Overload
Open Line 1-2	Line 1-3 Overload	51.1	33.2
Open Line 2-6	Line 2-5 Overload	3.3	3.3
Open Line 7-5	Line 2-5 Overload	15.1	15.1

The system aggregate MVA overload metric is calculated in (3.1).

$$MVA_{AO}^{SYS} = 33.2 + 3.3 + 15.1 = 51.6 \text{ MVA} \quad (3.1)$$

Where

$MVA_{AO}^{SYS}$  represents the system total aggregated MVA overload.

Figure 3.4 shows the connection diagram of Bus 4 with the Type two wind farm and the result of power flow analysis. Bus 4 is modeled as PV bus. No extra capacitor is connected to Bus 4 in this case. It also shows that after conducting the power flow analysis, the wind farm will provide 100 MW of real power and 18 Mvar of reactive power to the system and the bus voltage is regulated at 1 pu.

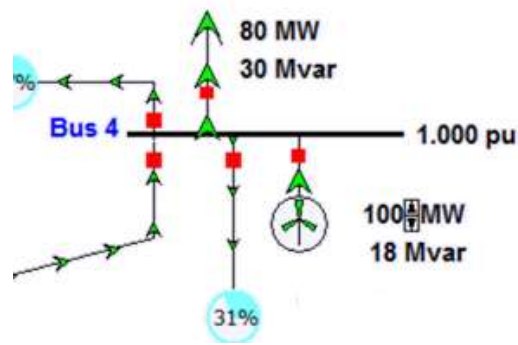


Figure 3.4 Connection of Bus 4 with A Type Two Wind Farm

Figure 3.5 shows the condition of Bus 4 with the Type two wind farm after opening Line 2-4. The voltage magnitude at Bus 4 is kept at the same value as the wind farm can provide reactive power to make up for the reactive power loss from Bus 2. The reactive power output of the wind farm increased from 18 Mvar to 43 Mvar to maintain the bus voltage.

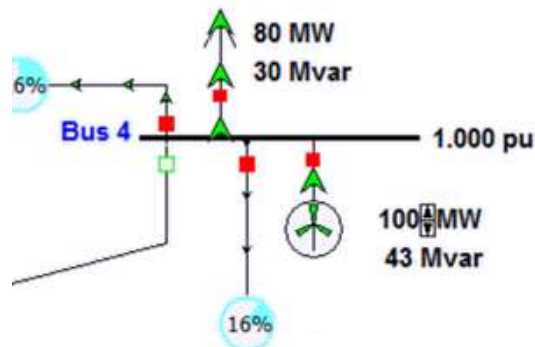


Figure 3.5 Contingency Condition of A Type Two Wind Farm

An N-1 contingency analysis is performed for the Type two wind farm condition. The line overload violations are shown in Table 3.2.

Table 3.2 Results of Contingency Analysis with A Type Two Wind Farm

Contingency Definitions	Contingencies	Percent Overload	MVA Overload
Open Line 1-2	Line 1-3 Overload	50.9	33.1
Open Line 2-6	Line 2-5 Overload	3	3
Open Line 7-5	Line 2-5 Overload	12.7	12.7

The system aggregate contingency overload is calculated in (3.2).

$$MVA_{AO}^{SYS} = 33.1 + 3 + 12.7 = 48.8 \text{ MVA} \quad (3.2)$$

Comparing the values of system aggregate contingency overload index  $MVA_{AO}^{SYS}$  from (3.1) and (3.2), it can be concluded that the power system aggregate MVA overload is reduced with a Type two wind farm.

This case study compares two types of wind farms through power flow analysis and contingency analysis. The wind generation units equipped with power electronic converters can provide reactive power to the grid instead of absorbing it from the grid. This advantage can reduce the cost of implementing external capacitor banks for wind farms, use wind farm to contribute to bus voltage regulation and improve the system security.

### 3.2 Wind Farm Planning

This section focuses on the planning of the location and integration scheme for a wind

farm considering the steady state operation. An index for ranking the locations is introduced and a case study is presented in subsection 3.2.1. Then, a more practical case of replacing a synchronous generator with a wind farm in a large system is presented in subsection 3.2.2.

### 3.2.1 Weighted Transmission Loading Relief

The index, Weighted Transmission Loading Relief (WTLR), is introduced in references [2- 4] for identifying and ranking the locations where the new extra wind farm added can enhance the system security.

In contingency analysis, Transmission Loading Relief (TLR) sensitivity is defined as the branch post-contingency flow change with respect to the injection at a certain bus, the equation for calculation is shown in (3.3) [15].

$$TLR_{BUSi, BRANCHjk, CONTc} = \frac{\Delta PostContMWFl_{BRANCHjk, CONTc}}{\Delta MWInjection_{BUSi}} \quad (3.3)$$

Where

$TLR_{BUSi, BRANCHjk, CONTc}$  represents the calculated TLR value by changing power flow at branch  $jk$  under contingency  $c$  with respect to injecting real power at bus  $i$ ,  $\Delta PostContMWFlow_{BRANCHjk, CONTc}$  represents the post-contingency real power flow change in branch  $jk$  under contingency  $c$  and  $\Delta MWInjection_{BUSi}$  represents real power injection at bus  $i$ .

To assess the effect of injecting power at a certain bus on all branches under all

contingencies, Equivalent Transmission Loading Relief (ETLR) is introduced. The ETLR value is the sum of all TLRs for one bus, using equation (3.4) [15].

$$ETR_{BUSi} = \sum_{jk} \sum_c TLR_{BUSi, BRANCHjk, CONTc} \quad (3.4)$$

However, ETLR does not consider the severity of the contingency overloads, WTLR is introduced by weighting TLRs by the aggregated contingency overload  $P_{ACO}$ . The calculation equation for WTLR is shown in (3.5) [15].

$$WTLR_{BUSi} = \frac{N_{CONT}}{P_{ACO}^{SYS}} \sum_{jk \in Branches} (CODir_{BRANCHjk} * TLR_{BUSi, BRANCHjk} * P_{ACO, BRANCHjk}) \quad (3.5)$$

Where

$N_{CONT}$  represents the number of contingencies,  $P_{ACO}^{SYS}$  and  $P_{ACO, BRANCHjk}$  represent aggregated contingency overload for the whole system and for single one branch and they are introduced in equations (3.6) and (3.7),  $CODir_{BRANCHjk}$  represents the overload direction defined as 1 if the line is overloaded in the forward direction during all the contingencies and 0 otherwise.

$$P_{ACO, BRANCHjk} = MVARating_{BRANCHjk} * \sum_{jk} (\%Overload - 100) \quad (3.6)$$

$$P_{ACO}^{SYS} = \sum_{Branchjk} P_{ACO, BRANCHjk} \quad (3.7)$$

The calculated WTLR values for each bus indicate that new generations will reduce the overloads and enhance system security if the values are negative and will increase the overloads if the values are positive. The calculations of the above indexes are incorporated in PowerWorld sensitivity analysis tool.

### 3.2.1.1 Case Study: Application of WTLR for Wind Farm Planning

This case study investigates the optimal integration location for adding a wind farm to better enhance the system security in the 7 Bus system with the aid of WTLR index.

The 7 Bus system is shown in Figure 3.6 and the ranking of weak elements is visualized by aggregated MVA overload. It is shown that transmission Lines 1-3 and 2-5 are the weak elements and will decrease the system security under contingencies.

The system aggregate MVA overload for this system is 47.73 MVA.

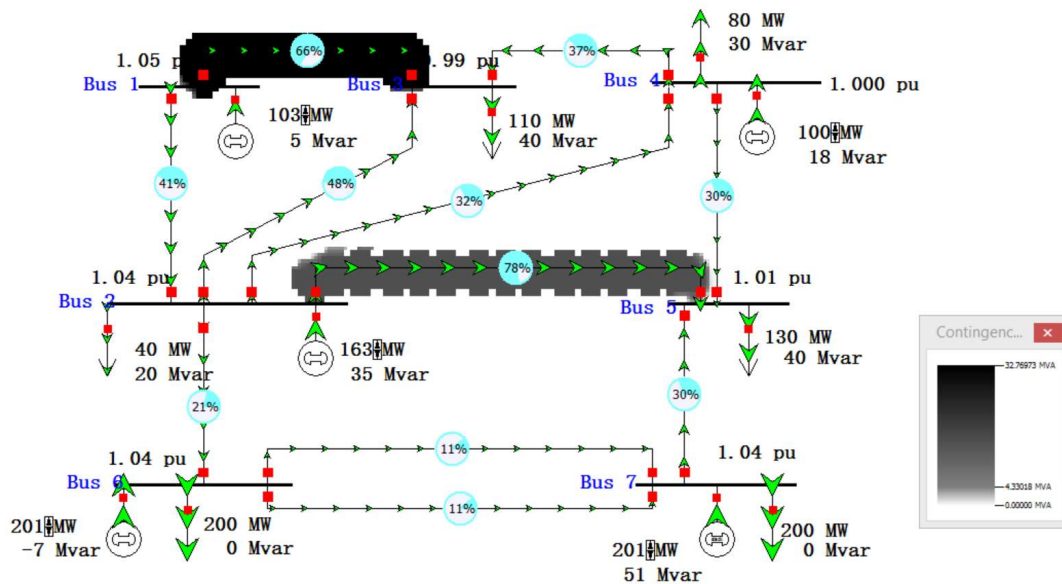


Figure 3.6 Weak Element Visualization

The WTLR values are calculated for each bus and visualized in Figure 3.7. The dark places represent negative WTLR values and indicate where the wind farm should be located to enhance the system security.

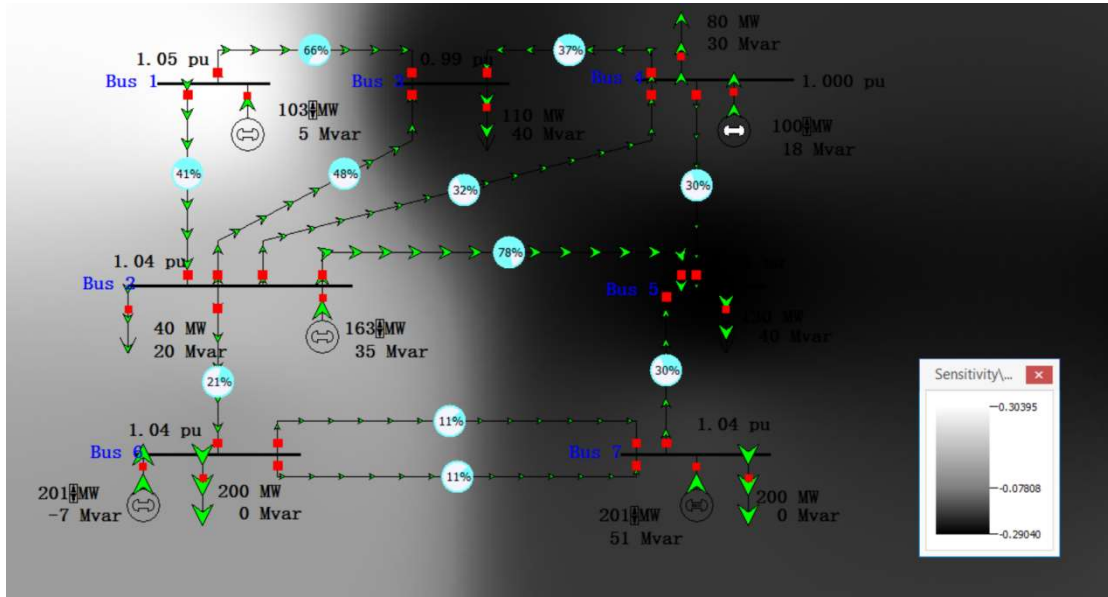


Figure 3.7 WTLR Sensitivity Visualization

Based on the information provided in Figure 3.7, Bus 5 and Bus 3 are chosen for connecting the new wind farm. The wind farm used here is the same Type two wind farm with rated 100 MW and reactive power output range of  $-50 \text{ Mvar} < Q < 50 \text{ Mvar}$ . As shown in Table 3.3, the system aggregated MVA overload values are calculated for different wind farm real power outputs considering the wind speed variations. It is shown that Bus 5 with lower value of WTLR is a better place to connect a new wind farm to enhance the system security.

Table 3.3 System Aggregated MVA Overload for a Wind Farm connected at Bus 5 and

Bus 3

Connected Bus	WTLR	ETLR	Wind Farm Real Power Output (MW)				
			100	75	50	25	0
Bus 5	-0.2905	-0.4274	0	6.86	15.41	24.32	40.06
Bus 3	-0.2561	-0.1683	2.36	6.63	19.35	32.35	47.73

Planning a wind farm with the aid of WTLR values is theoretically effective. However, the location of a wind farm may not be changeable in a real power system as the wind resource is distributed unevenly. The location of a wind farm is decided by the available of wind resource. The next subsection discusses how to integrate the wind substation into a large system when the site of wind farm has already been decided.

### **3.2.2 Case Study: Wind Farm Planning in a Large System**

This case study investigates the impact on the steady state operation of a large system when a synchronous machine is replaced by a wind farm. The system used for this case study is a regional power system of Island Electric Company (IEC) [16]. The existing 300 MW generator at the Pheasant Substation is replaced by a new 600 MW wind farm. Due to the variability of wind speed, the power output of the wind farm varies from 0 MW to 600 MW. The wind farm is the Type two wind farm. Thus, for a given wind speed, it will be modeled as PV bus generator with fixed real power and limited reactive power range of  $-250 \text{ Mvar} < Q < 250 \text{ Mvar}$ . The one line diagram of the IEC power system is shown in Figure 3.8 and the details are summarized in Appendix B.

In this case study, the base case without wind farm replacement is analyzed first. The case of disconnecting a synchronous generator is then discussed. Finally, several schemes of connecting a new wind farm to replace the disconnected synchronous generator are presented and compared.

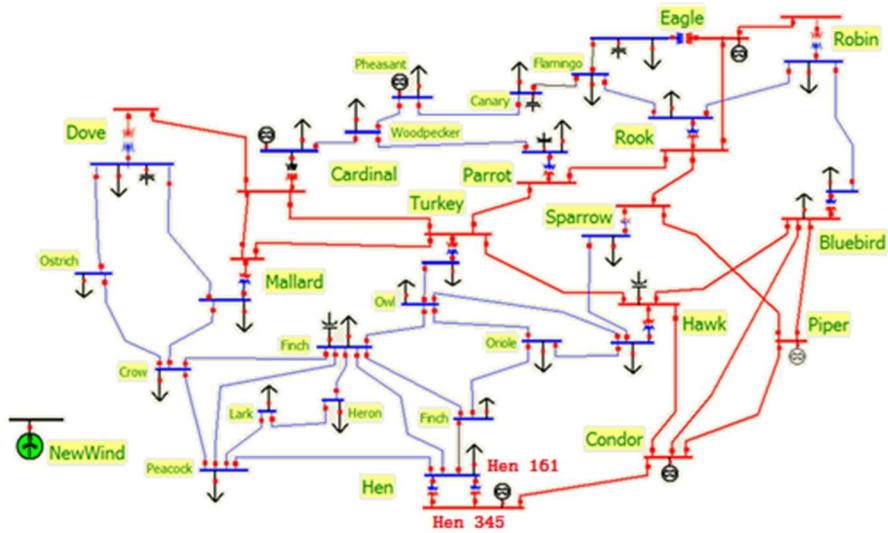
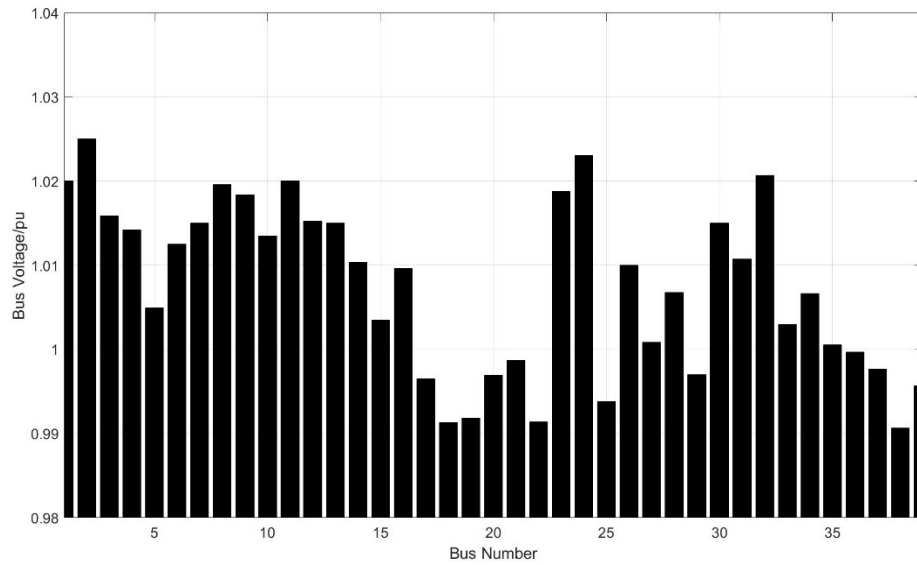


Figure 3.8 One Line Diagram of Island Electric Company (IEC) Power System [16]

### 3.2.2.1 Analysis of Base Case

After performing power flow analysis for the base case, the voltage magnitudes at all buses are shown in Figure 3.9. It is illustrated in Figure 3.9 that the bus voltage magnitudes vary within the range of 1.03 pu and 0.99 pu. The bus voltage at the Pheasant substation is regulated at 1.01 pu and the generator outputs are 300 MW and -20.409 Mvar.



*Figure 3.9 Bus Voltage Magnitude Variations of IEC Power System Base Case*

After performing the N-1 contingency analysis for the base case, it is found that the violations are between substations of Hen 345 and Hen 161. In here, N-1 contingency analysis assesses the system security when one of the system elements is opened. There are two transformers between them as shown in Figure 3.8. When one transformer opened, the other one will overload.

### **3.2.2.2 Analysis of Disconnecting a Synchronous Generator**

This subsection analyzes the condition where the 300 MW synchronous generator at the Pheasant substation is disconnected. Figure 3.10 shows the bus voltage magnitudes after the generator at the Pheasant Substation is opened. The bus voltages dropped down on some buses and the minimum bus voltage is below 0.99 pu due to the loss of the generator.

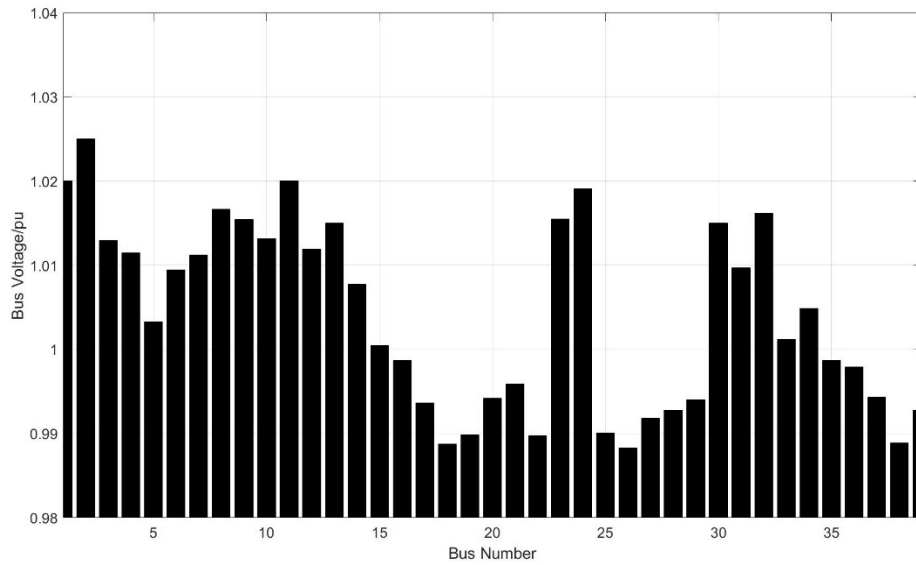


*Figure 3.10 Bus Voltage Magnitude Variations of IEC Power System with Synchronous Generator Disconnection*

The results of N-1 contingency analysis are the same as in the base case, except that the transmission line overload is higher, increasing from 101.5% to 104.8%.

### **3.2.2.3 Analysis of Planning a Wind Farm**

In this section, a new 600 MW wind farm is connected to the IEC power system to replace the old 300 MW synchronous generator. Six connection schemes are designed and compared to assess how the wind farm connection schemes affect the system operation.

To simplify the analysis, the wind farm is connected at the 161 kV level and requires at least two transmission lines for the NewWind substation. Table 3.4 shows the available approaches for constructing transmission lines to connect the wind farm into

the IEC system.

*Table 3.4 Available Approaches for Construction*

Substations	Distance (KM)
NewWind to Ostrich	15
NewWind to Dove	55
NewWind to Crow	30
NewWind to Peacock	53
NewWind to Hen	70
Ostrich to Mallard	45
Peacock to Hen	20
Dove to Cardinal	40

The line parameters are listed below [13].

$$r = 0.037 \ \Omega/km \quad (3.8)$$

$$x = 0.367 \ \Omega/km \quad (3.9)$$

$$b = 4.518 \ \mu s/km \quad (3.10)$$

Six connection schemes are designed as shown in Table 3.5. Schemes 1-3 build 2 transmission lines that connect NewWind substation with other two substations while Schemes 4-5 add an extra line.

*Table 3.5 NewWind Substation Connection Schemes*

Scheme 1	NewWind-Ostrich & NewWind-Crow
Scheme 2	NewWind-Dove & NewWind-Peacock
Scheme 3	NewWind-Dove & NewWind-Hen
Scheme 4	NewWind-Ostrich & Ostrich-Mallard & NewWind-Crow
Scheme 5	NewWind-Dove & Dove-Cardinal & NewWind-Peacock
Scheme 6	NewWind-Peacock & Peacock-Hen & NewWind-Dove

Both power flow and contingency analysis are performed for each scheme. From the results of power flow analysis, it is found that there are little differences on the bus voltage magnitudes between these six schemes. This system is a large system, which makes the power from the wind farm have less impact on the system bus voltages.

Figure 3.11 shows the aggregated MVA overload for each scheme from contingency analysis with the wind farm at 100 MW. When the wind farm has 600 MW output, all the contingencies are eliminated for all schemes. Scheme 4 is adding a transmission line of Ostrich-Mallard to Scheme 1. The system aggregated MVA overload for scheme 4 is 10.92 MVA which is lower than Scheme 1 of 11.28 MVA. By adding additional transmission line, the system security is enhanced. It is also the same for

Scheme 2 and Scheme 5, with aggregated MVA overload decreased from 4.26 MVA to 0 MVA by adding line Dove-Cardinal. However, comparing Scheme 2 with Scheme 6, by adding an extra line of Peacock-Hen, the aggregated MVA overload increased from 30.52 MVA to 52.7 MVA.

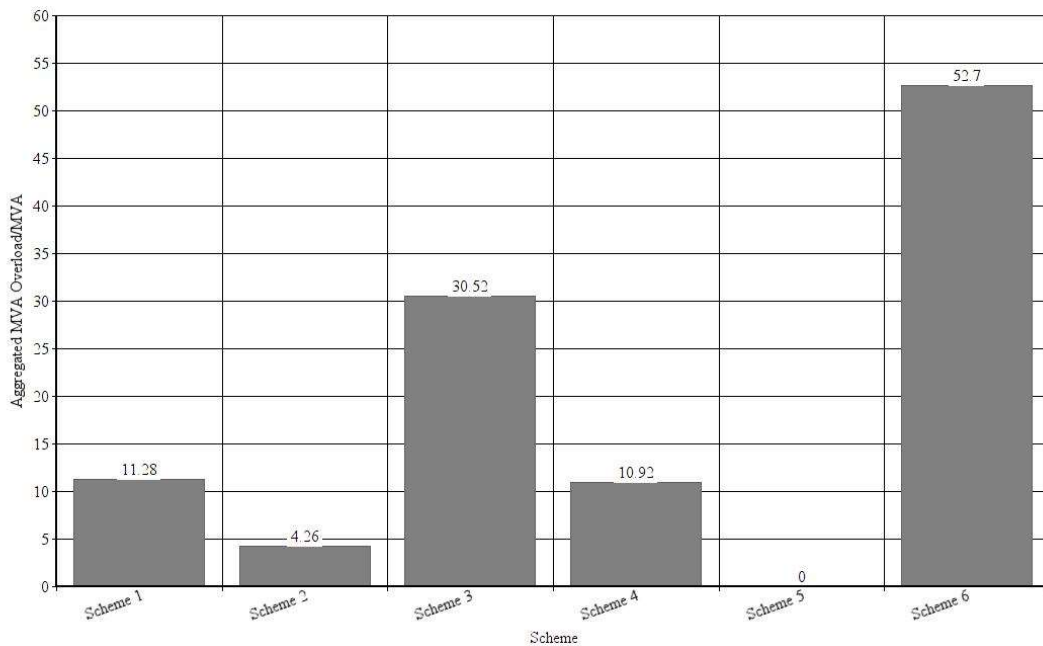


*Figure 3.11 Aggregated MVA Overload of Different Connection Schemes at 100 MW*

### *Output*

Connecting a newly built wind farm into a relatively large power system may have little effect on bus voltages. This case study compares six connection schemes and it is found that the system security can be enhanced by adding an extra line. It should be noted that this case study does not consider the cost of building transmission lines.

### **3.3 Wind Farm Temporal Intermittency**

One of the biggest disadvantages of using wind energy for electricity generation is that wind is unpredictable. Wind speed is characterized by its high variability, both spatially and temporally [17]. The wind speed varies both from region to region and from time to time. This renders great variability to the outputs of wind farms. The intermittent power output from a wind farm cannot meet the power system requirements for stable and flexible power supply. It is significant to investigate how much the intermittency characteristics of a wind farm can affect the power system operation.

#### **3.3.1 Case Study: Wind Farm Temporal Intermittency**

The case study in this section focuses on the impact of the temporal intermittency of a wind farm power output on power system steady state operation.

This case study also adopts the 7 Bus system for analysis. The system one line diagram is shown in Figure 3.1. In this system, a wind farm is connected to Bus 4. In this section, a powerful tool is introduced for analyzing the intermittent characteristics of a wind farm. The tool Time Step Simulation (TSS) provided by PowerWorld is suitable for analyzing the system operation over a period.

The data for varying the system load demands and wind farm power outputs are taken from the daily records of Ontario on Feb 18<sup>th</sup>, 2016 [18]. The load demands and wind

farm outputs are given in Table 3.6. To fit the data into the 7 Bus system, the data is first scaled into the range of 1- 2. Figure 3.12 shows the graph of comparison between load demands and wind farm outputs. The desirable pattern of the wind farm outputs is to have the same trend as load demands. It is shown in Figure 3.12 that the biggest difference between load demand and wind farm output happened at 8:00 AM.

*Table 3.6 Varying Actual and Scaled Data of Load Demand and Wind Farm Output*

Time	Load Demand (MW)	Load Demand (scaled)	Wind Farm Output (MW)	Wind Farm Output (scaled)
0:00	16701	1.31	310	1.04
1:00	15934	1.11	260	1.01
2:00	15571	1.02	240	1.00
3:00	15500	1.00	236	1.00
4:00	15490	1.00	252	1.01
5:00	15764	1.07	299	1.04
6:00	16271	1.20	278	1.02
7:00	17602	1.54	281	1.03
8:00	18933	1.87	382	1.08
9:00	18498	1.76	479	1.14
10:00	17994	1.64	510	1.16
11:00	17579	1.53	564	1.19
12:00	17380	1.48	610	1.21
13:00	17068	1.40	684	1.26

14:00	16874	1.35	620	1.22
15:00	16700	1.31	617	1.22
16:00	16811	1.34	520	1.16
17:00	17559	1.53	980	1.42
18:00	18611	1.79	1455	1.69
19:00	19425	2.00	1810	1.90
20:00	19427	2.00	1738	1.86
21:00	19111	1.92	1435	1.68
22:00	18480	1.76	1894	1.94
23:00	17242	1.45	1851	1.92
0:00	16133	1.16	1990	2.00

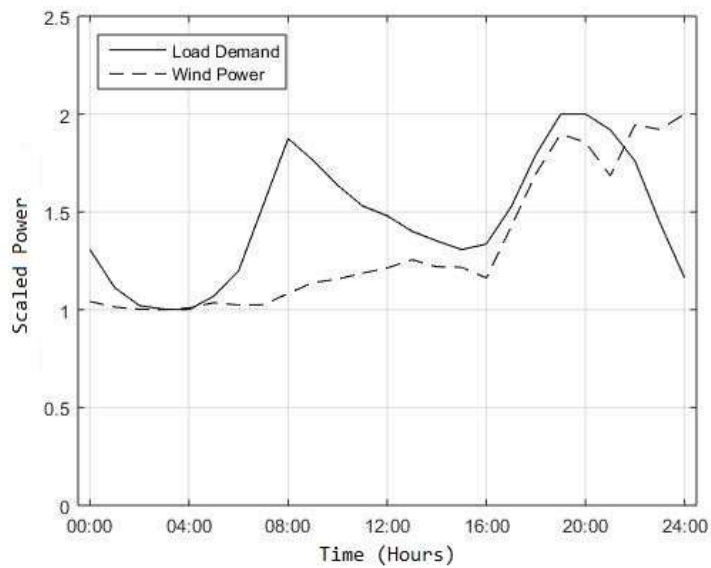


*Figure 3.12 Varying Scaled Load Demand and Wind Farm Output*

The scaled data is then transferred into appropriate input data for performing TSS on the 7 Bus system. The transfer equations for load demand and wind farm output are

presented in (3.11) and (3.12).

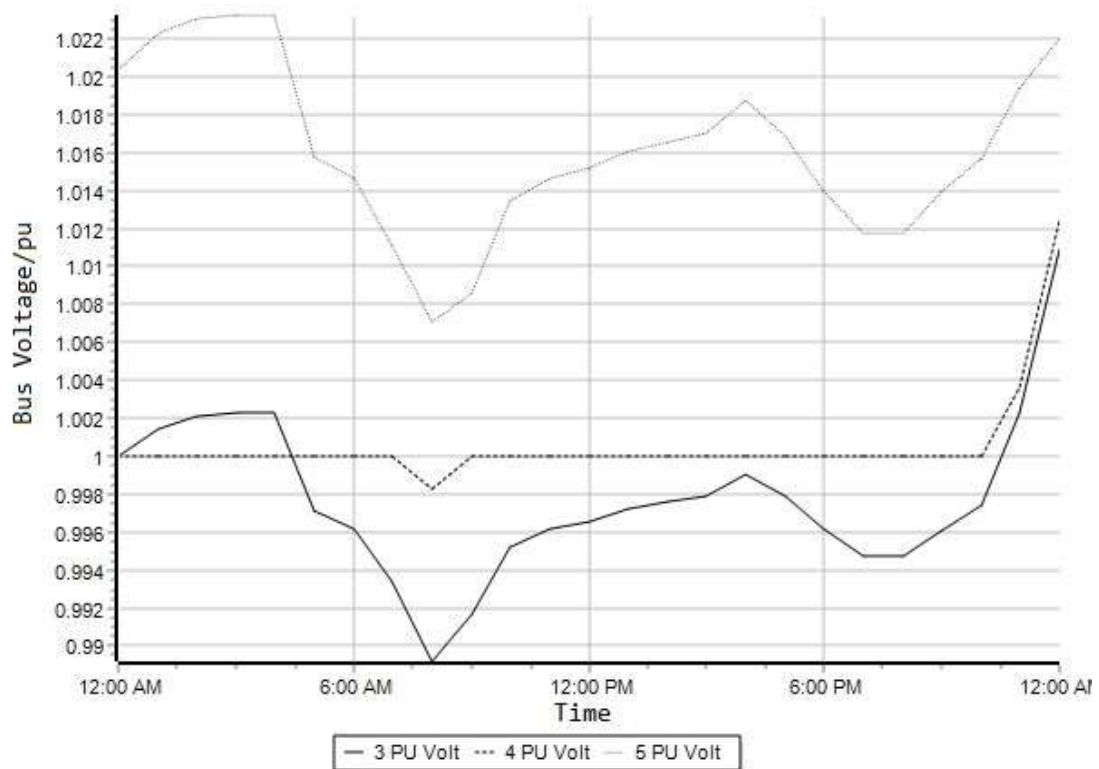
$$LoadDemand = 600ScaleData - 200 \quad (3.11)$$

$$WindOutput = 180ScaleData - 160 \quad (3.12)$$

Where

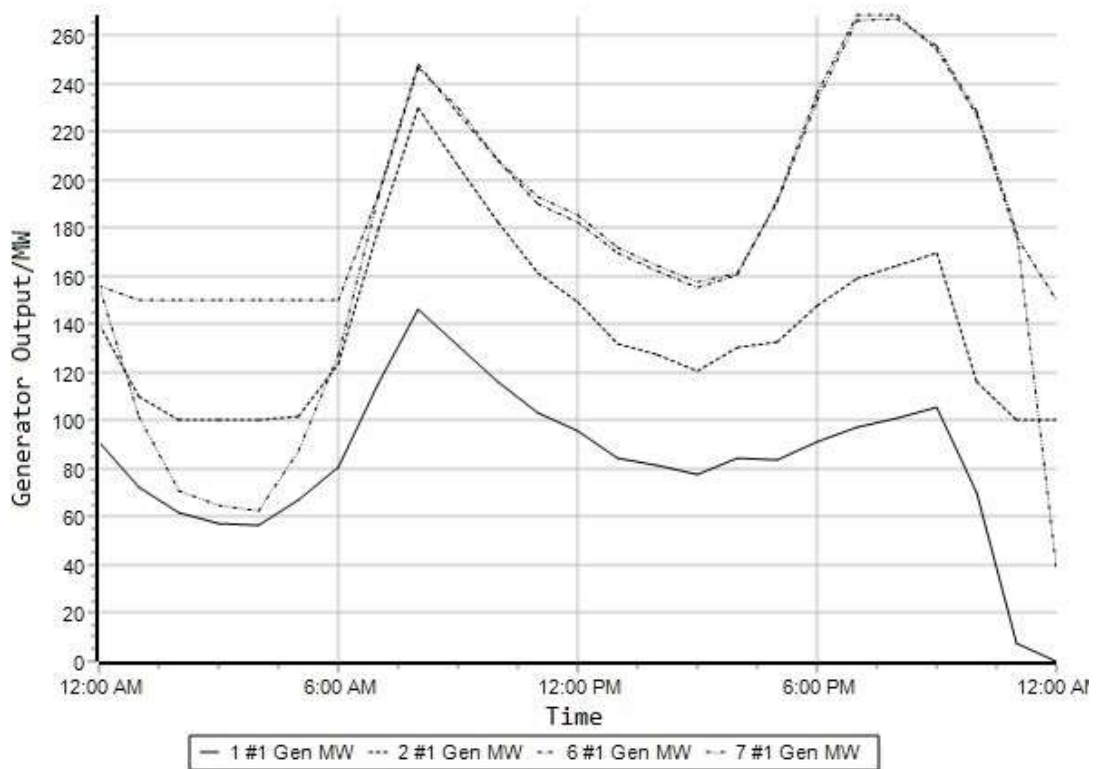
*LoadDemand* represents the total load demand in the 7 Bus system, *WindOutput* represents the wind farm outputs in the 7 Bus system and *ScaleData* represents the scaled data calculated in Table 3.7.

Both power flow and N-1 contingency analysis are performed for each time point of TSS. Voltage magnitudes at bus 1, 2, 6 and 7 stay as the same values throughout TSS. The variation of bus voltage magnitudes at bus 3-5 is shown in Figure 3.13. It is shown that all three buses experienced a decrease at 8:00 AM, because wind farm output cannot 'keep up with' load demand as shown in Figure 3.12.



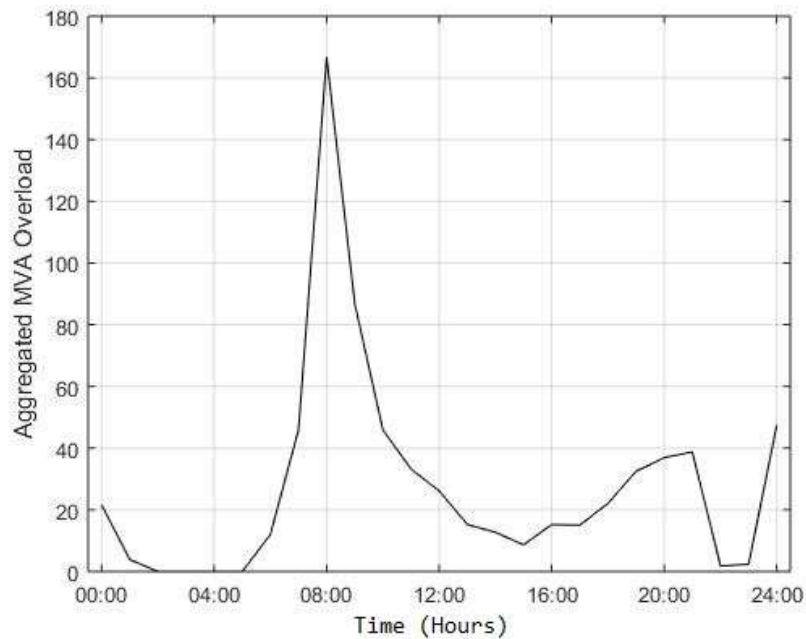
*Figure 3.13 Bus Voltage Magnitude Variations of the 7 Bus System over 24 Hours*

Figure 3.14 shows the real power outputs of synchronous generators. It is shown that at 8:00 AM and 8:00 PM, the synchronous generators outputs increase to meet the peak hour load demand. The wind farm power output depends on the wind speed, which is not changeable to meet the load demand. With the wind energy integration, the synchronous generators within the power system need to be adjusted based on both the load changes and wind power outputs.



*Figure 3.14 Synchronous Generator Output Variations of the 7 Bus System over 24 Hours*

Performing an N-1 contingency analysis for each time point and the system aggregated MVA overload variation is presented in Figure 3.15. There is a dramatic increase of system aggregated MVA overload at 8:00 AM, where the wind farm output did not match with the load demand. This causes the system to be operated insecurely. The system aggregated MVA overload values for other time points are relatively low.



*Figure 3.15 System Aggregated MVA Overload Variations of the 7 Bus System over 24 Hours*

This case study uses Time Step Simulation (TSS) tool for assessing the intermittency of a wind farm power outputs. It is found that the intermittent power outputs from a wind farm affect the system steady state operation. The wind power outputs may keep at low level while the load demand increases sharply as in this case study. This will cause the bus voltages to drop and system security to decrease. The synchronous generators within the system have to adjust their power outputs to meet both the load demands and the wind farm power outputs. This is a challenge encountered in real world. This may cause bus voltage decrease, more contribution from traditional synchronous generators and system insecurity. Before a practical storage solution is developed to smooth the wind farms power outputs, this characteristic will still be a challenge for wind energy development.

### **3.4 Summary**

This chapter demonstrates the characteristics of wind farms in power system steady state operation. Three aspects focusing on the features of different wind farms, planning a new wind farm and the wind power intermittency are presented. All aspects are illustrated by case studies. Power flow analysis, N-1 contingency analysis and time step simulation are the main tools for the case studies.

The results illustrate that wind farms equipped with power electronic devices can contribute to bus voltage regulations and have superior performance under contingencies. When planning a wind farm, the locations of the wind farm can be chosen based on WTLR index. Different connection schemes also have an impact on the power system operation. Due to the intermittency characteristics of the wind farm power outputs, the system steady state operation is influenced. When the wind farm output cannot meet the load demand, it will cause bus voltages to drop and system aggregated MVA overload to increase.

# **Chapter 4**

## **Conventional Small Signal Stability Analysis**

### **4.0 Introduction**

This chapter introduces conventional small signal stability analysis of power systems. It gives the basic understanding of the power system small signal stability and its analysis methods. Section 4.1 gives an overview of power system stability and important concepts related to it. The focus of Chapter 4 is given in section 4.2, where two small signal stability analysis methods are presented and compared using case studies. Small signal stability analysis of a large power system is presented in section 4.3. A summary is given in section 4.4.

### **4.1 Power System Stability**

Maintaining the stable condition of a power system is of great significance for safe and reliable electricity transmission. Many efforts have been devoted to defining and classifying power system stability. The most accepted definition is presented in [19],

which states that ‘power system stability is the ability of an electric power system, for a given initial operating condition, to regain a state of operating equilibrium after being subjected to a physical disturbance, with most system variables bounded so that practically the entire system remains intact.’

The power system stability problem can be generally classified into rotor angle stability, voltage stability and frequency stability depending on the quantity of interest. The active power transmission causes rotor angle separation and reactive power results in voltage variation. Depending on the size of disturbances, power system stability can also be divided into small signal stability and transient stability. Different analysis methods are developed and applied to small signal stability and transient stability analysis.

The rest of this section is dedicated to the fundamental swing equation and power system oscillations.

#### **4.2.1 Swing Equation**

Swing equation gives the motion of a synchronous machine. It is a fundamental equation for understanding the rotor angle stability phenomenon. The rotor motion is determined by Newton’s second law, given in (4.1) [16].

$$J \frac{d\omega_r}{dt} = T_m - T_e \quad (4.1)$$

Where

$J$  represents the inertia of the rotating masses,  $\omega_r$  represents the rotor angular velocity,  $T_m$  represents the mechanical torque and  $T_e$  represents the electrical torque.

The rotor angular velocity  $\omega_r$  is the derivation of  $\theta$  with respect to time, where  $\theta$  is the rotor angular position with respect to a stationary axis. In power system, it is more common to use the term ‘ $\delta$ ’ as the rotor angle, which is the rotor angular position with respect to a synchronously rotating axis. The relation between  $\theta$  and  $\delta$  is explained in (4.2) [16].

$$\theta = \omega_s t + \delta \quad (4.2)$$

Then, (4.3) can be obtained from (4.2).

$$\frac{d\omega_r}{dt} = \frac{d}{dt} \left( \omega_s + \frac{d\delta}{dt} \right) = \frac{d^2\delta}{dt^2} \quad (4.3)$$

In many literatures, the inertia constant  $H$  is used in swing equation. The relation of  $J$  and  $H$  is shown by (4.4) [16].

$$J = \frac{2H}{\omega_s} \quad (4.4)$$

Combining (4.1) and (4.4), (4.5) is obtained.

$$\frac{2H}{\omega_s} \frac{d^2\delta}{dt^2} = T_m - T_e \quad (4.5)$$

The swing equation explains the basic relation between the motion of rotor and mechanical and electrical power of the generator. It clearly shows that the change of

rotor angle can be caused by primary mover or electrical components of the power system.

#### **4.2.2 Synchronous and Damping Torques**

The change of electrical torque  $\Delta T_e$  caused by a perturbation can be divided into two components as in (4.6) [13].

$$\Delta T_e = K_s \Delta \delta + K_D \Delta \omega \quad (4.6)$$

Where

$K_s$  represents synchronous torque coefficient,  $K_D$  represents damping torque coefficient,  $\Delta \delta$  represents rotor angle deviation,  $\Delta \omega$  represents speed deviation,  $K_s \Delta \delta$  represents synchronous torque and  $K_D \Delta \omega$  represents damping torque.

The small signal stability of a power system depends on both components. Lack of sufficient synchronous torque will cause steady increase in rotor angle and lack of sufficient damping torque will cause rotor oscillation of increasing amplitude. In a practical power system, the small signal stability is more concerned with sufficient damping of oscillation [13].

#### **4.2.3 Power System Oscillation**

Oscillations are due to natural modes of the system and therefore cannot be eliminated [20]. The small signal stability problem in a practical power system heavily depends

on the damping of oscillations. The electromechanical oscillation can be divided into:

- Local plant mode oscillation;
- Interarea mode oscillation;
- Torsional mode oscillation;
- Control mode oscillation.

The general form of damped power system oscillation is shown in Figure 4.1 [21].

This figure shows the generator speed oscillation obtained from time domain simulation. The oscillation is damped as the magnitude of the oscillation is getting smaller. To maintain system stability, it is important to ensure all oscillations are effectively damped.

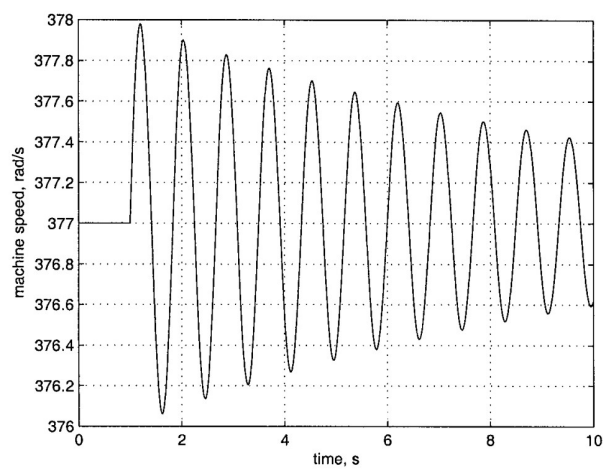


*Figure 4.1 Illustration of Power System Oscillation [21]*

## **4.2 Analysis Methods for Small Signal Stability**

Two methods are used and compared here for analyzing power system small signal stability. One is time domain simulation and the other one is eigenvalue analysis. Two case studies are conducted on the same Two Area power system [13]. The simulation software used is Power System Analysis Tool (PSAT) [22].

### **4.2.1 Time Domain Simulation**

Time domain simulation applies numerical integration to solve differential algebra equations (DAEs) step-by-step formed by the given system. It gives the result of the variation of assessed quantity with time. It is a more common method for transient stability analysis, which is investigated in detail in Chapters 6 and 7.

#### **4.2.1.1 Case Study: Time Domain Simulation for Small Signal Stability Analysis**

This case study and the next case study in subsection 4.2.2.1 are conducted on Two Area power system, shown in Figure 4.2 [13]. Two generators lie in ‘Area 1’ while the other two are included in ‘Area 2’. The two areas are connected by transmission lines. The data of this system is provided in Appendix C.

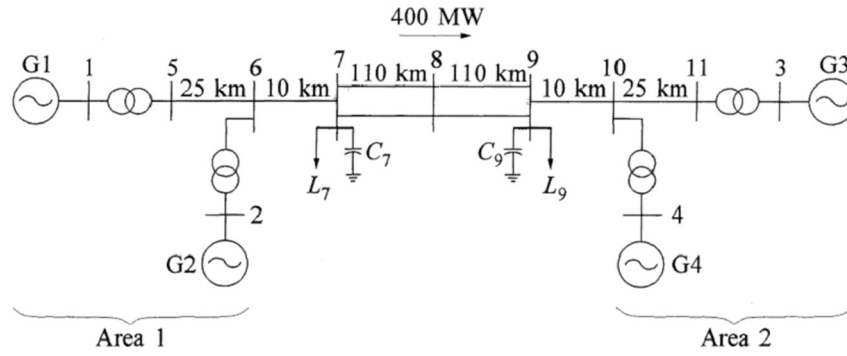


Figure 4.2 One Line Diagram of Two Area Power System [13]

In this case study, time domain simulation is used to analyze small signal stability of the given Two Area system. Two scenarios are considered. Scenario One is the system without adding control of automatic voltage regulators (AVRs) and power system stabilizers (PSSs), while Scenario Two adds an AVR and a PSS to each generator. The small disturbance adopted is the load demand increase of 10% for all loads during the time period of 1s to 1.1s.

Time domain simulation is used to obtain the system responses of this disturbance numerically. Power system stability is determined by observing the obtained system responses.

When the load increase disturbance is applied to Scenario One system, the responses for the rotor angles and rotor speeds are obtained from time domain simulation, shown in Figure 4.3 and 4.4 respectively. It is shown that under the given disturbance, the rotor angles of synchronous generators 3 and 4 drop dramatically, while the rotor speeds of all generators continue to increase. This indicates that after the disturbance, the system is not stable.

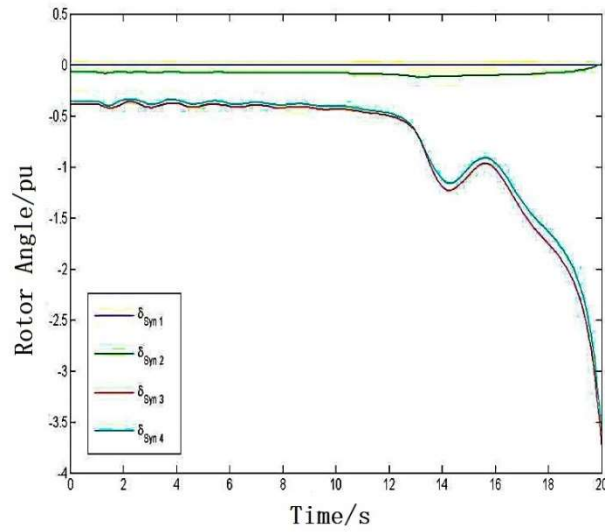


Figure 4.3 Responses of Rotor Angles When Load Increase is Applied (Scenario One)

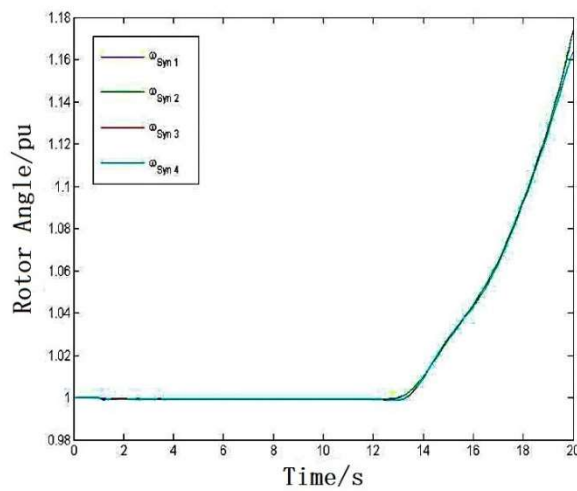


Figure 4.4 Responses of Rotor Speeds When Load Increase is Applied (Scenario One)

The same load increase disturbance is applied to Scenario Two system. In a modern power system, it is a common practice to add sufficient controllers for a generation plant to maintain effective operation. The system responses obtained from time domain simulation are presented in Figure 4.5 and 4.6. It is shown that under the given disturbance, the rotor angles and rotor speeds of all generators can be stable at a

new equilibrium point after a period of oscillations. It indicates that the system is stable. With the additional controllers for the generation plants, the system small signal stability is enhanced.

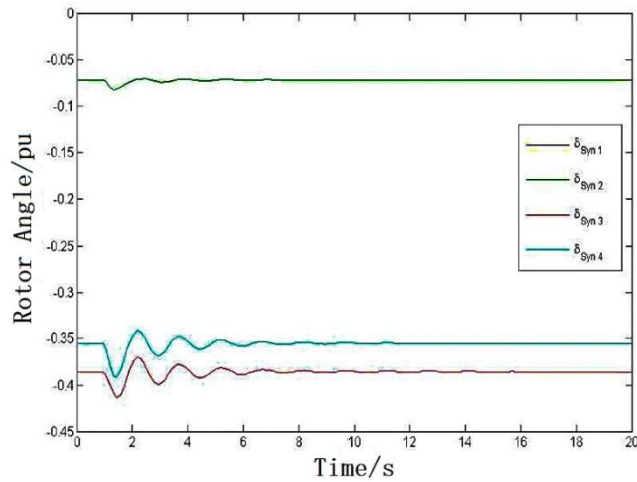


Figure 4.5 Responses of Rotor Angles When Load Increase is Applied (Scenario Two)

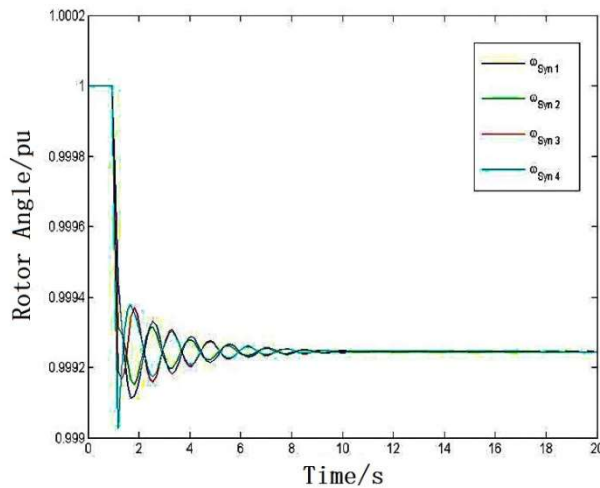


Figure 4.6 Responses of Rotor Speeds When Load Increase is Applied (Scenario Two)

This subsection presents small signal stability analysis using time domain simulation. The power system small signal stability condition is determined by observing the

system responses to a specific disturbance. The two main limitations for time domain simulation are that the observed system responses are restricted to one specific disturbance at one specific location and it cannot reveal relations between the system instability and system states.

#### 4.2.2 Eigenvalue Analysis

Eigenvalue analysis takes advantage of the small disturbance in small signal stability problem to linearize the power system around the equilibrium point.

A power system can be described by state space representation, shown in equations (4.7) and (4.8) [13].

$$\dot{x} = f(x, z, u) \quad (4.7)$$

$$0 = g(x, z, u) \quad (4.8)$$

Where

$x$  represents the state variable,  $z$  represents the algebraic variable,  $u$  represents the input variable and  $t$  represents the time.

The system can be linearized when subjected to a small disturbance. The linearized equations are shown in the general form in (4.9) and (4.10) [20].

$$\Delta\dot{x} = A\Delta x + B\Delta z + C\Delta u \quad (4.9)$$

$$0 = D\Delta x + E\Delta z + F\Delta u \quad (4.10)$$

Where

$$A = \begin{bmatrix} \frac{\partial f_1}{\partial x_1} & \dots & \frac{\partial f_1}{\partial x_n} \\ \vdots & \ddots & \vdots \\ \frac{\partial f_n}{\partial x_1} & \dots & \frac{\partial f_n}{\partial x_n} \end{bmatrix}, B = \begin{bmatrix} \frac{\partial f_1}{\partial z_1} & \dots & \frac{\partial f_1}{\partial z_r} \\ \vdots & \ddots & \vdots \\ \frac{\partial f_n}{\partial z_1} & \dots & \frac{\partial f_n}{\partial z_r} \end{bmatrix}, C = \begin{bmatrix} \frac{\partial f_1}{\partial u_1} & \dots & \frac{\partial f_1}{\partial u_p} \\ \vdots & \ddots & \vdots \\ \frac{\partial f_n}{\partial u_1} & \dots & \frac{\partial f_n}{\partial u_p} \end{bmatrix},$$

$$D = \begin{bmatrix} \frac{\partial g_1}{\partial x_1} & \dots & \frac{\partial g_1}{\partial x_n} \\ \vdots & \ddots & \vdots \\ \frac{\partial g_m}{\partial x_1} & \dots & \frac{\partial g_m}{\partial x_n} \end{bmatrix}, E = \begin{bmatrix} \frac{\partial g_1}{\partial z_1} & \dots & \frac{\partial g_1}{\partial z_r} \\ \vdots & \ddots & \vdots \\ \frac{\partial g_m}{\partial z_1} & \dots & \frac{\partial g_m}{\partial z_r} \end{bmatrix}, F = \begin{bmatrix} \frac{\partial g_1}{\partial u_1} & \dots & \frac{\partial g_1}{\partial u_p} \\ \vdots & \ddots & \vdots \\ \frac{\partial g_m}{\partial u_1} & \dots & \frac{\partial g_m}{\partial u_p} \end{bmatrix}.$$

The state matrix  $A_{sys}$  can be calculated by (4.11).

$$A_{sys} = A - BE^{-1}D \quad (4.11)$$

The matrix  $A_{sys}$  is called state matrix, which characterizes the stability of the linearized system. The values of  $\lambda$  satisfying (4.12) is the eigenvalues of matrix  $A_{sys}$ .

$$\det(\lambda I - A_{sys}) = 0 \quad (4.12)$$

The stability of the system can be determined by the eigenvalues. The negative real eigenvalues correspond to decaying non-oscillation modes while positive real eigenvalues correspond to aperiodic instability modes. The complex eigenvalues with negative real parts correspond to damped oscillation modes while complex eigenvalues with positive real parts correspond to increasing oscillation modes. For eigenvalues with zero real parts, it is difficult to decide its stability in general, which are not given attention in this thesis.

For an eigenvalue  $\lambda_i$ , the right eigenvector  $\Phi_i$  and left eigenvector  $\Psi_i$  of matrix  $A_{sys}$  associated with it are presented in (4.13) and (4.14).

$$A_{sys}\Phi_i = \lambda_i\Phi_i \quad (4.13)$$

$$\Psi_i A_{sys} = \lambda_i \Psi_i \quad (4.14)$$

The participation factor is defined in equation (4.15).

$$p_{ki} = \psi_{ki}\phi_{ik} \quad (4.15)$$

Where

$p_{ki}$  represents the participation factor,  $\phi_{ki}$  is the  $k^{th}$  entry of the right eigenvector  $\Phi_i$  and  $\psi_{ki}$  is the  $k^{th}$  entry of the left eigenvector  $\Psi_i$ .

The participation factor determines the relative participation of certain state variable in a certain mode, and vice versa [13]. It gives information on how much a state variable is involved in a specific mode and the most related state variable in a mode can be found by comparing the values of participation factors. This gives eigenvalue analysis method a great advantage over the time domain simulation method in small signal stability analysis. In time domain simulation, it is difficult to find out the source of certain instabilities.

#### **4.2.2.1 Case Study: Eigenvalue Analysis for Small Signal Stability Analysis**

In this section, eigenvalue analysis method is used for analyzing the small signal stability of the Two Area system. The same two scenarios are also considered for small signal stability analysis of Two Area system using eigenvalue analysis.

Figure 4.7 shows the eigenvalues in the complex plane for Scenario One. It shows that there are two eigenvalues on the right side of the complex plane, which indicates the system is unstable.

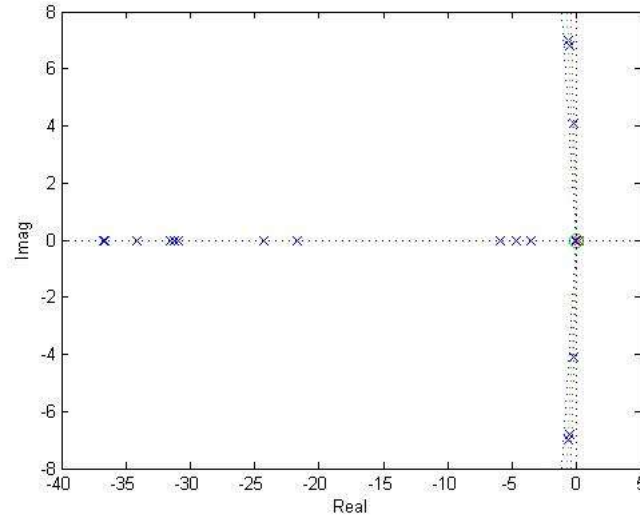


*Figure 4.7 Eigenvalues on Complex plane of Two Area Power System (Scenario One)*

The two real positive eigenvalues are given in Table 4.1. One of the eigenvalues is 0.50337 with the most associated state from synchronous generator 2 while the other one is 0.01977 which is most related to synchronous generator 3. The positive real eigenvalues correspond to aperiodic unstable modes which match with the one obtained from time domain simulation.

*Table 4.1 Instable Modes of Two Area Power System (Scenario One)*

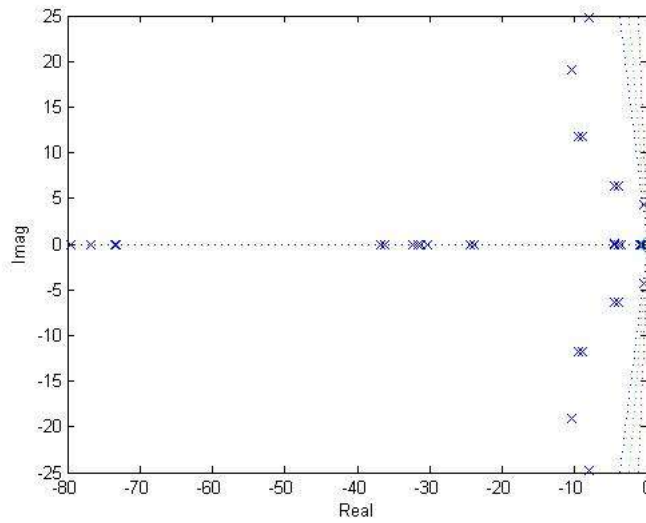
Mode	Eigenvalue	Most Associated States
$\lambda_{19}$	0.50337	$E'_{q2}$
$\lambda_{22}$	0.01977	$E'_{q3}$

Table 4.2 gives the oscillation modes under scenario one. It shows the frequency and damping ratio of an oscillation mode and the participation factors of most associated states. The mode of  $\lambda_9$  and  $\lambda_{10}$  having a frequency of 1.0446 Hz is a local oscillation mode in area one. The mode of  $\lambda_{11}$  and  $\lambda_{12}$  having a frequency of 1.0679 Hz is a local oscillation mode in area two. The mode of  $\lambda_{13}$  and  $\lambda_{14}$  having a frequency of 0.654 Hz is an inter area oscillation mode between area one and two. All the oscillation modes have a low damping as the system is not equipped with any generation controllers.

Table 4.2 Oscillation Modes of Two Area Power System (Scenario One)

Mode	Eigenvalue	Frequency (HZ)	Damping Ratio	Participation Factors of Most Associated States
$\lambda_9, \lambda_{10}$	$-0.57158 \pm j 6.5632$	1.0446	0.0868	$\delta_1 = \omega_1 = 16.865\%$ $\delta_2 = \omega_2 = 20.633\%$
$\lambda_{11}, \lambda_{12}$	$-0.58148 \pm j 6.7099$	1.0679	0.0863	$\delta_3 = \omega_3 = 17.795\%$ $\delta_4 = \omega_4 = 19.956\%$
$\lambda_{13}, \lambda_{14}$	$-0.26224 \pm j 3.3208$	0.5285	0.0787	$\delta_1 = \omega_1 = 15.792\%$ $\delta_3 = \omega_3 = 10.506\%$

Figure 4.8 and Table 4.3 give eigenvalues in complex plane and oscillation modes of Scenario Two of the Two Area power system with AVRs and PSSs. It is shown in Figure 4.8 that all the system eigenvalues are on the left side of complex plane, which indicate that the system is stable. With employing the AVRs and PSSs, the two unstable modes in Scenario One are eliminated. By adding AVRs and PSSs, the power system small signal stability is enhanced. This conclusion also matches with the one obtained from the observation of time domain simulation.



*Figure 4.8 Eigenvalues on Complex Plane of Two Area Power System (Scenario Two)*

From Table 4.3, there are totally 9 oscillation modes containing 8 local modes and 1 inter area mode. Comparing the damping ratios between Table 4.1 and 4.2, the damping values of power system oscillations in Scenario Two are generally higher than in Scenario One. The system small signal stability is enhanced by adding the controllers.

Table 4.3 Oscillation Modes of Two Area Power System (Scenario Two)

Mode	Eigenvalue	Frequency (HZ)	Damping Ratio	Participation Factors of Most Associated States
$\lambda_9, \lambda_{10}$	$-6.7026 \pm j26.6642$	4.2437	0.2438	$E'_{q4}=18.653\%$ $E''_{q4}=14.396\%$
$\lambda_{11}, \lambda_{12}$	$-9.81 \pm j20.5769$	3.2749	0.4303	$E'_{q1}=15.864\%$ $E'_{q2}=15.628\%$
$\lambda_{17}, \lambda_{18}$	$-30.2395 \pm j0.09673$	0.0154	1.0	$V_{2\_pss3}=19.42\%$ $V_{2\_pss1}=20.872\%$
$\lambda_{21}, \lambda_{22}$	$-9.8255 \pm j13.3165$	2.1194	0.5937	$E'_{q1}=14.465\%$ $E'_{q2}=11.803\%$
$\lambda_{23}, \lambda_{24}$	$-9.676 \pm j13.2867$	2.1146	0.5887	$E'_{q3}=14.872\%$ $E'_{q4}=11.314\%$
$\lambda_{25}, \lambda_{26}$	$-3.1115 \pm j5.983$	0.9522	0.4614	$\delta_2=11.882\%$ $\omega_2=10.625\%$
$\lambda_{27}, \lambda_{28}$	$-3.3777 \pm j6.0761$	0.9670	0.4859	$\delta_4=11.424\%$ $\omega_4=10.32\%$
$\lambda_{29}, \lambda_{30}$	$-0.28649 \pm j3.6675$	0.5837	0.0779	$\delta_1=14.559\%$ $\omega_1=12.852\%$
$\lambda_{31}, \lambda_{32}$	$-4.6326 \pm j0.06785$	0.0108	0.9999	$E'_{d2}=37.944\%$ $E'_{d4}=30.086\%$

This section introduces two common methods for analyzing power system small signal stability. Case studies are presented on Two Area power system and two

scenarios are considered. Through these two scenarios, it is shown that power system stability is enhanced by adding AVRs and PSSs, which is widely adopted controllers in modern power systems. By comparing these two methods, it is found that time domain simulation has limitations, while eigenvalue analysis is a more effective method for small signal stability analysis. Time domain simulation gives the system responses to a certain disturbance and cannot indicate the relation between system oscillations and system states. Eigenvalue analysis gives overall system modes to assess stability and provides the information on the most associated states to a certain mode. Eigenvalue analysis is a more effective way for investigating power system small signal stability.

### **4.3 Small Signal Stability of a Large System**

As shown in the comparison in the previous section, eigenvalue analysis is a more effective way for analyzing power system small signal stability. In this section, the eigenvalue analysis method is applied to the small signal stability analysis of the 10-Machine New England power system. The objective of this section is to demonstrate how eigenvalue analysis is applied to a practical large power system.

### 4.3.1 Case Study: Small Signal Stability Analysis of New England Power System

The one line diagram of the New England power system is shown in Figure 4.9 [24].

The system data is provided in Appendix D. All generators are equipped with AVRs and PSSs to enhance the system stability.

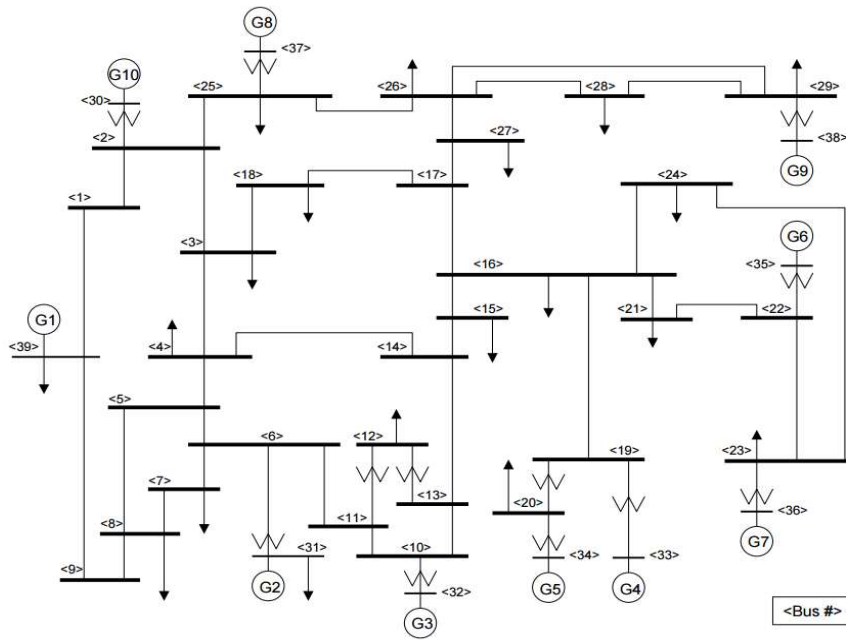


Figure 4.9 One Line Diagram of New England Power System [24]

Figure 4.10 shows the eigenvalues of New England power system in complex plane.

All the eigenvalues are on the left side of the panel indicating the system is stable. As this is a relatively large system, more states are involved in the eigenvalue analysis.

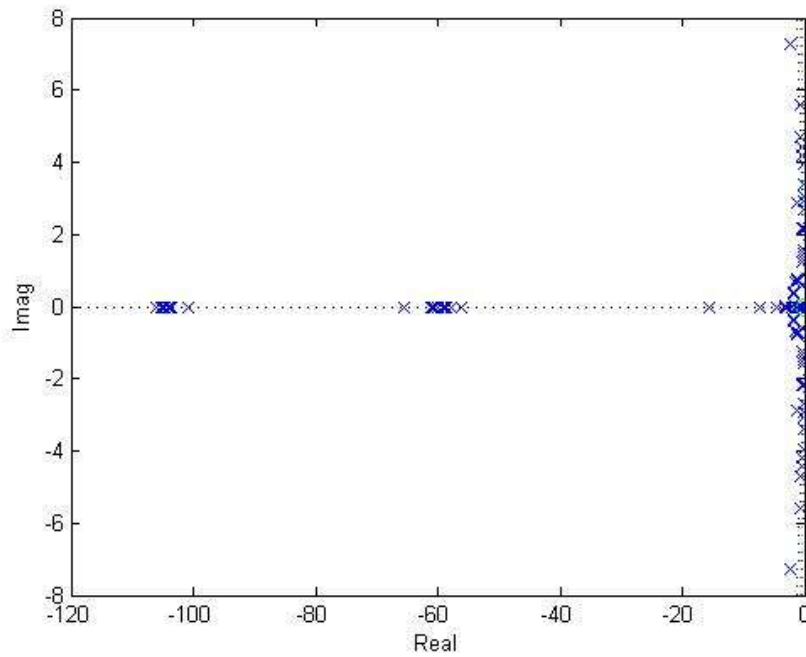


Figure 4.10 Eigenvalues on Complex Plane of New England Power System

All the oscillation modes in New England power system are presented in Table 4.4. The lowest damping ratio is 0.03, which is under the mode of  $\lambda_{44}$ ,  $\lambda_{45}$  and the most associated states are the rotor angle and speed of synchronous generator 4. The damping can be improved by putting more control over the rotor. From Table 4.4, it can be found that most of the inter-area oscillations are well damped while the local oscillations have lower damping ratios.

Table 4.4 Oscillation Modes Of the New England Power System

Mode	Eigenvalue	Frequency (HZ)	Damping Ratio	Most Associated States
$\lambda_{22}, \lambda_{23}$	$-2.30 \pm 7.29j$	1.22	0.30	$V_{3pss-6}, V_{2pss-6}$
$\lambda_{25}, \lambda_{26}$	$-0.64 \pm 5.57j$	0.89	0.11	$\delta_2, \omega_2$
$\lambda_{27}, \lambda_{28}$	$-0.60 \pm 4.69j$	0.75	0.13	$\delta_8, \omega_8$

$\lambda_{29}, \lambda_{30}$	$-0.44 \pm 4.40j$	0.7	0.10	$\delta_5, \omega_5$
$\lambda_{31}, \lambda_{32}$	$-0.33 \pm 4.17j$	0.67	0.08	$\delta_3, \omega_3$
$\lambda_{33}, \lambda_{34}$	$-0.16 \pm 4.00j$	0.63	0.04	$\delta_{10}, \omega_{10}$
$\lambda_{36}, \lambda_{37}$	$-0.27 \pm 3.39j$	0.54	0.08	$\delta_6, \omega_6$
$\lambda_{38}, \lambda_{39}$	$-1.31 \pm 2.87j$	0.50	0.42	$V_{3pss-8}, V_{2pss-8}$
$\lambda_{40}, \lambda_{41}$	$-0.23 \pm 3.08j$	0.49	0.07	$\delta_9, \omega_9$
$\lambda_{42}, \lambda_{43}$	$-0.21 \pm 2.92j$	0.47	0.07	$V_{3pss-5}, V_{2pss-5}$
$\lambda_{44}, \lambda_{45}$	$-0.09 \pm 2.67j$	0.43	0.03	$\delta_4, \omega_4$
$\lambda_{46}, \lambda_{47}$	$-3.25 \pm 0.04j$	0.52	1.00	$E'_{q4}, E'_{q3}$
$\lambda_{49}, \lambda_{50}$	$-0.44 \pm 2.17j$	0.35	0.20	$V_{3pss-9}, V_{2pss-9}$
$\lambda_{51}, \lambda_{52}$	$-0.21 \pm 2.12j$	0.34	0.10	$V_{3pss-7}, V_{2pss-7}$
$\lambda_{53}, \lambda_{54}$	$-0.23 \pm 2.16j$	0.34	0.11	$V_{3pss-3}, V_{2pss-3}$
$\lambda_{56}, \lambda_{57}$	$-0.11 \pm 1.57j$	0.25	0.07	$V_{2pss-10}, V_{3pss-10}$
$\lambda_{58}, \lambda_{59}$	$-0.11 \pm 1.47j$	0.24	0.07	$V_{3pss-4}, \omega_1$
$\lambda_{60}, \lambda_{61}$	$-0.09 \pm 1.37j$	0.22	0.07	$V_{3pss-4}, V_{2pss-4}$
$\lambda_{63}, \lambda_{64}$	$-0.41 \pm 1.22j$	0.21	0.32	$V_{3pss-1}, V_{2pss-1}$
$\lambda_{65}, \lambda_{66}$	$-1.83 \pm 0.09j$	0.29	1.00	$V'_{r3}, E'_{q8}$
$\lambda_{67}, \lambda_{68}$	$-1.73 \pm 0.35j$	0.28	0.98	$V'_{r9}, E'_{q9}$
$\lambda_{69}, \lambda_{70}$	$-1.69 \pm 0.41j$	0.28	0.97	$V'_{r7}, E'_{q6}$
$\lambda_{71}, \lambda_{72}$	$-1.48 \pm 0.66j$	0.26	0.91	$V'_{r1}, E'_{q1}$
$\lambda_{74}, \lambda_{75}$	$-1.35 \pm 0.74j$	0.24	0.88	$V'_{r10}, E'_{q10}$
$\lambda_{76}, \lambda_{77}$	$-0.28 \pm 0.59j$	0.10	0.43	$V'_{r2}, E'_{q2}$
$\lambda_{78}, \lambda_{79}$	$-1.10 \pm 0.75j$	0.21	0.83	$V'_{r8}, E'_{q7}$

$\lambda_{80}, \lambda_{81}$	$-1.29 \pm 0.76j$	0.24	0.86	$V'_{r4}, E'_{q3}$
$\lambda_{82}, \lambda_{83}$	$-1.23 \pm 0.78j$	0.23	0.84	$V'_{r6}, E'_{q5}$

Illustrations of time domain simulation are given in Figure 4.11 and 4.12, which show the rotor speed and angle responses to 20% load increase from 1s to 1.1s respectively. It is shown that the magnitudes of oscillations are all generally decreased under this disturbance, indicating the system is stable.

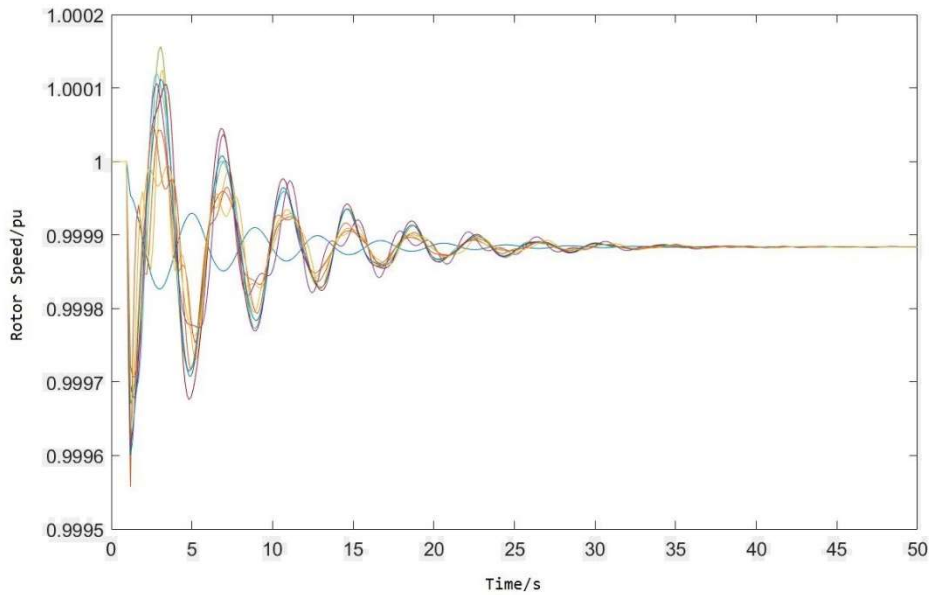


*Figure 4.11 Rotor Speed of New England Power System*

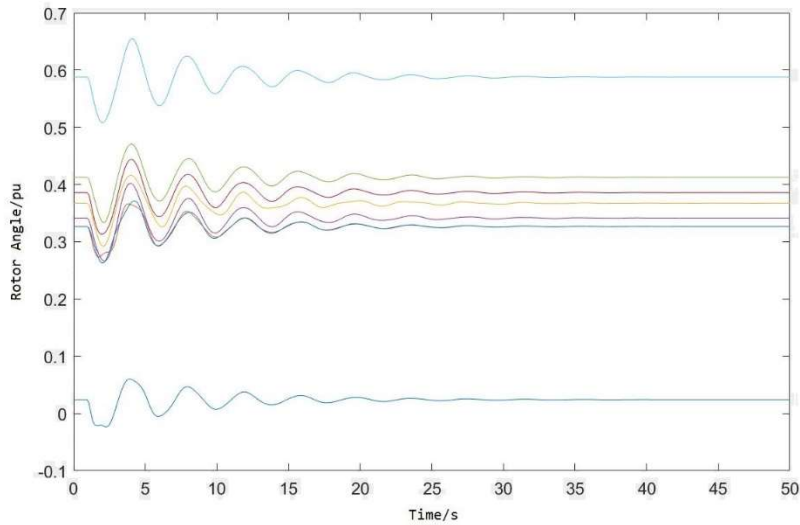


*Figure 4.12 Rotor Angle of New England Power System*

This section performs eigenvalue analysis on New England power system and the results are presented. It gives a more comprehensive demonstration on the effectiveness of eigenvalue analysis in power system small signal stability analysis.

#### **4.4 Summary**

This chapter introduces the conventional power system small signal stability analysis. Basic concepts related to small signal stability are introduced. Two analysis methods are presented and compared on the Two Area power system. The results agree with previous works that eigenvalue analysis is a more effective method for analyzing small signal stability compared with time domain simulation. A case study on the large 10-Machine New England power system is also presented to give a more comprehensive analysis.

## **Chapter 5**

# **Power System Small Signal Stability Analysis with Wind Energy Integrations**

### **5.0 Introduction**

This chapter investigates how power system small signal stability is affected when wind energy is integrated into the system. Section 5.1 presents small signal stability analysis on two single machine infinite bus (SMIB) systems with a synchronous generator and a doubly fed induction generator (DFIG). Section 5.2 presents small signal stability analysis with wind energy integrations using Power System Analysis Toolbox (PSAT). A summary is given in section 5.3.

### **5.1 Small Signal Stability Analysis of SMIB Systems**

A SMIB system is frequently used in electrical power system engineering to reveal concepts and perform analysis in an easy-to-understand way. In this section, small signal stability analysis is performed on two SMIB systems. One SMIB system

containing a traditional synchronous generator connected to an infinite bus is presented first in 5.1.1. Then, the other SMIB system with a DFIG connected to an infinite bus is analyzed in 5.1.2.

This section presents the basic procedures of eigenvalue analysis and gives an insight into the small signal stability of traditional synchronous generators and DFIGs. This section aims to give a detail description of small signal stability with a DFIG connected to an infinite bus and compare with the synchronous generator.

### **5.1.1 Small Signal Stability Analysis of a SMIB System with a Synchronous Generator**

Synchronous generators are the dominant generators in modern power systems. Depending on the requirements for calculation time and accuracy, different models of a synchronous generator have been proposed [13, 25, 26]. The Two-Axis model is studied here.

Eigenvalue analysis is performed on a SMIB system with a synchronous generator. The SMIB system is shown in Figure 5.1. A synchronous generator is connected to an infinite bus through a transmission line. The synchronous generator is represented by the Two-Axis model, the transmission line is represented by a reactance for simplicity and the infinite bus is the bus with fixed voltage and angle.

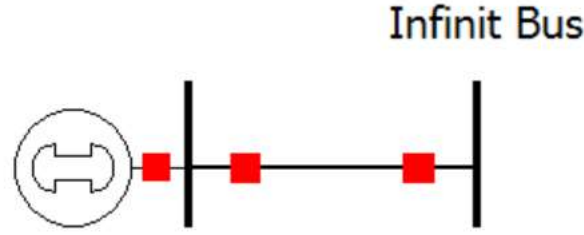


Figure 5.1 SMIB System with a Synchronous Generator Connected to an Infinite Bus

The generation units can be described by differential equations while the outside networks form the algebraic equations. The system in Figure 5.1 can be modelled by differential algebraic equations (DAEs) in the form of (4.7) and (4.8). The dynamic Two-Axis generator model used here is given in equations (5.1) - (5.4) [16, 25].

$$\frac{d\delta}{dt} = \omega_r - \omega_s \quad (5.1)$$

$$\frac{d\omega_r}{dt} = \frac{\omega_s}{2H} (T_m - T_e) \quad (5.2)$$

$$\frac{dE'_q}{dt} = \frac{1}{T'_{d0}} [-E'_q - (X_d - X'_d)I_d + E_{fd}] \quad (5.3)$$

$$\frac{dE'_d}{dt} = \frac{1}{T'_{q0}} [-E'_d + (X_q - X'_q)I_q] \quad (5.4)$$

Where

$T_e = E'_d I_d + E'_q I_q + (X'_q - X'_d) I_d I_q$  is the electromagnetic torque,  $\delta$  represents rotor angle,  $\omega_r$  represents rotor speed,  $E'_q$  and  $E'_d$  are equivalent internal voltage source in d-q frame,  $I_q$  and  $I_d$  are stator currents,  $X_q$  and  $X_d$  are steady-state reactance,  $X'_q$  and  $X'_d$  are transient reactance,  $T'_{q0}$  and  $T'_{d0}$  are transient time constants,  $H$  is inertia constant,  $T_m$  is the mechanical torque and  $E_{fd}$  is field voltage.

The exciter and governor models are not considered here. The mechanical torque  $T_m$  and the field voltage  $E_{fd}$  are kept constant.

The interactions between the synchronous generator and the transmission line form the network algebraic equations, shown in (5.5) - (5.8) [25].

$$-(X'_q + X_t)I_q - E'_d + E_b \sin \delta = 0 \quad (5.5)$$

$$(X'_d + X_t)I_d - E'_q + E_b \cos \delta = 0 \quad (5.6)$$

$$-X_t I_q + E_b \sin \delta = V_d \quad (5.7)$$

$$X_t I_d + E_b \cos \delta = V_q \quad (5.8)$$

Where

$E_b$  represents the infinite bus voltage and  $X_t$  is the transmission line reactance.

In this system,  $\delta$ ,  $\omega_r$ ,  $E'_q$  and  $E'_d$  are state variables.  $V_q$ ,  $V_d$ ,  $I_q$  and  $I_d$  are algebraic variables.  $T_m$  and  $E_{fd}$  are input variables.

Equations (5.5) and (5.6) describe the transmission between the generator internal voltages and the infinite bus through the internal reactance and transmission line.

Equations (5.7) and (5.8) describe the algebraic relations between the generator internal voltages and the generator terminal bus through the internal reactance.

Setting all the derivative terms to 0 in (5.1) - (5.4) and combining with (5.5) - (5.8), the initial values of variables can be obtained.

Linearizing (5.1) - (5.4) gives (5.9) - (5.12).

$$\Delta\dot{\delta} = \Delta\omega_r \quad (5.9)$$

$$\Delta\dot{\omega}_r = \frac{\omega_s}{2H} [-I_{d0}\Delta E'_d - I_{q0}\Delta E'_q - (E'_{d0} + (X'_q - X'_d)I_{q0})\Delta I_d - (E'_{q0} + (X'_q - X'_d)I_{d0})\Delta I_q + \Delta T_m] \quad (5.10)$$

$$\Delta\dot{E}'_q = \frac{1}{T'_{d0}} [-\Delta E'_q - (X_d - X'_d)\Delta I_d + \Delta E_{fd}] \quad (5.11)$$

$$\Delta\dot{E}'_d = \frac{1}{T'_{q0}} [-\Delta E'_d + (X_q - X'_q)\Delta I_q] \quad (5.12)$$

Representing (5.9)- (5.12) in the matrix form results in (5.13).

$$\begin{bmatrix} \Delta\dot{\delta} \\ \Delta\dot{\omega}_r \\ \Delta\dot{E}'_q \\ \Delta\dot{E}'_d \end{bmatrix} = \begin{bmatrix} 0 & 1 & 0 & 0 \\ 0 & 0 & -\frac{\omega_s}{2H}I_{q0} & -\frac{\omega_s}{2H}I_{d0} \\ 0 & 0 & -\frac{1}{T'_{d0}} & 0 \\ 0 & 0 & 0 & -\frac{1}{T'_{q0}} \end{bmatrix} \begin{bmatrix} \Delta\delta \\ \Delta\omega_r \\ \Delta E'_q \\ \Delta E'_d \end{bmatrix} + \begin{bmatrix} 0 & 0 & 0 & 0 \\ 0 & 0 & -\frac{\omega_s}{2H}[E'_{q0} + (X'_q - X'_d)I_{d0}] & -\frac{\omega_s}{2H}[E'_{d0} + (X'_q - X'_d)I_{q0}] \\ 0 & 0 & 0 & -\frac{X_d - X'_d}{T'_{d0}} \\ 0 & 0 & \frac{X_q - X'_q}{T'_{q0}} & 0 \end{bmatrix} \begin{bmatrix} \Delta V_q \\ \Delta V_d \\ \Delta I_q \\ \Delta I_d \end{bmatrix} + \begin{bmatrix} 0 & 0 \\ \frac{\omega_s}{2H} & 0 \\ 0 & \frac{1}{T'_{d0}} \\ 0 & 0 \end{bmatrix} \begin{bmatrix} \Delta T_m \\ \Delta E_{fd} \end{bmatrix} \quad (5.13)$$

Linearizing (5.5) - (5.8) gives (5.14) - (5.17).

$$-(X'_q + X_t)\Delta I_q - \Delta E'_d + E_b \cos \delta_0 \Delta\delta = 0 \quad (5.14)$$

$$(X'_d + X_t)\Delta I_d - \Delta E'_q - E_b \sin \delta_0 \Delta\delta = 0 \quad (5.15)$$

$$-X_t \Delta I_q + E_b \cos \delta_0 \Delta\delta - \Delta V_d = 0 \quad (5.16)$$

$$X_t \Delta I_d - E_b \sin \delta_0 \Delta\delta - \Delta V_q = 0 \quad (5.17)$$

Arranging (5.14)- (5.17) into the matrix form results in (5.18).

$$0 = \begin{bmatrix} E_b \cos \delta_0 & 0 & 0 & -1 \\ -E_b \sin \delta_0 & 0 & -1 & 0 \\ E_b \cos \delta_0 & 0 & 0 & 0 \\ -E_b \sin \delta_0 & 0 & 0 & 0 \end{bmatrix} \begin{bmatrix} \Delta \delta \\ \Delta \omega_r \\ \Delta E'_q \\ \Delta E'_d \end{bmatrix} + \begin{bmatrix} 0 & 0 & -X'_q - X_t & 0 \\ 0 & 0 & 0 & X'_d + X_t \\ 0 & -1 & -X_t & 0 \\ -1 & 0 & 0 & X_t \end{bmatrix} \begin{bmatrix} \Delta V_q \\ \Delta V_d \\ \Delta I_q \\ \Delta I_d \end{bmatrix} + \begin{bmatrix} 0 & 0 \\ 0 & 0 \\ 0 & 0 \\ 0 & 0 \end{bmatrix} \begin{bmatrix} \Delta T_m \\ \Delta E_{fd} \end{bmatrix} \quad (5.18)$$

From the above equations, the four differential equations describe the dynamic performances of a synchronous generator and the four algebraic equations represent connecting the synchronous generator to the outside network. In a system containing more than two generators, the interactions between generators are dependent on the algebraic equations. Combining (5.13) and (5.18) gives the small signal DAEs representing the SMIB system with a synchronous generator. Equations (5.13) and (5.18) give the matrix form as shown in (4.9) and (4.10) and the state matrix  $A_{sys}$  can be calculated.

The system eigenvalues are calculated and plotted in Figure 5.2. All the parameters used for the calculation are given in Appendix E. There are totally four eigenvalues as the state matrix  $A_{sys}$  is a 4\*4 matrix. It is shown that all the eigenvalues are on the left side of the complex plane, which indicates the system is stable for small disturbances.

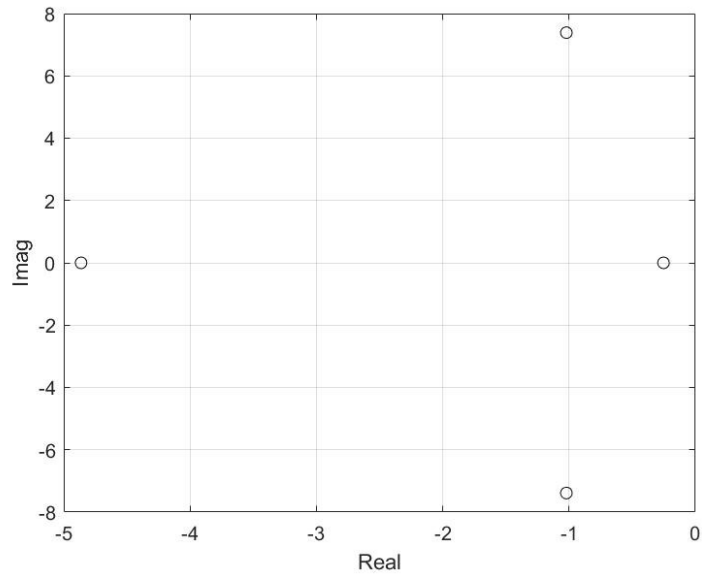


*Figure 5.2 Eigenvalues on Complex Plane of SMIB System with a Synchronous Generator*

The eigenvalues of the system and the corresponding frequency and damping are provided in Table 5.1. Two eigenvalues are negative real values representing the decaying non-oscillation modes. Eigenvalues  $\lambda_3$  and  $\lambda_4$  are the damped oscillation mode with damping of 0.1369 N/(m/s).

*Table 5.1 Eigenvalues of SMIB System with a Synchronous Generator*

Mode	Eigenvalues	Frequency	Damping
$\lambda_1$	-4.8632	0	1
$\lambda_2$	-0.2524	0	1
$\lambda_3, \lambda_4$	$-1.0213 \pm j7.3883$	1.1759	0.1369

The participation factors calculated for each eigenvalue are given in Table 5.2. This table gives all the participation factors between each state variable and mode which

reveals the relative participation between the state variable and the mode. It is shown that non-oscillation modes  $\lambda_1$  and  $\lambda_2$  are most related to  $E'_d$  and  $E'_q$  respectively. The oscillation modes  $\lambda_1$  and  $\lambda_2$  are most related to the rotor angle  $\delta$  and  $\omega$ . This gives valuable information that the system oscillations can be better damped by adding controllers for the rotor dynamics.

*Table 5.2 Participation Factors of SMIB System with a Synchronous Generator*

	$\lambda_1$	$\lambda_2$	$\lambda_3$	$\lambda_4$
$\delta$	-0.0794	-0.0042	0.5418-j0.0487	0.5418+j0.0487
$\omega$	-0.0794	-0.0042	0.5418-j0.0487	0.5418+j0.0487
$E'_q$	0.0307	0.9507	0.0093+j0.0372	0.0093-j0.0372
$E'_d$	1.1281	0.0576	-0.0928+j0.0602	-0.0928-j0.0602

The transmission line reactance  $X_t$  can be changed to simulate the synchronous generator connected to different grids. Normally, the longer the transmission line, the larger the transmission line reactance  $X_t$ . A long transmission line means a weak grid connection for the generation units. The movement of the eigenvalues are shown in Figure 5.3 when  $X_t$  varies from 0.1 pu (strong grid) to 1.0 pu (weak grid). The point ‘\*’ represents the starting (0.1 pu) and the triangle points mean the end (1.0 pu). It is shown that the eigenvalues move to right when  $X_t$  increases. From Figure 5.3, it is shown that a strong grid can enhance the system small signal stability.



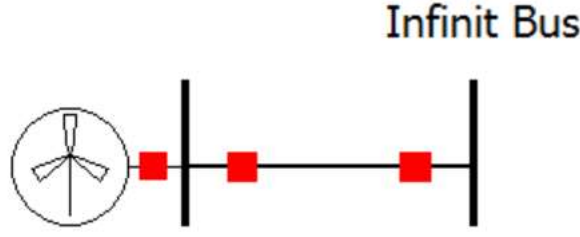


Figure 5.4 SMIB System with a DFIG connected to an Infinite Bus

The differential equations of a doubly fed induction generator are present in (5.19)-(5.23). It is the same model as introduced in Chapter 2 and repeated here.

$$\frac{X'_s}{\omega_s} \frac{dI_{ds}}{dt} = V_{ds} - \left( R_s + \frac{X_s - X'_s}{T'_0} \right) I_{ds} - \frac{\omega_r}{\omega_s} E'_d - \frac{L_m}{L_{rr}} V_{dr} + \frac{1}{T'_0} E'_q + X'_s I_{qs} \quad (5.19)$$

$$\frac{X'_s}{\omega_s} \frac{dI_{qs}}{dt} = V_{qs} - \left( R_s + \frac{X_s - X'_s}{T'_0} \right) I_{qs} - \frac{\omega_r}{\omega_s} E'_q - \frac{L_m}{L_{rr}} V_{qr} - \frac{1}{T'_0} E'_d - X'_s I_{ds} \quad (5.20)$$

$$\frac{dE'_d}{dt} = (\omega_s - \omega_r) E'_q - \frac{\omega_s L_m}{L_{rr}} V_{qr} - \frac{\omega_s}{T'_0} [E'_d - (X_s - X'_s) I_{qs}] \quad (5.21)$$

$$\frac{dE'_q}{dt} = -(\omega_s - \omega_r) E'_d + \frac{\omega_s L_m}{L_{rr}} V_{dr} - \frac{\omega_s}{T'_0} [E'_q + (X_s - X'_s) I_{ds}] \quad (5.22)$$

$$\frac{d\omega_r}{dt} = \frac{1}{2H} (T_m - E'_d I_{ds} - E'_q I_{qs}) \quad (5.23)$$

The algebraic equations can be formed by using power balance, given in (5.24) and (5.25).

$$P_{out} = P_s + P_r \quad (5.24)$$

$$Q_{out} = Q_s + Q_r \quad (5.25)$$

Where

$P_{out}$  and  $Q_{out}$  are real and reactive power output of a DFIG transferred through the

transmission line.  $P_s$  and  $Q_s$  are real and reactive power from the stator.  $P_r$  is the real power from the rotor and  $Q_r$  is the reactive power from the rotor. The rotor side power  $P_r$  and  $Q_r$  are transferred through the rotor side and grid side converters to the grid. The grid side converter is normally controlled to operate at unity power factor. Then, the reactive power from the rotor  $Q_r$  equals to zero.

From the basic equations (2.15) and (2.16), the rotor side currents can be represented by (5.26) and (5.27).

$$I_{dr} = \frac{E'_q}{L_m} - \frac{L_m}{L_{rr}} I_{ds} \quad (5.26)$$

$$I_{qr} = -\frac{E'_d}{L_m} - \frac{L_m}{L_{rr}} I_{qs} \quad (5.27)$$

The algebraic equations for the SMIB system with a DFIG are given in (5.28) and (5.29) using the power balancing equations.

$$V_{ds}I_{ds} + V_{qs}I_{qs} + V_{dr} \left( \frac{E'_q}{L_m} - \frac{L_m}{L_{rr}} I_{ds} \right) + V_{qr} \left( -\frac{E'_d}{L_m} - \frac{L_m}{L_{rr}} I_{qs} \right) - \frac{\sqrt{V_{ds}^2 + V_{qs}^2} E_b \sin\left(\tan^{-1}\left(\frac{V_{qs}}{V_{ds}}\right)\right)}{X_t} = 0 \quad (5.28)$$

$$V_{qs}I_{ds} - V_{ds}I_{qs} + \frac{(V_{ds}^2 + V_{qs}^2) - \sqrt{V_{ds}^2 + V_{qs}^2} E_b \cos\left(\tan^{-1}\left(\frac{V_{qs}}{V_{ds}}\right)\right)}{X_t} = 0 \quad (5.29)$$

In this system,  $I_{ds}$ ,  $I_{qs}$ ,  $E'_d$  and  $E'_q$  are state variables,  $V_{ds}$  and  $V_{qs}$  are algebraic variables and  $T_m$ ,  $V_{dr}$  and  $V_{qr}$  are input variables.

Linearizing (5.19) - (5.23), (5.30) - (5.34) can be obtained.

$$\Delta \dot{I}_{ds} = \frac{\omega_s}{X'_s} \left[ \Delta V_{ds} - \left( R_s + \frac{X_s - X'_s}{T_0} \right) \Delta I_{ds} - \frac{E'_{d0}}{\omega_s} \Delta \omega_r - \frac{\omega_{r0}}{\omega_s} \Delta E'_d - \frac{L_m}{L_{rr}} \Delta V_{dr} + \frac{1}{T_0} \Delta E'_q + \right.$$

$$X'_s \Delta I_{qs} \Big] \quad (5.30)$$

$$\Delta \dot{I}_{qs} = \frac{\omega_s}{X'_s} \left[ \Delta V_{qs} - \left( R_s + \frac{X_s - X'_s}{T_0} \right) \Delta I_{qs} - \frac{E'_{q0}}{\omega_s} \Delta \omega_r - \frac{\omega_{r0}}{\omega_s} \Delta E'_q - \frac{L_m}{L_{rr}} \Delta V_{qr} - \frac{1}{T_0} \Delta E'_d - X'_s \Delta I_{ds} \right] \quad (5.31)$$

$$\Delta \dot{E}'_d = (\omega_s - \omega_{r0}) \Delta E'_q - E'_{q0} \Delta \omega_r - \frac{\omega_s}{T_0} (\Delta E'_d + (X_s - X'_s) \Delta I_{qs}) - \frac{\omega_s L_m}{L_{rr}} \Delta V_{qr} \quad (5.32)$$

$$\Delta \dot{E}'_q = -(\omega_s - \omega_{r0}) \Delta E'_d + E'_{d0} \Delta \omega_r - \frac{\omega_s}{T_0} (\Delta E'_q + (X_s - X'_s) \Delta I_{ds}) + \frac{\omega_s L_m}{L_{rr}} \Delta V_{dr} \quad (5.33)$$

$$\Delta \dot{\omega}_r = \frac{1}{2H} (\Delta T_m - E'_{d0} \Delta I_{ds} - I_{ds0} \Delta E'_d - E'_{q0} \Delta I_{qs} - I_{qs0} \Delta E'_q) \quad (5.34)$$

Putting (5.30) - (5.34) into the matrix form gives (5.35).

$$\begin{bmatrix} \Delta \dot{I}_{ds} \\ \Delta \dot{I}_{qs} \\ \Delta \dot{E}'_d \\ \Delta \dot{E}'_q \\ \Delta \dot{\omega}_r \end{bmatrix} = \begin{bmatrix} -\frac{\omega_s}{X'_s} \left( R_s + \frac{X_s - X'_s}{T_0} \right) & \omega_s & -\frac{\omega_{r0}}{X'_s} & \frac{\omega_s}{T_0 X'_s} & -\frac{E'_{d0}}{X'_s} \\ -\omega_s & -\frac{\omega_s}{X'_s} \left( R_s + \frac{X_s - X'_s}{T_0} \right) & -\frac{\omega_s}{T_0 X'_s} & -\frac{\omega_{r0}}{X'_s} & -\frac{E'_{q0}}{X'_s} \\ 0 & -\frac{\omega_s}{T_0} (X_s - X'_s) & -\frac{\omega_s}{T_0} & (\omega_s - \omega_{r0}) & -E'_{q0} \\ -\frac{\omega_s}{T_0} (X_s - X'_s) & 0 & -(\omega_s - \omega_{r0}) & -\frac{\omega_s}{T_0} & E'_{d0} \\ -\frac{E'_{d0}}{2H} & -\frac{E'_{q0}}{2H} & -\frac{I_{ds0}}{2H} & -\frac{I_{qs0}}{2H} & 0 \end{bmatrix} \begin{bmatrix} \Delta I_{ds} \\ \Delta I_{qs} \\ \Delta E'_d \\ \Delta E'_q \\ \Delta \omega_r \end{bmatrix} + \begin{bmatrix} \frac{\omega_s}{X'_s} & 0 \\ 0 & \frac{\omega_s}{X'_s} \\ 0 & 0 \\ 0 & 0 \\ 0 & 0 \end{bmatrix} \begin{bmatrix} \Delta V_{ds} \\ \Delta V_{qs} \end{bmatrix} + \begin{bmatrix} 0 & -\frac{\omega_s L_m}{X'_s L_{rr}} & 0 \\ 0 & 0 & -\frac{\omega_s L_m}{X'_s L_{rr}} \\ 0 & 0 & -\frac{\omega_s L_m}{L_{rr}} \\ 0 & \frac{\omega_s L_m}{L_{rr}} & 0 \\ \frac{1}{2H} & 0 & 0 \end{bmatrix} \begin{bmatrix} \Delta T_m \\ \Delta V_{dr} \\ \Delta V_{qr} \end{bmatrix} \quad (5.35)$$

Linearizing (5.28) and (5.29), (5.36) and (5.37) can be obtained.

$$\left(V_{ds0} - \frac{L_m}{L_{rr}} V_{dr0}\right) \Delta I_{ds} + \left(V_{qs0} - \frac{L_m}{L_{rr}} V_{qr0}\right) \Delta I_{qs} - \frac{V_{qr}}{L_m} \Delta E'_d + \frac{V_{dr0}}{L_m} \Delta E'_q + \left(I_{ds0} + \frac{E_b}{X_t} A\right) \Delta V_{ds} + \left(I_{qs0} + \frac{E_b}{X_t} B\right) \Delta V_{qs} + \left(\frac{E'_{q0}}{L_m} - \frac{L_m}{L_{rr}} I_{ds0}\right) \Delta V_{dr} + \left(-\frac{E'_{d0}}{L_m} - \frac{L_m}{L_{rr}} I_{qs0}\right) \Delta V_{qr} = 0 \quad (5.36)$$

$$V_{qs0} \Delta I_{ds} - V_{ds0} \Delta I_{qs} + (-I_{qs0} + C) \Delta V_{ds} + (I_{ds0} + D) \Delta V_{qs} = 0 \quad (5.37)$$

Putting (5.36) and (5.37) into the matrix form gives (5.38).

$$0 = \begin{bmatrix} V_{ds0} - \frac{L_m}{L_{rr}} V_{dr0} & V_{qs0} - \frac{L_m}{L_{rr}} V_{qr0} & -\frac{V_{qr0}}{L_m} & \frac{V_{dr0}}{L_m} & 0 \\ V_{qs0} & -V_{ds0} & 0 & 0 & 0 \end{bmatrix} \begin{bmatrix} \Delta I_{ds} \\ \Delta I_{qs} \\ \Delta E'_d \\ \Delta E'_q \\ \Delta \omega_r \end{bmatrix} + \begin{bmatrix} I_{ds} + \frac{E_b}{X_t} A & I_{qs0} + \frac{E_b}{X_t} B \\ -I_{qs0} + C & I_{ds0} + D \end{bmatrix} \begin{bmatrix} \Delta V_{ds} \\ \Delta V_{qs} \end{bmatrix} + \begin{bmatrix} 0 & \frac{E'_{q0}}{L_m} - \frac{L_m}{L_{rr}} I_{ds} & -\frac{E'_{d0}}{L_m} - \frac{L_m}{L_{rr}} I_{qs0} \\ 0 & 0 & 0 \end{bmatrix} \begin{bmatrix} \Delta T_m \\ \Delta V_{dr} \\ \Delta V_{qr} \end{bmatrix} \quad (5.38)$$

Where

$$A = \frac{V_{qs0}}{\sqrt{\frac{V_{qs}^2}{V_{ds0}^2} + 1} \sqrt{V_{ds}^2 + V_{qs}^2}} - \frac{V_{qs} \sqrt{V_{ds0}^2 + V_{qs0}^2}}{V_{ds0}^2 \sqrt{\frac{V_{qs0}^2}{V_{ds0}^2} + 1}} + \frac{V_{qs0}^3 \sqrt{V_{ds0}^2 + V_{qs}^2}}{V_{ds0}^4 \sqrt{\left(\frac{V_{qs}^2}{V_{ds0}^2} + 1\right)^3}} \quad (5.39)$$

$$B = \frac{\sqrt{V_{ds0}^2 + V_{qs}^2}}{V_{ds0} \sqrt{\frac{V_{qs0}^2}{V_{ds0}^2} + 1}} + \frac{V_{qs0}^2}{V_{ds0} \sqrt{\frac{V_{qs0}^2}{V_{ds}^2} + 1} \sqrt{V_{ds}^2 + V_{qs0}^2}} - \frac{V_{qs0}^2 \sqrt{V_{ds}^2 + V_{qs}^2}}{V_{ds0}^4 \sqrt{\left(\frac{V_{qs}^2}{V_{ds}^2} + 1\right)^3}} \quad (5.40)$$

$$C = 2V_{ds0} - \frac{E_b V_{ds0}}{\sqrt{\frac{V_{qs0}^2}{V_{ds0}^2} + 1} \sqrt{V_{ds0}^2 + V_{qs}^2}} - \frac{E_b V_{qs}^2 \sqrt{V_{ds}^2 + V_{qs0}^2}}{V_{ds0}^3 \sqrt{\left(\frac{V_{qs}^2}{V_{ds}^2} + 1\right)^3}} \quad (5.41)$$

$$D = 2V_{qs} - \frac{E_b V_{qs}}{\sqrt{\frac{V_{qs0}^2}{V_{ds0}^2} + 1} \sqrt{V_{ds0}^2 + V_{qs}^2}} + \frac{E_b V_{qs0} \sqrt{V_{ds}^2 + V_{qs}^2}}{V_{ds0}^2 \sqrt{\left(\frac{V_{qs}^2}{V_{ds}^2} + 1\right)^3}} \quad (5.42)$$

With matrices (5.35) and (5.38), the SMIB system state matrix can be obtained and the eigenvalues of the system can be found. The system parameters for simulation are given in Appendix F. The eigenvalues of the SMIB system with a DFIG is presented in Figure 5.5. Four of the eigenvalues of the system are on the left side of the plane, while one eigenvalue is on the zero point. There are two damped oscillation modes in the system. The zero point brings uncertainty to system stability evaluation.

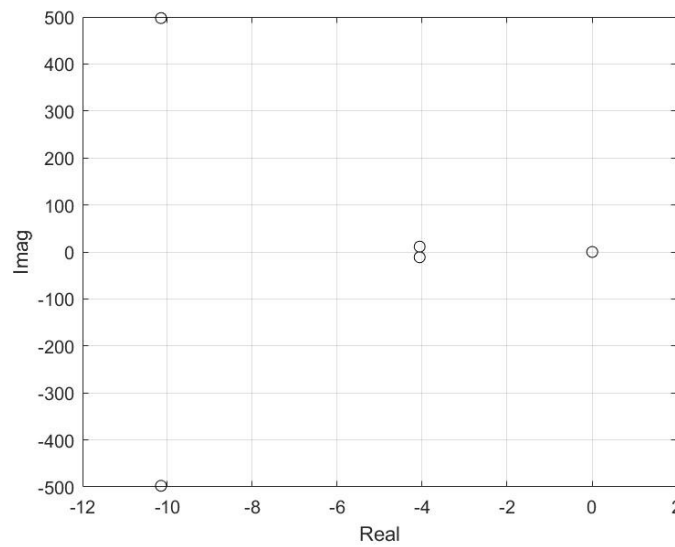


*Figure 5.5 Eigenvalues on Complex Plane of SMIB System with A DFIG*

Table 5.3 shows the eigenvalues and the frequency and damping of each mode. There are two oscillation modes in this system. The first mode has high frequency and not well damped, while the second mode has lower frequency with better damping.

Table 5.3 Eigenvalues of SMIB System with A DFIG

Mode	Eigenvalues	Frequency	Damping
$\lambda_1, \lambda_2$	$-10.15 \pm j497.64$	79.2019	0.0204
$\lambda_3, \lambda_4$	$-4.06 \pm j11.25$	1.7905	0.3395
$\lambda_5$	0	N/A	N/A

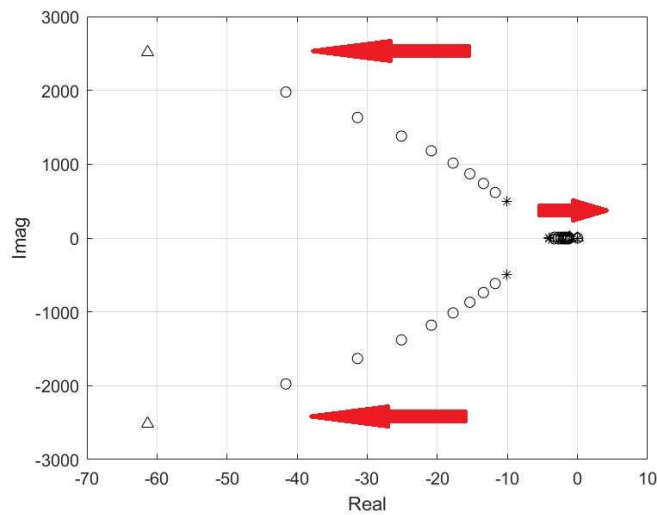
The participation factors calculated for the SMIB system with a DFIG are given in Table 5.4. The first oscillation mode of  $\lambda_1$  and  $\lambda_2$  has the highest participation factors with the stator currents  $I_{ds}$  and  $I_{qs}$ . This can be referred to as ‘stator mode’. The second low frequency better damped oscillation mode of  $\lambda_3$  and  $\lambda_4$  is most related to the internal voltages  $E'_d$  and  $E'_q$ , which can be considered as ‘electrical mode’. The zero-point mode is most related to the rotor speed  $\omega_r$ .

Table 5.4 Participation Factors of SMIB System with A DFIG

	$\lambda_1$	$\lambda_2$	$\lambda_3$	$\lambda_4$	$\lambda_5$
$I_{ds}$	0.5003-j0.0082	0.5003+j0.0082	-0.0003+j0.0039	-0.0003-j0.0039	0
$I_{qs}$	0.4999+j0.0162	0.4999-j0.0162	0.0001+j0.004	0.0001-j0.004	-0.0001
$E'_d$	-0.0001-j0.004	-0.0001+j0.004	0.498-j0.0041	0.498+j0.0041	0.0042
$E'_q$	-0.0001-j0.004	-0.0001+j0.004	0.5-j0.0033	0.5+j0.0033	0.0002
$\omega_r$	0	0	0.0022-j0.0006	0.0022+j0.006	0.9956

Figure 5.6 shows the eigenvalue movement when the transmission line parameter  $X_t$  increases from 0.1 pu to 1.0 pu. The point ‘\*’ represents the starting (0.1 pu) and the triangle points represent the end (1.0 pu). The low value of  $X_t$  represents the DFIG

connected to a strong grid. It is shown in Figure 5.6 that the eigenvalues of ‘stator mode’ move to left while the eigenvalues of ‘electrical mode’ move to right in the complex plane. Both the imaginary and real part of ‘stator mode’ are decreasing which is difficult to determine the change of the damping value from the plot. The real part of ‘electrical mode’ increases more obviously, which indicates the damping is reducing.



*Figure 5.6 Eigenvalues of SMIB System with A DFIG Corresponding to Different  $X_t$*

The damping values of the system oscillation modes for different  $X_t$  are given in Table 5.5. It is shown that the damping value of ‘stator mode’ is decreasing when  $X_t$  increases from 0.1 pu to 0.5 pu. The damping value of ‘stator mode’ starts to increase after 0.5 pu while the damping keeps at relatively low value for this mode. The ‘electrical mode’ keeps decreasing when  $X_t$  increases from 0.1 pu to 1.0 pu. In general, the system small signal stability is reduced when the DFIG is connected to a weak grid.

*Table 5.5 Eigenvalues of SMIB System with A DFIG Corresponding to Different  $X_t$*

$X_t$	0.1	0.2	0.3	0.4	0.5	0.6	0.7	0.8	0.9	1.0
Damping	0.0204	0.191	0.0182	0.0177	0.0175	0.0177	0.0182	0.0192	0.021	0.0244
	0.3395	0.2806	0.2377	0.2049	0.1789	0.1578	0.1402	0.1253	0.1126	0.1016

In this section, the analysis of the SMIB systems with a synchronous generator and a DFIG are presented and compared. The detailed calculations of the eigenvalues are given. The participation factors and the movement of the eigenvalues with respect to the transmission line reactance are discussed. It is found that both the synchronous generators and DFIGs should be connected to a strong grid in order to enhance the small signal stability.

## **5.2 Small Signal Stability Analysis with Wind Energy Integrations using PSAT**

Building the DAEs and forming the state matrix gives a good insight into the small signal stability as shown in the previous section.

In this section, the studies are done on the Two Area and New England power systems when wind energy is integrated using PSAT. It makes modeling and simulation easier with the pre-defined models and user friendly interface in PSAT.

A DFIG based wind farm is integrated into the Two Area power system to replace one

of the synchronous generators. The effects of introducing the wind energy into the system are presented. The different connection locations are compared and the movements of eigenvalue are provided to demonstrate how it influences the power system small signal stability. A DFIG based wind farm is then connected into a larger 10-Machine New England power system to show the wind energy impacts on a large system.

### **5.2.1 Small Signal Stability Analysis of Two Area Power System with Wind Energy Integrations**

The conventional small signal stability analysis of the Two Area power system is presented in Chapter 4. In this section, a DFIG based wind farm is connected to the Two Area power system and the comparison of eigenvalue movement is presented. The Two Area power system without and with automatic voltage regulators (AVRs) and power system stabilizers (PSSs) are both considered. As presented in Chapter 4, the Two Area power system without AVRs and PSSs has two real eigenvalues on right side of the complex plane, while all the eigenvalues of the Two Area system with AVR and PSS are on the left side of the complex panel.

The complete results are given in Appendix G. The complex and positive real eigenvalues are included while the negative real eigenvalues representing the decaying stable modes and the zero eigenvalues are not included.

In the Two Area power system without AVRs and PSSs, the synchronous generator at

Bus 1 is replaced by a DFIG based wind farm with the same capacity. The complex eigenvalues representing the oscillation modes of the system with and without a wind farm are shown in Figure 5.7. It is shown that the eigenvalues move to right and an oscillation mode is induced when wind energy is connected into the system. However, it should be noted that the two negative real eigenvalues representing instability modes reduced to one as shown in Table G.1 in Appendix G. It can be assumed that the undamped unstable mode converts to a damped oscillation mode by introducing the wind energy into the system. It could be concluded that the system small signal stability is enhanced.

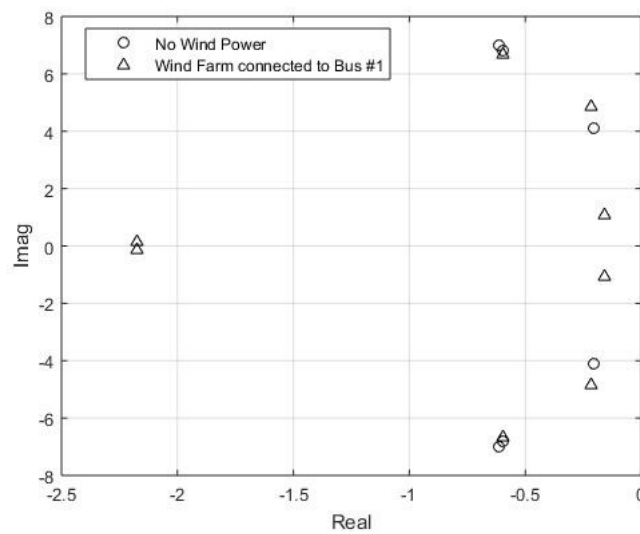


*Figure 5.7 Comparisons of the Two Area System without Wind Energy Integrations and with DFIG connected to Bus 1*

The damping values of oscillations are presented in Table 5.6 for the above eigenvalues. The integration of wind energy increases the damping of two existing oscillation mode and it converts one of the unstable modes into a well damped

oscillation mode. In general, the small signal stability of the system is increased when wind energy is introduced to the system.

*Table 5.6 Comparisons of the Two Area System without Wind Energy Integrations and with DFIG connected to Bus 1*

System	Damping of Oscillation			
	1	2	3	4
With Wind	0.0887	0.0445	0.1432	0.9973
No Wind	0.0876	0.0873	0.0502	N/A

The locations of wind farm can have an impact on the system small signal stability. Figure 5.8 compares the complex eigenvalues of a DFIG replacing a synchronous at different buses. It shows that the locations do have an influence on the system eigenvalues. From Figure 5.8, when the DFIG replaces the synchronous generator at Bus 3, it has the complex eigenvalues that are closest to the y axis.

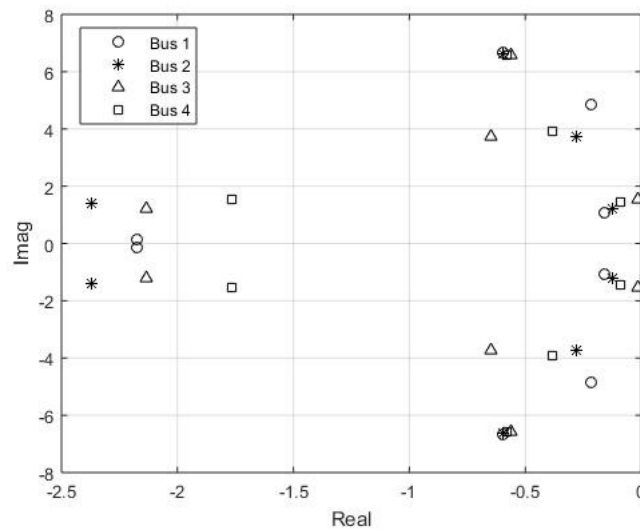


*Figure 5.8 Effects of Different Wind Farm Locations on the Two Area Power System*

Table 5.7 presents the damping of each wind farm connection. It is shown that the system with a DFIG based wind farm replacing generator at Bus 3 produces the oscillation mode with the highest damping. The location of the DFIG has an impact on the system small signal stability. Connecting the DFIG base wind farming to certain locations can have better damping effects on the oscillations.

*Table 5.7 Comparisons of Damping of Different Wind Farm Locations in the Two Area Power System*

System	Damping of Oscillation			
	1	2	3	4
Bus 1	0.0445	0.0887	0.1432	0.0997
Bus 2	0.0751	0.0895	0.1006	0.0863
Bus 3	0.0111	0.0849	0.1711	0.0867
Bus 4	0.0619	0.0878	0.0967	0.0756

The wind energy impacts on small signal stability of the Two Area system without AVR and PSS are provided above. As presented in Chapter 4, negative real eigenvalues are eliminated when AVR and PSS are used. The DFIG based wind farms replacing synchronous generators equipped with AVR and PSS is discussed below.

Five situations are considered, namely the base case with only synchronous generators, and four cases with a DFIG based wind farm replacing synchronous generators at different buses. The results of the eigenvalue analysis are given in Table G.2 in Appendix G. The complex eigenvalues of the Two Area system with AVR and PSS for different situations are shown in Figure 5.9. From Figure 5.9, it is shown that there are complex eigenvalues with positive real parts, which means the system is unstable when a DFIG based wind farm replaces a synchronous generator at certain bus.

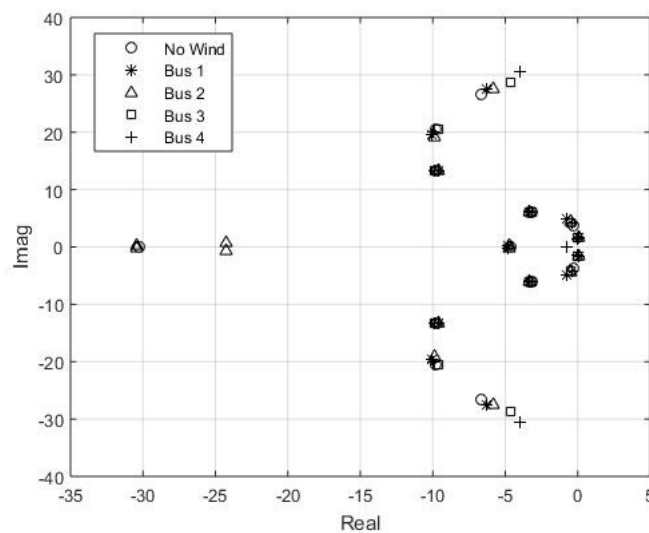


*Figure 5.9 Comparisons of the Two Area Power System with AVR and PSSs with DFIGs connected to Different Locations*

For each situation, the complex eigenvalues with the lowest damping are shown in Figure 5.10. From Figure 5.10, when a DFIG based wind farm replaces the synchronous generator at Bus 1 or 2, the system has eigenvalues with positive real parts indicating the system is unstable. In general, the complex eigenvalues with the lowest damping move to the right when wind energy is introduced into the system. The values of the lowest damping are shown in Table 5.9. It is shown that the base case has the highest damping value. The wind energy integration has a negative influence on the system small signal stability. When the DFIG based wind farm replaces the synchronous generator at Bus 1 or 2, the lowest damping becomes a negative value. However, the connection at Bus 3 or 4 shows a positive damping value. A suitable location should be found to integrate wind energy into the system in order to avoid system insatiability.

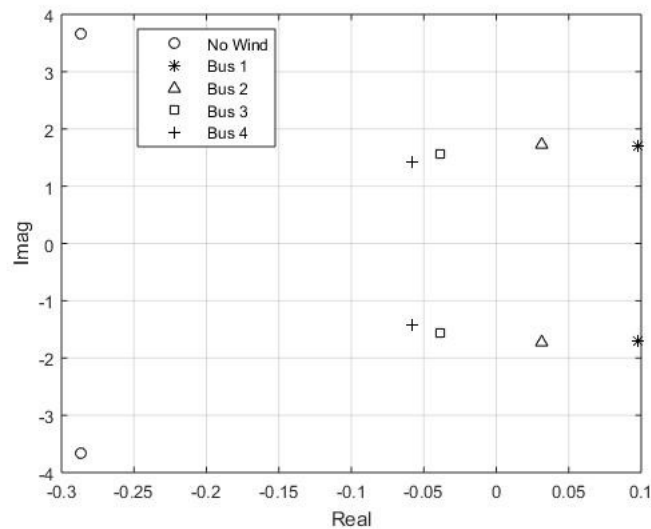


*Figure 5.10 Comparisons of the Lowest Damping of the Two Area System with AVR and PSS*

*Table 5.9 Comparisons of the Lowest Damping of the Two Area System with AVR and PSS*

Base Case	Bus 1	Bus 2	Bus 3	Bus 4
0.0779	-0.0573	-0.0179	0.0245	0.0407

In 5.2.1, eigenvalue analysis is used for small signal stability analysis of the Two Area systems without and with AVRs and PSSs when wind energy is integrated. The DFIG based wind farm in the Two Area system without AVRs and PSSs shows a positive effect while it shows a negative effect with the inclusion of AVRs and PSSs.

### **5.2.2 Small Signal Stability Analysis of New England Power System with Wind Energy Integrations**

The small signal stability analysis of New England power system without wind energy integration was presented in Chapter 4. All generators in New England power system are equipped with AVRs and PSSs. In this section, the wind energy is introduced into New England power system.

To investigate how wind energy integrations influence the small signal stability of New England power system, the synchronous generator at Bus 32 is replaced by a DFIG based wind farm with the same capacity. The complex eigenvalues are calculated for both without and with wind energy by PSAT and plotted in Figure 5.11.

All eigenvalues of both situations are on the left side. It is shown in Figure 5.11 that the complex eigenvalues of the case without wind energy integration move to right when the synchronous generator at Bus 32 is replaced by a wind farm. The system small signal stability is decreased. However, the system is still stable as the New England system is a large system with 10 machines and 39 buses. The effects of replacing a single synchronous generator with a DFIG based wind farm are diminished in a large system.

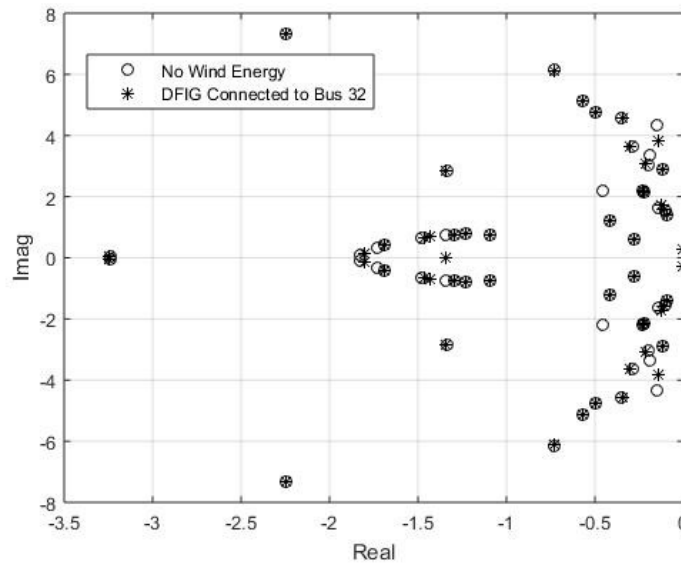


*Figure 5.11 Comparisons of New England Power System without Wind Energy Integrations and with DFIGs connected to Bus 32*

The eigenvalues with the lowest damping of both situations are compared in Table 5.10. It is shown that the lowest damping is smaller when the wind farm replaces the synchronous generator. The system small signal stability is reduced by the integration of the DFIG based wind farm.

*Table 5.10 Comparisons of the Lowest Damping of New England Power System without Wind Energy Integration and with DFIG connected to Bus 32*

System	Mode	Frequency	Damping
Without Wind Energy	$-0.1475 \pm j4.3329$	0.6896	0.034
With Wind Energy	$-0.0007 \pm j0.27$	0.043	0.0026

The rotor speed and rotor angle responses of New England power system with the wind farm replacement are shown in Figure 5.12 and 5.13 respectively. The disturbance applied to the system is 20% load increase from 1s to 1.1s. The responses show the system is stable under this disturbance.

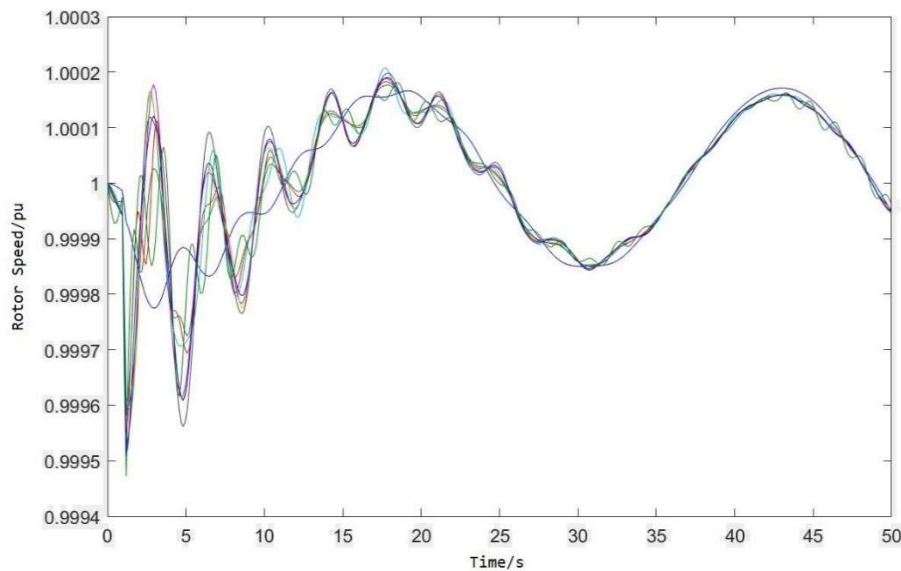


*Figure 5.12 Rotor Speed of New England Power System with Wind Energy*

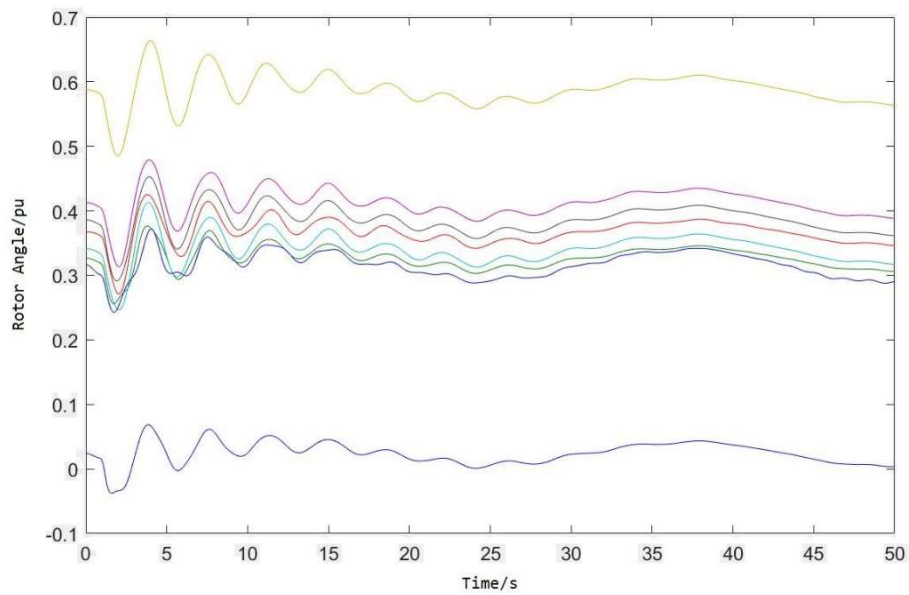


*Figure 5.13 Rotor Angle of New England Power System with Wind Energy*

#### **5.4 Summary**

This chapter discusses the impacts of wind energy integrations on power system small signal stability. The detailed analysis of the SMIB systems with a synchronous generator and a DFIG are given and compared. It gives an insight into the small signal stability problem. It is shown that both the integrations of synchronous generators and DFIGs require a strong grid to maintain small signal stability.

Two examples are given to investigate the influences of DFIG based wind farms replacement on Two Area and New England power systems. The analysis software is PSAT and the model of the DFIG based wind farm is the PSAT built-in model. The conclusions are summarized below.

- It is found that there are beneficial effects on small signal stability when a synchronous generator is replaced by a DFIG based wind farm in Two Area system without AVRs and PSSs. DFIGs equipped with power electronic converters have better dynamic performances than synchronous generators without suitable controllers.
- In Two Area system, the DFIG replacements have negative impacts on the system small signal stability as all the replaced synchronous generators are equipped with AVRs and PSSs. The replacement of synchronous generators with DFIGs generally has a negative impact on power system small signal stability as sophisticated controllers are normally included in the generation units in a modern power system.
- In New England power system, the wind energy integration also shows a detrimental effect as all the synchronous generators are equipped with AVRs and PSSs. However, the negative effect is smaller as the system is larger and the relative wind energy integration scale is lower.
- More advanced dynamic control systems should be developed to facilitate the integration of DFIGs.

# Chapter 6

## Conventional Transient Stability Analysis

### 6.0 Introduction

Transient stability of a power system should be maintained for secure and reliable operation. This chapter focuses on the conventional transient stability analysis of power systems. In section 6.1, the equal area criterion method is presented for demonstrating and explaining the transient stability phenomenon and the importance of critical fault clearing time. Then, more complex systems are presented in 6.2 for performing transient stability analysis on multimachine power systems using PowerWorld simulator. A summary is given in section 6.3.

### 6.1 Power System Transient Stability Analysis

Since maintaining the transient stability of a power system is of great importance, appropriate analysis methods have been developed to assess power system transient stability. Numerical, direct, pattern recognition, probabilistic, probabilistic, neural

network and expert system methods have been used for power system transient stability analysis. The detailed descriptions of these six methods are presented in [28]. At present, the most practical available method for transient stability analysis is time domain simulation where the nonlinear differential equations are solved using step-by-step numerical integration techniques [13]. The time domain simulation for systems without wind energy integrations is presented in this chapter.

Time domain simulation is a widely-used method for power system transient stability analysis. This method requires the solution of the differential algebraic equations (DAEs) formed by the generation units and power system networks. Many specialized simulation software have been developed incorporating the time domain simulation, such as PowerWorld [14]. The models in the software are determined by the balance of accuracy and simulation time.

### 6.1.1 Equal Area Criterion

An easy-to-understand way of introducing the transient stability is equal area criterion, which can illustrate the system stability visually and determine the critical fault clearing time using the energy balance. However, it is not suitable for multimachine transient stability analysis.

The swing equation in (4.5) can be transformed into (6.1).

$$\left(\frac{d\delta}{dt}\right)^2 = \int \frac{\omega_s(P_m - P_e)}{H} d\delta \quad (6.1)$$

The term  $\frac{d\delta}{dt}$  should be zero before the disturbance. For stable system, it should remain zero after the disturbance. After the disturbance, (6.2) can be obtained from (6.1).

$$\int_{\delta_0}^{\delta_m} (P_m - P_e) d\delta = 0 \quad (6.2)$$

Where

$\delta_0$  is the initial rotor angle and  $\delta_m$  is the maximum rotor angle.

It can be interpreted from the energy balance aspect. Assuming that  $\delta_1$  is the angle when the fault is cleared, the rotor energy gain is presented in (6.3) and the energy loss is presented in (6.4).

$$E_{gain} = \int_{\delta_0}^{\delta_1} (P_m - P_e) d\delta = A_1 \quad (6.3)$$

$$E_{lost} = \int_{\delta_1}^{\delta_m} (P_e - P_m) d\delta = A_2 \quad (6.4)$$

Figure 6.1 shows the relationships between power transfer curves and the rotor energy [13].

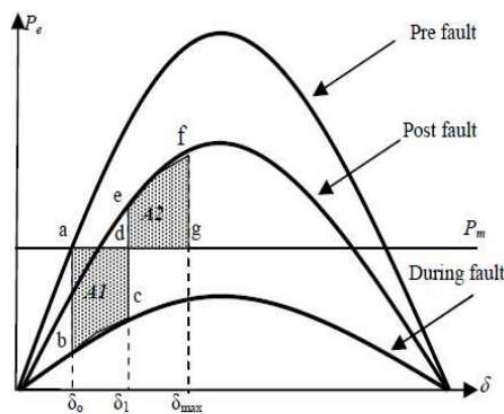


Figure 6.1 Relationship of Power Transfer Curve and Energy [13]

For a stable condition, area  $A_1$  should be equal to  $A_2$ . If area  $A_1$  is larger than  $A_2$ , it is an unstable condition. It can be interpreted as the energy gained is more than the energy lost, causing the rotor angle increase and making the system unstable. The pre-fault condition is at point a in Figure 6.1 where the mechanical power is equal to the electrical power transferred. During the fault, the power transfer curve changes and the mechanical power is larger than the electrical power transferred. The excess mechanical power causes the rotor angle to increase. The fault clearing angle  $\delta_1$  determines the energy gain area  $A_1$ . After the fault, the electrical power transferred is larger than the mechanical power which consumes the energy gained during the fault. The lost part of energy is area  $A_2$ . If  $\delta_1$  is too large, area  $A_2$  cannot be equal to  $A_1$ . The energy gained cannot be consumed, resulting in system instability.

### **6.1.2 Case Study: Equal Area Criterion**

This case study is aimed demonstrating how to use equal area criterion for determining the critical fault clearing time. It gives the system tolerance for a specific large disturbance. The results are verified by numerical analysis using Matlab [29].

Figure 6.2 presents a simplified system of a synchronous generator connected to a large system through transmission lines. All the values of the parameters are shown in the figure. A three-phase fault occurs at Bus 3 of this system. It is assumed that the internal voltage of the synchronous generator does not change and the infinite bus voltage remains constant. Before the fault, the real power supplied to the infinite bus

is 1 pu at 0.95 power factor lagging. The fault is cleared by opening the circuit breakers at the end of Line 1-3 and 2-3. These circuit breakers then remain open.

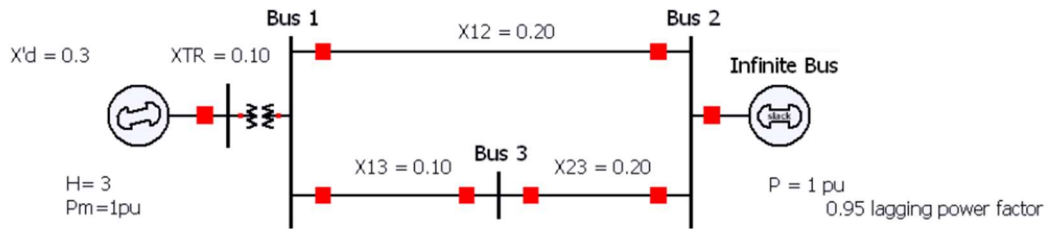


Figure 6.2 Simplified System

The basic power transfer function through a transmission line is shown in (6.5).

$$P = \frac{E' E_b}{X_t} \sin \delta \quad (6.5)$$

Where

$E'$  is the internal voltage of synchronous generator,  $E_b$  is the infinite bus voltage,  $X_t$  is the equivalent reactance of the transmission line between synchronous generator internal voltage and infinite bus and  $P$  is the real power transferred from the synchronous generator to the infinite bus.

The initial condition can be found from the steady state analysis. The internal voltage  $E'$  is 1.2812 pu and it is assumed constant. The initial rotor angle  $\delta_0$  is 0.4179 radians. Before the disturbance,  $X_t$  is calculated as (6.6).

$$X_t^{pre} = X'_d + X_{TR} + \frac{X_{12}(X_{13} + X_{23})}{X_{12} + X_{13} + X_{23}} = 0.52 \text{ pu} \quad (6.6)$$

During the three-phase fault at Bus 3, Bus 3 is grounded and the system equivalent

circuit is shown in Figure 6.3 [16]. Using Thevenin equivalent theory, the equivalent reactance and voltage are calculated in (6.7) and (6.8) respectively.

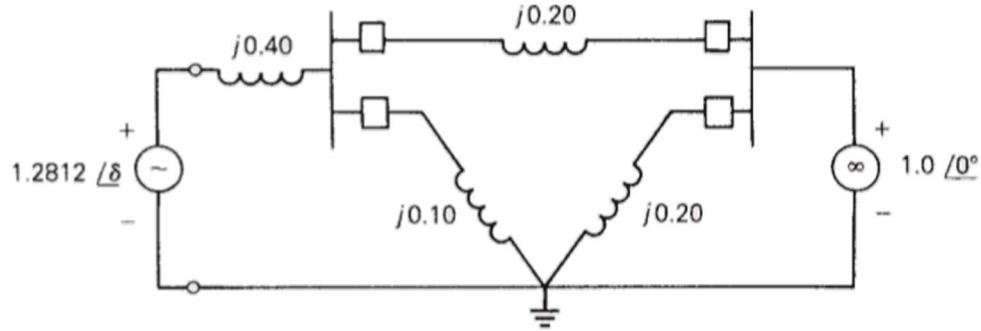


Figure 6.3 Simplified System Equivalent Circuit during Fault [16]

$$X_t^{during} = X'_d + X_{TR} + \frac{X_{12}X_{13}}{X_{12}+X_{13}} = 0.4667 \text{ pu} \quad (6.7)$$

$$E_B^{eq} = E_B \frac{X_{13}}{X_{13}+X_{12}} = 0.3333 \text{ pu} \quad (6.8)$$

To clear the fault, Line 1-3 and 2-3 are opened and the equivalent reactance between synchronous generator internal voltage and infinite bus becomes  $X_T^{after}$ , as shown in (6.9).

$$X_t^{after} = X'_d + X_{TR} + X_{12} = 0.6 \text{ pu} \quad (6.9)$$

According to the variation of the equivalent reactance and voltage connected to the internal voltage of synchronous generator, the power transfer equations before, during and after fault are calculated below in (6.10) - (6.12).

$$P_{pre} = 2.4638 \sin \delta \quad (6.10)$$

$$P_{during} = 0.9152 \sin \delta \quad (6.11)$$

$$P_{after} = 2.1353 \sin \delta \quad (6.12)$$

The rotor mechanical power input  $P_m$  is assumed constant as 1 pu. The equations used to calculate  $A_1$  and  $A_2$  are given in (6.13) and (6.14).

$$A_1 = \delta_1 + 0.9152 \cos \delta_1 - (\delta_0 + 0.9152 \cos \delta_0) \quad (6.13)$$

$$A_2 = -2.1353 \cos \delta_m - \delta_m + 2.1353 \cos \delta_1 + \delta_1 \quad (6.14)$$

Critical clearing angle can be calculated by making  $A_1$  equals to  $A_2$ . The critical clearing angle here is 1.9812 radians. Then, the critical clearing time can be obtained from the swing equation (4.5) as 0.3934 seconds.

The numerical analysis is performed in Matlab to verify the calculated critical fault clearing time. Setting the clearing time to 0.34 seconds, the plot of rotor angle is shown in Figure 6.4, which is stable. Increasing the clearing time to 0.4 seconds, the plot of rotor angle is shown in Figure 6.5, which is unstable. It is shown that fault clearing time is critical for transient stability. Reducing the clearing time can enhance the system transient stability.

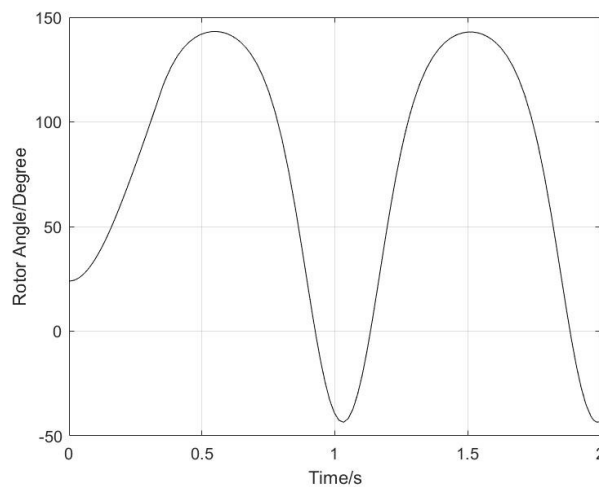


*Figure 6.4 Generator Rotor Angle when Fault Clearing Time is 0.34 seconds*

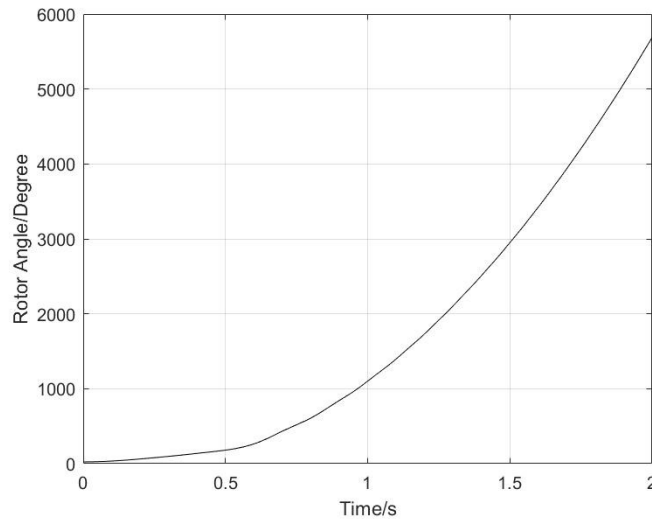


*Figure 6.5 Generator Rotor Angle when Fault Clearing Time is 0.4 seconds*

Equal area criterion serves as an introduction to the analysis of power system transient stability. A case study is given in this section to use the equal area criterion to determine the critical fault clearing time. The critical fault clearing time is verified by numerical analysis. It is shown that fault clearing time is critical for maintaining transient stability of power systems.

## **6.2 Transient Stability Analysis using PowerWorld**

When a power system contains more than one generator, equal area criterion is not suitable to solve the problem. Time domain simulation should be employed for transient stability analysis of multimachine systems. PowerWorld simulator provides time domain simulation for power system transient stability analysis. The detailed implementation of time domain simulation will be presented in the next chapter. In

this section, two case studies are provided using PowerWorld for transient stability analysis.

### 6.2.1 Case Study: Transient Stability Analysis of Five-Bus Two-Machine Power System

The Five-Bus Two-Machine power system used for this case study is shown in Figure 6.6. This system contains two generators, one generator connected to Bus One and the other generator connected to Three. Loads are connected at Bus Two and Bus Three. The machine models for representing the dynamics of synchronous generators are included. The system parameters are given in Appendix H.

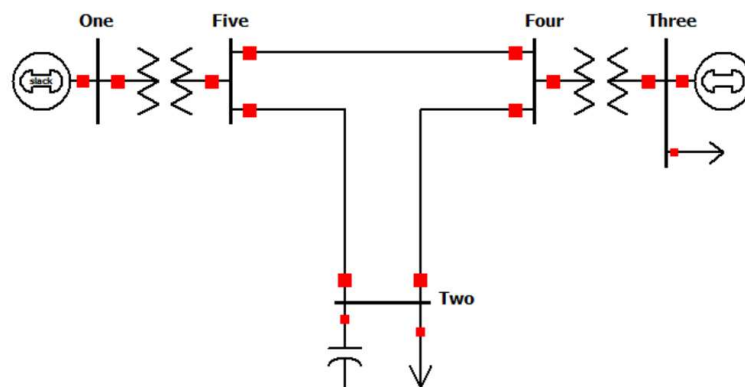


*Figure 6.6 Five-Bus Two-Machine Power System*

A three-phase fault occurs at Bus 4 at 0 s and cleared at 0.05 s. The rotor angles of the two generators from time domain simulation are shown in Figure 6.7. The solid line represents the rotor angle of generator at Bus One, while the dash line represents the rotor angle of generator at Bus Three. It is shown that the magnitudes of both

oscillations are decreasing. Under the fault clearing time of 0.05 seconds the rotor angle oscillations are damped indicating the system is stable. The damping effect is not very effective in this case as the synchronous generators are only represented by simple machine models in PowerWorld.

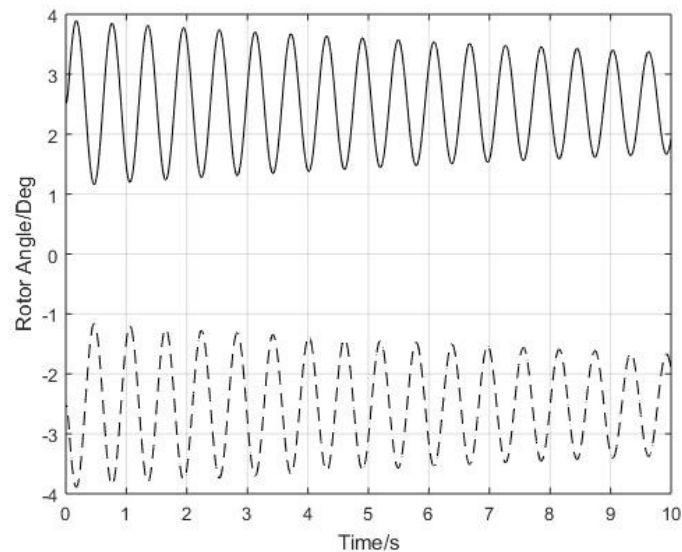


*Figure 6.7 Generator Rotor Angles when Fault Clearing Time is 0.05 seconds of the Five-Bus Two-Machine System*

The rotor angles of the two generators are shown in Figure 6.8 when fault clearing time increases to 2.5 seconds. The system is unstable under this condition as the rotor angles continue to increase. Fault clearing time is critical for maintaining system transient stability. By trying different fault clearing time, the critical fault clearing time is found at around 2 s.

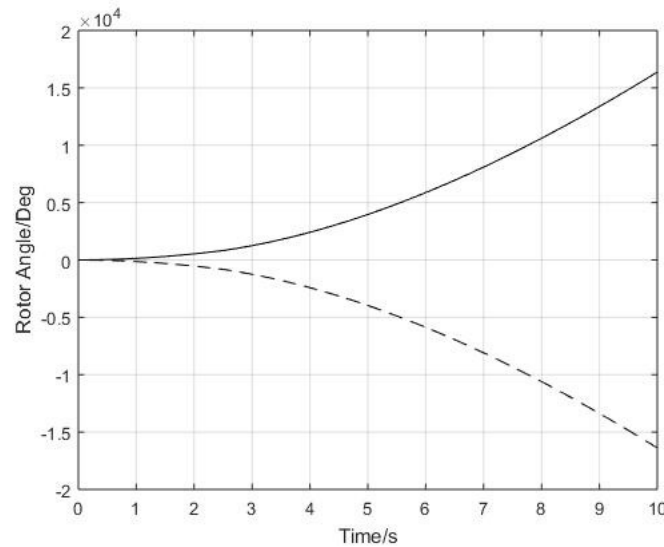


*Figure 6.8 Generator Rotor Angles when Fault Clearing Time is 2.5 seconds in the Five-Bus Two-Machine System*

In this case study, time domain simulation for multimachine power system transient stability analysis is discussed. It presents how to determine the stability condition and the critical fault clearing time using time domain simulation. The fault clearing time is crucial for ensuring system transient stability.

### **6.2.2 Case Study: Transient Stability Analysis of New England Power System**

In this case study, the transient stability of the 10-machine New England power system is investigated. The one line diagram of the New England power system is given in Figure 4.9. The machine models and exciter models are included in the representation of the synchronous generators. This will be used as base case in 7.5.3 in the following chapter. A three-phase fault is applied at Bus 16 occurring at 0.5 s and it is cleared after 0.05 second.

The rotor angles of generators at Bus 30 and Bus 34 are chosen within New England power system. The results from time domain simulation of generator rotor angles at Bus 30 and Bus 34 are shown in Figure 6.9 and 6.10 respectively. With a fault clearing time of 0.05 seconds, the system is stable as the oscillations are damped.

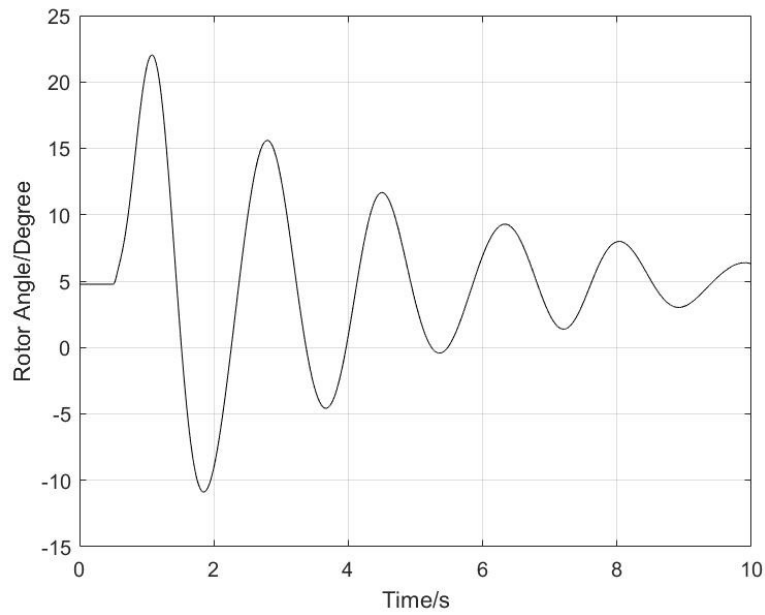


*Figure 6.9 Generator Rotor Angle at Bus 30 of the New England Power System*

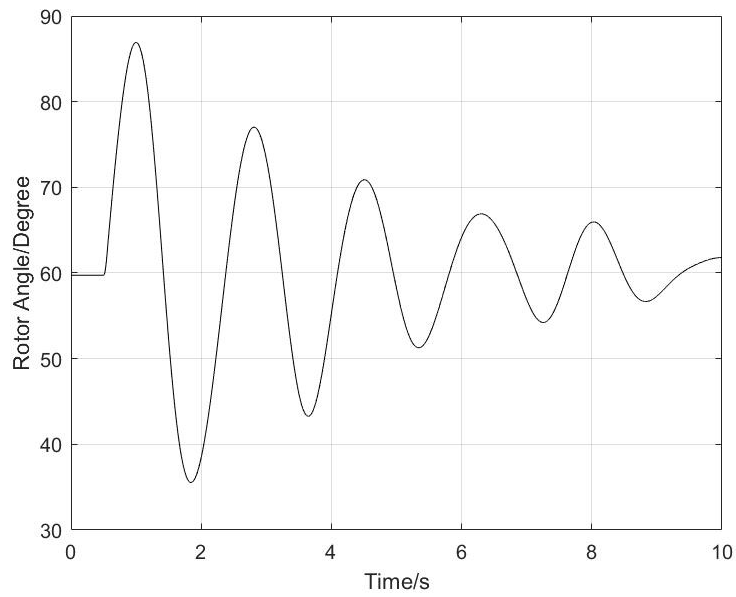


*Figure 6.10 Generator Rotor Angle at Bus 34 of the New England Power System*

The rotor angle responses of the generators at Bus 30 and Bus 34 are shown in Figure 6.11 and 6.12 respectively, when the fault clearing time is increased from 0.05 second to 0.2 second. The rotor angles of both generators are increasing. The system is unstable when the fault clearing time is increased.

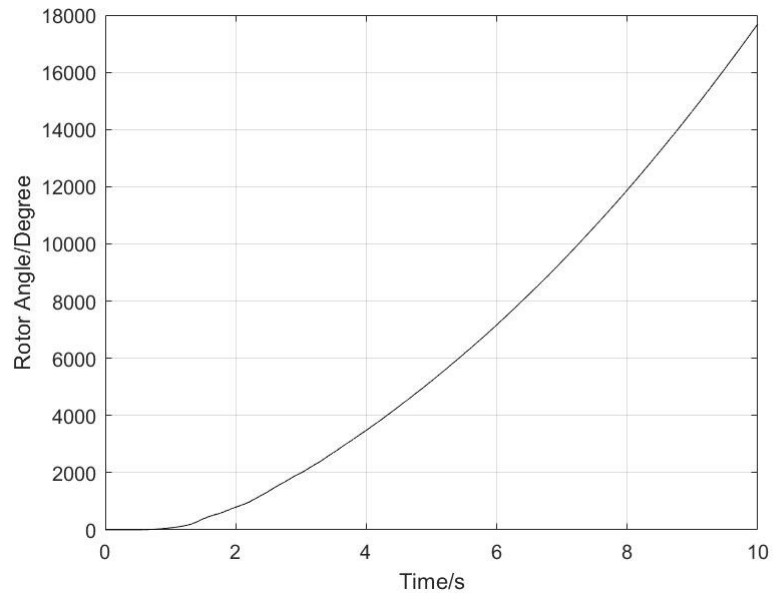


*Figure 6.11 Generator Rotor Angle at Bus 30 of the New England Power System  
(Increased Fault Clearing Time)*

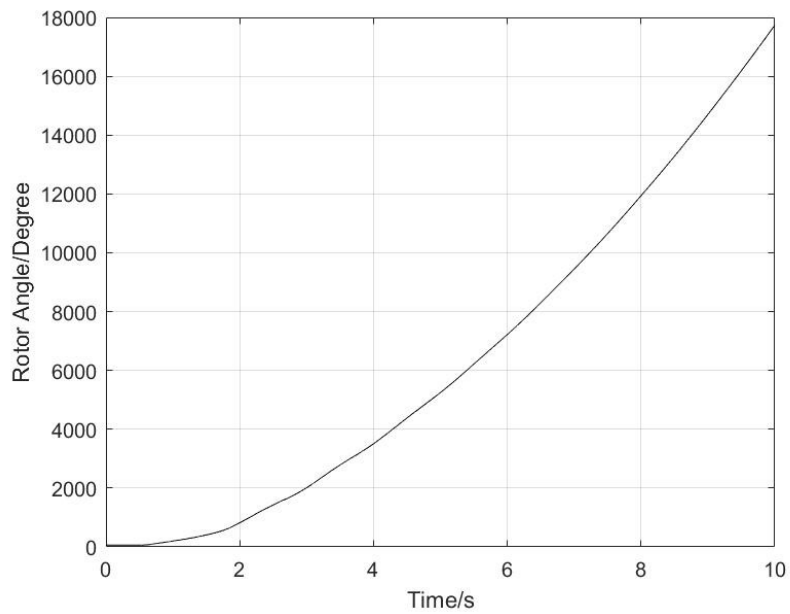


*Figure 6.12 Generator Rotor Angle at Bus 34 of the New England Power System  
(Increased Fault Clearing Time)*

This section presented two case studies to demonstrate time domain simulation for

power system transient stability analysis using PowerWorld.

### **6.3 Summary**

This chapter introduces the conventional power system transient stability analysis without wind energy integrations. The equal area criterion is presented first and a case study is also given. It is shown that the equal area criterion can be used to determine the critical fault clearing time for a simple system. Then, time domain simulation is performed on multimachine systems with more machines and buses. Case Studies show the importance of faulting clearing time in maintaining power system transient stability and the time domain simulation application in transient stability analysis.

# Chapter 7

## Power System Transient Stability Analysis with Wind Energy Integrations

### 7.0 Introduction

This chapter presents how power system transient stability is affected when wind energy is integrated into a power system. The computational method of time domain simulation is presented in 7.1. The time domain simulation application on the SMIB with a synchronous generator is discussed in 7.2. The time domain simulations of 5<sup>th</sup> and 3<sup>rd</sup> order models of DFIGs are compared in 7.3. A mathematical model of a DFIG based wind generator system is built in Simulink and its transient behaviors are presented in 7.4. For transient stability analysis of large systems with wind energy integrations, PowerWorld simulator is used. Two case studies using PowerWorld are presented in 7.5. A summary is given in 7.6.

## 7.1 Time Domain Simulation for Transient Stability Analysis

Unlike small signal stability analysis where the set of system equations can be linearized and the stability information is obtained from eigenvalue analysis, the differential algebraic equations (DAEs) are solved in transient stability analysis and the stability condition is observed from the system responses. It is not possible to solve DAEs analytically. Numerical analysis method is applied.

Time domain simulation uses numerical analysis to get the system responses with respect to time. As mentioned in the previous chapters, the system dynamic behaviors can be described by DAEs, as shown in (7.1) and (7.2).

$$\dot{x} = f(x, z, u) \quad (7.1)$$

$$0 = g(x, z, u) \quad (7.2)$$

The method of numerical integration is to get the next values of state variables from the current values by solving differential equations. The algebraic variables can then be obtained from the algebraic equations. The values of state and algebraic variables are updated step by step.

The technique of numerical integration includes Euler method, Modified Euler method, Runge-Kutta (R-K) method and implicit integration method [13, 16]. Euler method is explained in detail here to illustrate how numerical method is applied to solve differential equations.

Considering a differential equation in (7.3).

$$\frac{dx}{dt} = f(x) \quad (7.3)$$

At beginning,  $x = x_1$ , calculating the slope at this point,  $\frac{dx_1}{dt} = f(x_1)$ . During a small interval  $\Delta t$ , it is assumed that the slope is constant. Then, the next state variable can be calculated by (7.4).

$$x_2 = x_1 + \Delta x = x_1 + \frac{dx_1}{dt} \Delta t \quad (7.4)$$

The slope at  $x = x_2$  then can be calculated. The searching for next point of  $x = x_3$  is same as above steps.

Euler method is a relatively simple method which requires a small interval  $\Delta t$  for accuracy [16]. In multimachine stability, the numerical integration is applied to solve the differential equations in (7.1) while the algebraic equations in (7.2) are solved by the power flow equations.

The ode15s solver in Matlab is employed in this chapter to solve the DAEs.

## 7.2 Time Domain Simulation Application on Synchronous Generators

This section presents the application of time domain simulation on transient stability analysis and gives an insight into how the system DAEs are formed and solved using practical examples. The same system in 6.1.2 is used here. The system diagram is shown in Figure 6.3. Instead of using equal area criterion to determine the critical fault clearing time, the system is solved using time domain simulation. Two types of

synchronous generator models are applied in subsection 7.2.1 and 7.2.2 respectively.

The system is solved by Matlab ode15s solver and verified by PowerWorld.

### 7.2.1 Time Domain Simulation of Classical Model of Synchronous Generators

The classical model is the most simplified model for a synchronous generator. The classical model of a synchronous generator is represented by a constant internal voltage  $E'$  behind its direct axis transient reactance  $X'_d$ . Only the dynamics of the rotor are expressed. The differential equations of the classical model are presented in (7.5) and (7.6).

$$\frac{d\delta}{dt} = \omega_r - \omega_s \quad (7.5)$$

$$\frac{d\omega_r}{dt} = \frac{1}{2H} [T_m - T_e] \quad (7.6)$$

The algebraic equation is formed by the power balance in (7.8)

$$P_e = \frac{E'E_b}{X_t} \sin \delta \quad (7.8)$$

In the per unit system,  $P_e$  and  $T_e$  are equal. Substituting (7.8) into (7.6) gives (7.9).

$$\frac{d\omega_r}{dt} = \frac{1}{2H} \left[ T_m - \frac{E'E_b}{X_t} \sin \delta \right] \quad (7.9)$$

The values of  $E_b$  and  $X_t$  in the above equation depend on the network condition as discussed in Chapter 6. Before the fault at Bus 3 in Figure 6.3,  $E_b$  and  $X_t$  are 1 pu and 0.52 pu respectively. Then, a three-phase fault occurs at Bus 3 resulting in the equivalent  $E_b$  and  $X_t$  change to 0.3333 pu and 0.4667 pu respectively. The fault is

cleared by opening Line 1-3 and 2-3 which results in new values of  $E_b$  and  $X_t$  at 1 pu and 0.6 pu respectively.

The mechanical torque  $T_m$  is assumed to be constant at 1 pu.

The system in Figure 6.3 with the classical model of synchronous generators is solved in Matlab using ode15s solver and the same system is simulated in PowerWorld using the same classical model. The comparisons of the generator rotor angle and speed are shown in Figure 7.1 and 7.2.

In Figure 7.1, the rotor angle oscillations from both Matlab and PowerWorld are decreasing with time. The system is stable under this disturbance. It is shown that the rotor angle and speed results from Matlab ode15s and PowerWorld are the same from 0 second to 1.5 second. After 1.5 second, the results become different and this difference increases. This is because the ode15s solver and PowerWorld use different methods for solving the differential equations numerically. As described in 7.1, there are many techniques for performing the time domain simulation. There will be certain differences by using different solvers and the size of the difference depends on the type of solver, step size and error tolerance.

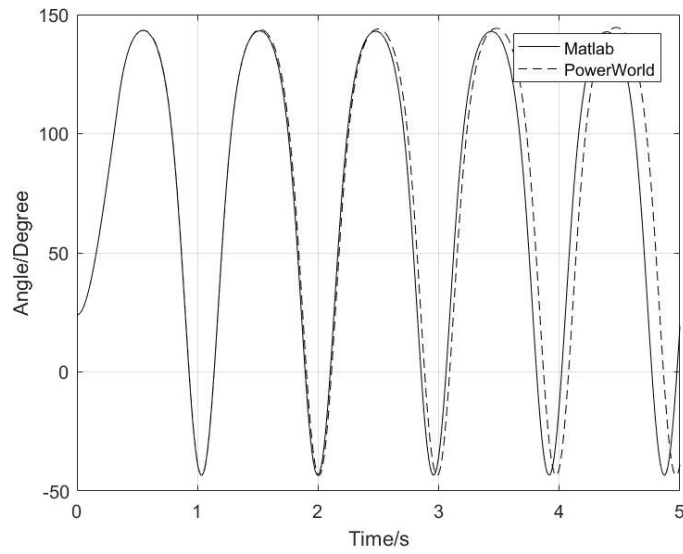


*Figure 7.1 Comparisons of Rotor Angles from Matlab and PowerWorld of the Classical Model*

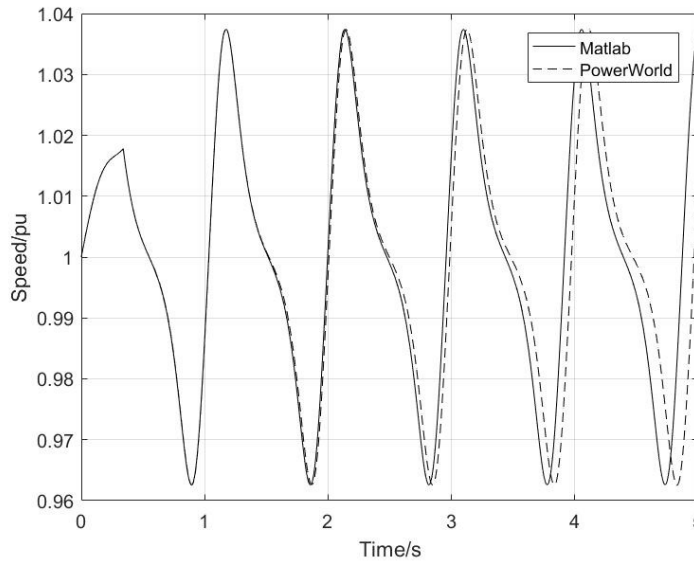


*Figure 7.2 Comparisons of Generator Speeds from Matlab and PowerWorld of the Classical Model*

This section applies the classical model of synchronous generators in time domain simulation using Matlab and compared the results with PowerWorld. It gives the basic

understanding of performing time domain simulation for transient stability analysis with the simplest example and illustrates the differences caused by different numerical solvers.

### 7.2.2 Time Domain Simulation of Two-Axis Model of Synchronous Generators

The classical model provides the simplest way for representing the synchronous generators in dynamic analysis. It is only appropriate for the most basic studies [16].

A more realistic Two-axis model is presented here.

The internal voltage of the synchronous generator is not represented by a constant voltage  $E'$  in the Two-axis model. It is represented by the dynamic internal voltages in d-q reference frame,  $E'_q$  and  $E'_d$ . The dynamics of  $E'_q$  and  $E'_d$  are given in the differential equations (7.10) and (7.11). As shown in (7.10), the dynamic of  $E'_q$  is related to the excitation voltage,  $E_{fd}$ , which is used for connecting the exciter model. However, the excitation system is not considered here and  $E_{fd}$  is assumed to be constant during the period of interest.

$$\frac{dE'_q}{dt} = \frac{1}{T'_{d0}} [-E'_q - (X_d - X'_d)I_d + E_{fd}] \quad (7.10)$$

$$\frac{dE'_d}{dt} = \frac{1}{T'_{q0}} [-E'_d + (X_q - X'_q)I_q] \quad (7.11)$$

Combining the above two equations with (7.5) and (7.6) gives the fourth order model for the synchronous generator. The dynamic model of the Two-axis model is the same as the one used for small signal stability analysis, given in (5.5)- (5.9).

The algebraic equations follow the reference [16] in order to be comparable with the results from PowerWorld. The algebraic equations that connect the internal voltages with the terminal bus voltage are shown in (7.12) and (7.13).

$$E'_q = V_q + X'_d I_d \quad (7.12)$$

$$E'_d = V_d - X'_q I_q \quad (7.13)$$

Equations (7.14) and (7.15) give the conversions of voltages and currents from in rotating d-q frame to in stationary network frame. These conversions connect the generator quantities with the network quantities.

$$\begin{bmatrix} V_r \\ V_i \end{bmatrix} = \begin{bmatrix} \sin \delta & \cos \delta \\ -\cos \delta & \sin \delta \end{bmatrix} \begin{bmatrix} V_d \\ V_q \end{bmatrix} \quad (7.14)$$

$$\begin{bmatrix} I_r \\ I_i \end{bmatrix} = \begin{bmatrix} \sin \delta & \cos \delta \\ -\cos \delta & \sin \delta \end{bmatrix} \begin{bmatrix} I_d \\ I_q \end{bmatrix} \quad (7.15)$$

The algebraic equations representing the generator terminal and the infinite bus are given in (7.16) and (7.17).

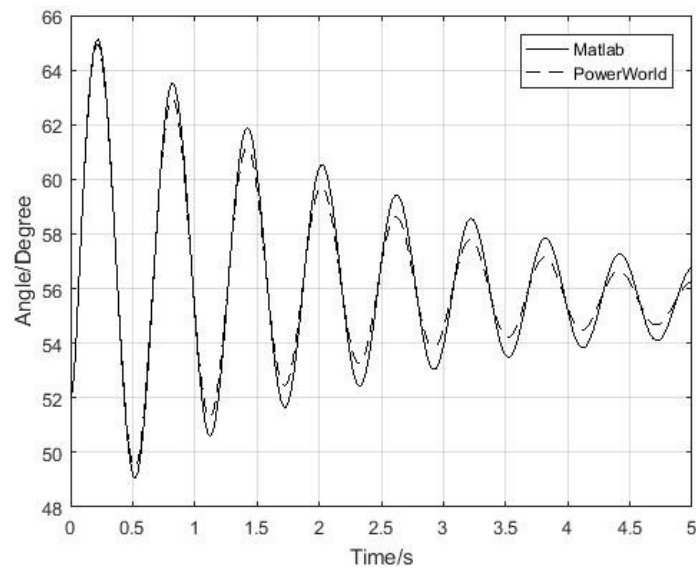
$$V_r = -X_t I_i + E_b \quad (7.16)$$

$$V_i = X_t I_r \quad (7.17)$$

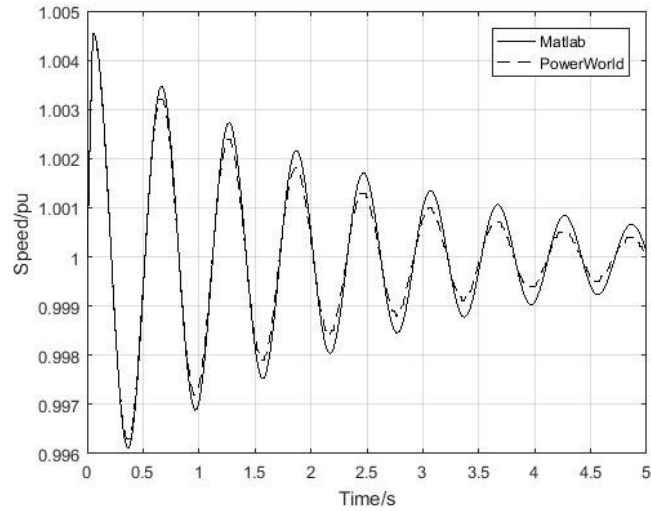
This model is also applied to the same system in Figure 6.3 and the same disturbance is employed as used in the subsection 7.2.1. The system responses obtained from Matlab ode15s solver and PowerWorld are given in Figure 7.3 - 7.6.

It is shown that the results from Matlab and PowerWorld basically match. The responses of the generator rotor angle and speed are shown in Figure 7.3 and 7.4.

Both oscillations are damped, indicating the system is stable. The fault clearing scheme works well to maintain the system transient stability. Comparing the results from ode15s solver and PowerWorld, the oscillation magnitudes are smaller in PowerWorld of both rotor angle and speed after 0.5 second. As mentioned before, the DAEs solver in PowerWorld is different from the one used in Matlab ode15s solver.

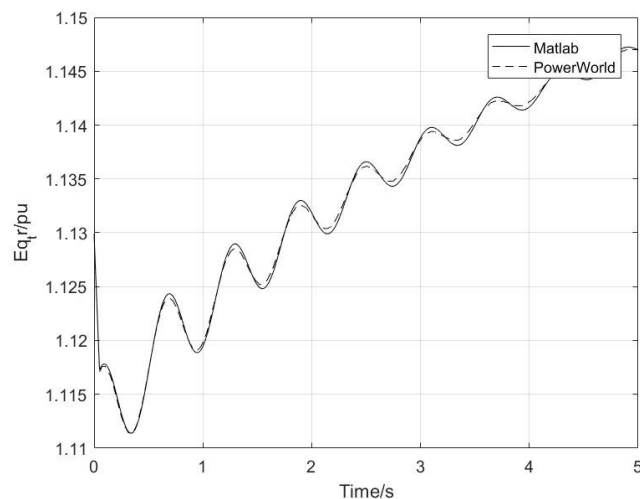


*Figure 7.3 Comparisons of Rotor Angles from Matlab and PowerWorld of the Two-Axis Model*



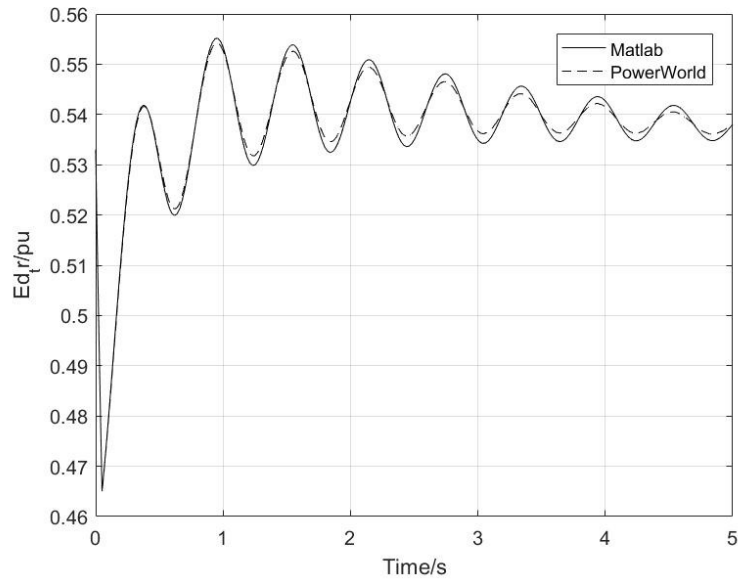
*Figure 7.4 Comparisons of Generator Speeds from Matlab and PowerWorld of the Two-Axis Model*

Figure 7.5 and 7.6 present the responses of the synchronous generator internal voltage in q and d axis. The variations of these two quantities come from (7.10) and (7.11), while the internal voltage is assumed constant in the classical model. The results from Matlab and PowerWorld are very close.



*Figure 7.5 Comparisons of Internal Voltage  $E'_q$  from Matlab and PowerWorld of the*

*Two-Axis Model*



*Figure 7.6 Comparison of Internal Voltage  $E_d'$  from Matlab and PowerWorld of the Two-Axis Model*

This section presented the time domain simulation for transient stability analysis of a SMIB system with a synchronous generator. Classical and Two-axis models are adopted for representing the synchronous machine. The DAEs are formed for the studied system and solved using Matlab ode15s solver. The results from ode15s solver are compared with the results from PowerWorld.

### **7.3 Analysis and Simulation of DFIGs**

The transient stability performances of a DFIG based wind generation system are presented in this section. This section introduces simulation of DFIGs using the ode15s solver and Simulink model. The 5<sup>th</sup> and 3<sup>rd</sup> order models of DFIGs are first

compared in subsection 7.3.1. A DFIG based system is implemented in Simulink and its transient behaviors during different disturbances are presented in subsection 7.3.2.

### 7.3.1 Comparison of 5<sup>th</sup> and 3<sup>rd</sup> Order DFIG Models

To analyze the impacts of DFIGs on power system transient stability, the DFIGs should be understood and appropriately modeled. This section performs analysis and simulation on a SMIB system with a DFIG. For modelling of DFIGs, choosing between 5<sup>th</sup> or 3<sup>rd</sup> order models are considered in power system analysis [30]. This section compares the 5<sup>th</sup> order and the 3<sup>rd</sup> order models. The DAEs formed are solved by ode15s solver.

The 5<sup>th</sup> order model has been given in (5.19) - (5.23) and repeated here in (7.18) - (7.22). This model includes the stator flux transients, which includes the differential equations for stator currents  $I_{ds}$  and  $I_{qs}$ .

$$\frac{X'_s}{\omega_s} \frac{dI_{ds}}{dt} = V_{ds} - \left( R_s + \frac{X_s - X'_s}{T'_0} \right) I_{ds} - \frac{\omega_r}{\omega_s} E'_d - \frac{L_m}{L_{rr}} V_{dr} + \frac{1}{T'_0} E'_q + X'_s I_{qs} \quad (7.18)$$

$$\frac{X'_s}{\omega_s} \frac{dI_{qs}}{dt} = V_{qs} - \left( R_s + \frac{X_s - X'_s}{T'_0} \right) I_{qs} - \frac{\omega_r}{\omega_s} E'_q - \frac{L_m}{L_{rr}} V_{qr} - \frac{1}{T'_0} E'_d - X'_s I_{ds} \quad (7.19)$$

$$\frac{dE'_d}{dt} = (\omega_s - \omega_r) E'_q - \frac{\omega_s L_m}{L_{rr}} V_{qr} - \frac{\omega_s}{T'_0} [E'_d - (X_s - X'_s) I_{qs}] \quad (7.20)$$

$$\frac{dE'_q}{dt} = -(\omega_s - \omega_r) E'_d + \frac{\omega_s L_m}{L_{rr}} V_{dr} - \frac{\omega_s}{T'_0} [E'_q + (X_s - X'_s) I_{ds}] \quad (7.21)$$

$$\frac{d\omega_r}{dt} = \frac{1}{2H} (T_m - E'_d I_{ds} - E'_q I_{qs}) \quad (7.22)$$

As presented in 5.1.2, the 5<sup>th</sup> order model of the DFIG has a high frequency low

damping mode from the eigenvalue analysis. This mode is referred to as ‘stator mode’ as it has the highest participation factor with stator currents  $I_{ds}$  and  $I_{qs}$ . As the focus of power system transient stability is on the low frequency oscillations, such high frequency oscillation is not of interest. The 3<sup>rd</sup> order model eliminates the differential equations for the stator currents to simplify the model.

In this 3<sup>rd</sup> order model, the stator flux transients are neglected in the basic equations. Thus, the differential terms of stator currents are eliminated and (7.8) and (7.9) become the algebraic equations, as given in (7.23) and (7.24).

$$-R_s I_{ds} + X'_s I_{qs} + E'_d - V_{ds} = 0 \quad (7.23)$$

$$-R_s I_{qs} - X'_s I_{ds} + E'_q - V_{qs} = 0 \quad (7.24)$$

The rotor voltages are assumed constant during the transient period when the focus is on the dynamics of the generator itself rather than the control schemes that are applied to it.

The DFIG is connected to an infinite bus through a transmission line as shown in Figure 5.4. The algebraic equations are the same as the one for small signal stability analysis in (5.28) and (5.29). The algebraic equations are repeated here in (7.25) and (7.26).

$$V_{ds} I_{ds} + V_{qs} I_{qs} + V_{dr} \left( \frac{E'_q}{L_m} - \frac{L_m}{L_{rr}} I_{ds} \right) + V_{qr} \left( -\frac{E'_d}{L_m} - \frac{L_m}{L_{rr}} I_{qs} \right) \frac{\sqrt{V_{ds}^2 + V_{qs}^2} E_b \sin\left(\tan^{-1}\left(\frac{V_{qs}}{V_{ds}}\right)\right)}{X_t} = 0 \quad (7.25)$$

$$V_{qs}I_{ds} - V_{ds}I_{qs} + \frac{(V_{ds}^2 + V_{qs}^2) - \sqrt{V_{ds}^2 + V_{qs}^2} E_b \cos\left(\tan^{-1}\left(\frac{V_{qs}}{V_{ds}}\right)\right)}{X_t} = 0 \quad (7.26)$$

A transmission line switch disturbance is applied here, causing the transmission line reactance  $X_t$  to drop from 0.55 pu to 0.192 pu. The above equations are solved in Matlab using ode15s solver. The system responses of the two models are plotted in Figure 7.7-7.10. All the plots stabilized at the new values, indicating the system is stable.

The electromagnetic torques and terminal bus voltage magnitudes are shown in Figure 7.7 and 7.8 respectively.

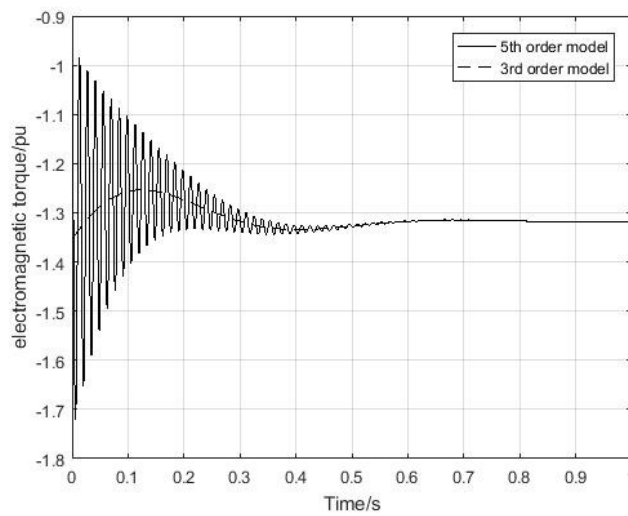


*Figure 7.7 Comparisons of Electromagnetic Torques of 5<sup>th</sup> Order and 3<sup>rd</sup> Order*

*Models of a DFIG*

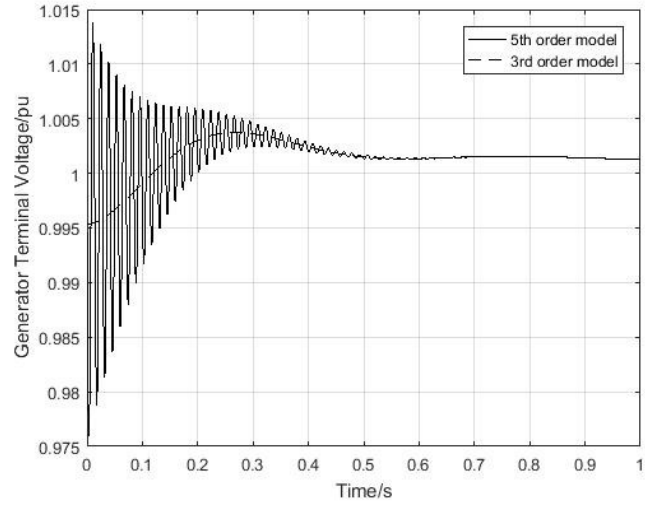


Figure 7.8 Comparisons of Generator Terminal Voltages of 5<sup>th</sup> Order and 3<sup>rd</sup> Order

*Models of a DFIG*

The inner voltages  $E'_d$  and stator currents  $I_{ds}$  of the two models are shown and compared in 7.9 and 7.10.

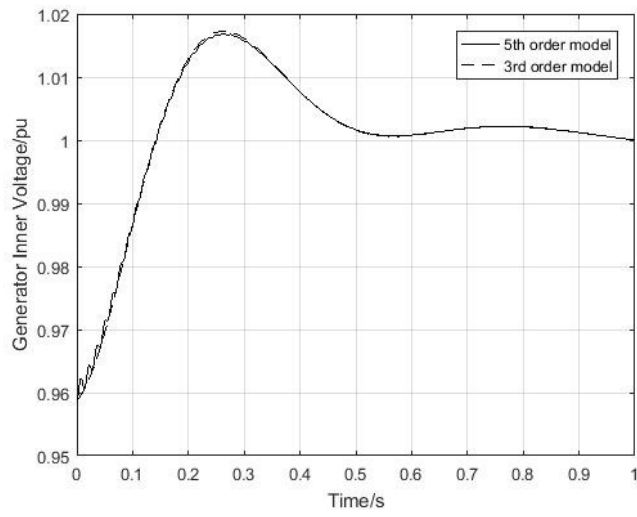
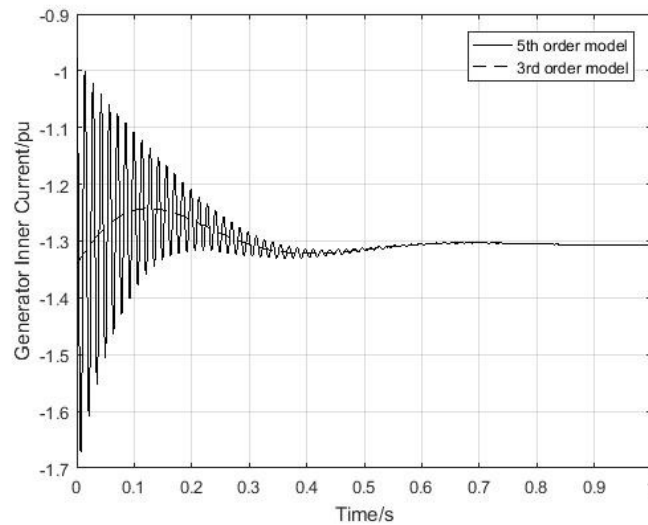


Figure 7.9 Comparisons of Generator Inner Voltages of 5<sup>th</sup> Order and 3<sup>rd</sup> Order

*Models of a DFIG ( $E'_d$ )*



*Figure 7.10 Comparisons of Generator Stator Currents of 5<sup>th</sup> Order and 3<sup>rd</sup> Order*

*Models of a DFIG ( $I_{ds}$ )*

As shown in the simulation results, extra high frequency oscillations are included in the 5<sup>th</sup> order model. The results match with the results of eigenvalues analysis. The high frequency oscillation is mostly related to the stator current as shown in Figure 7.10, while it does not affect the internal voltage shown in Figure 7.9. However, the trend for low frequency oscillation is the same. In the 5<sup>th</sup> order model, more accurate simulation results are obtained with the inclusion of the stator flux transients. In the 3<sup>rd</sup> order model, the stability can be determined from the low frequency oscillation and computational burden can be reduced with the exclusion of the stator flux transients. As the main concern of power system stability is the low frequency oscillation, it is practical to use the 3<sup>rd</sup> order model. Choosing between these two models depends on the balancing between simulation accuracy and computation time.

### **7.3.2 Simulation and Analysis of a DFIG based Wind Generation System and its Transient Behaviors**

A DFIG based wind generation system is discussed here and its mathematical model is implemented in Simulink. Two disturbances are applied to it to investigate its transient behaviors.

The overall DFIG based wind generation system block diagram is shown in Figure 7.11. The DFIG is modeled as the 3<sup>rd</sup> order model which only gives out the low frequency oscillations of the system dynamics. The rotor is modeled as a two-mass model and the wind turbine is also included. The rotor side converter provides the decoupled control to the rotor. The grid side converter is not considered in this model, which is not necessary for power system low frequency oscillation studies. It can be assumed the grid side converter manages to keep DC capacitor voltage constant and supply power at unity power factor.

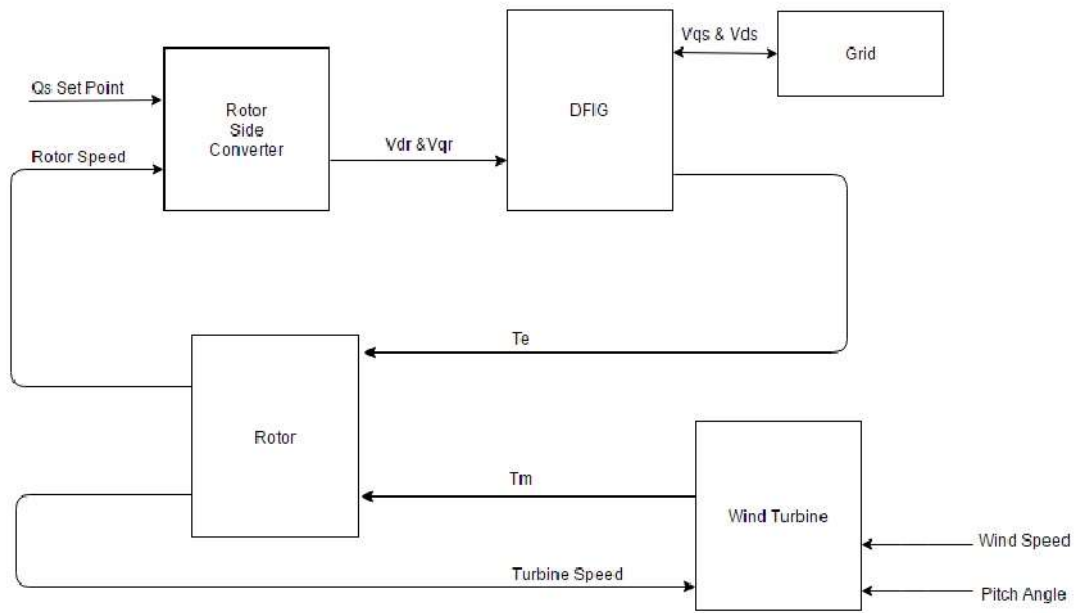


Figure 7.11 DFIG based Wind Generation System Block Diagram

The simulated system implemented in Simulink is shown in Figure 7.12.

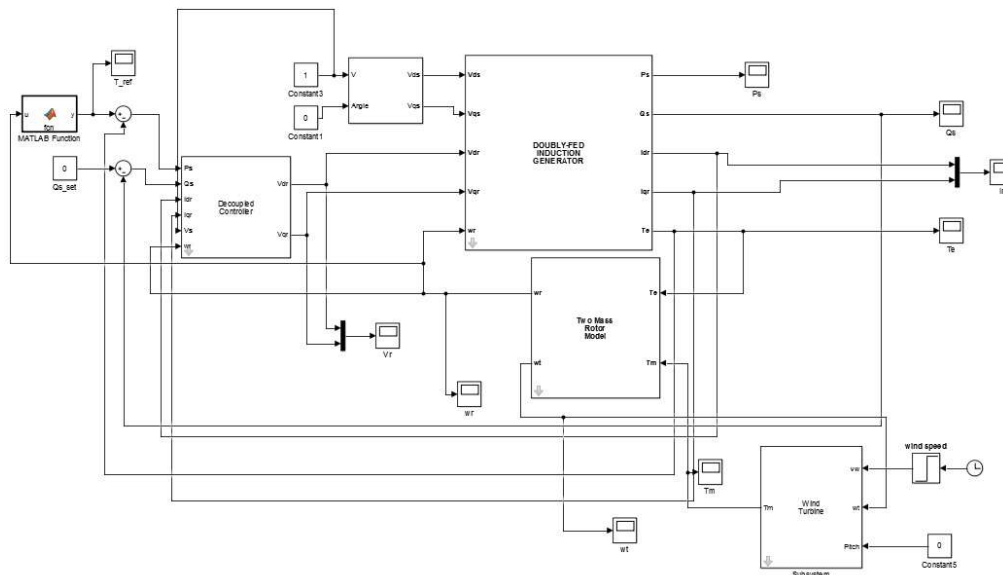


Figure 7.12 Model Implemented in Simulink

The 3<sup>rd</sup> order model of a DFIG is given above in (7.20), (7.21), (7.23) and (7.24)

while the two-mass model introduced in Chapter 2 in (2.5) - (2.7) is used to replace the one-mass model in (7.22).

The wind turbine mechanical model has been discussed in Chapter 2 in 2.6.2.1. The control aim is to operate at the optimal point to extract maximum power from the wind under the rated wind speed. In this model, only the speed below the rated wind speed is considered.

The variation of the mechanical torque with respect to the rotor speed under different wind speeds from 6 m/s to 14 m/s is plotted in Figure 7.31 using (2.1). It is shown that for a specific wind speed, there is a peak mechanical torque. Under the rated wind speed, the control goal is to get the maximum mechanical power. This is achieved by forming an optimal curve to find the optimal point for each wind speed and feeding to the torque controller as the reference torque [31]. The maximum points for each wind speed is found and connected by the red line in Figure 7.13. The optimal power curve is found using these maximum points and is plotted in the dash line in Figure 7.13. Equation (7.27) is used as the optimal curve for torque control to extract the maximum power from the wind under the rated wind speed.

$$T_{opt} = 0.2821\omega_r^3 + 0.3241\omega_r^2 + 0.4386\omega_r - 0.0992 \quad (7.27)$$

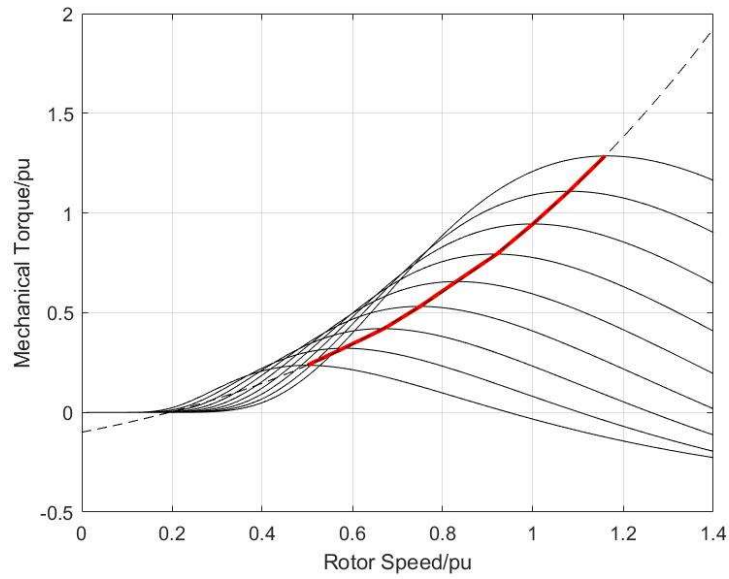


Figure 7.13 Mechanical Torque vs Rotor Speed

The decoupled control of the rotor side converter has been discussed in 2.6.2.4. As shown in (2.36) and (2.35), the electromagnetic torque  $T_e$  and stator reactive power  $Q_s$  determine the rotor currents  $I_q$  and  $I_d$ . The rotor currents then determine the rotor voltages  $V_{qr}$  and  $V_{dr}$ . A two stage PI controller is applied for electromagnetic torque  $T_e$  and stator reactive power  $Q_s$  control respectively, as shown in Figure 7.14 and 7.15.

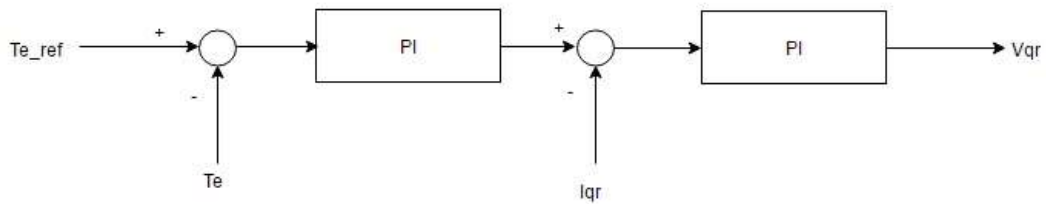
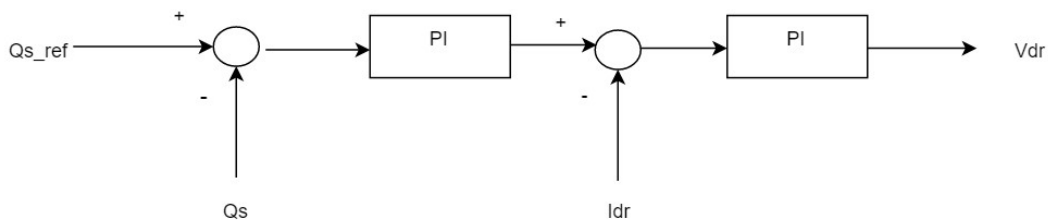


Figure 7.14 Torque Controller for Rotor Side Converter



*Figure 7.15 Reactive Power Controller for Rotor Side Converter*

The common disturbances for a wind generation system are the variations of wind speed and terminal bus voltage. Two disturbances are applied to the above system. One is the wind speed changing from 12 m/s to 13 m/s at 20 seconds and the other one is the terminal voltage dropping from 1 pu to 0.5 pu at 40 seconds. These two are the most common and significant disturbances that a wind generator encounters in the real world. The system responses are shown in Figure 7.16-7.24.

The mechanical torque from the wind turbine increases at 20 s in Figure 7.16. As shown in Figure 7.17 and 7.18, the rotor speed and the turbine speed are all increased due to the increase of the wind speed. The calculated reference torque for electromagnetic torque in Figure 7.19 also increases and the electromagnetic torque in Figure 7.20 follows. The active power and reactive power from the stator are shown in Figure 7.21 and 7.22. As the wind speed increases, the active power also increases while the reactive power is kept at zero. The rotor currents  $I_{dr}$  and  $I_{qr}$  are shown in Figure 7.23 and 7.24 respectively. At 20 s,  $I_{dr}$  increases to maintain the reactive power at zero and  $I_{qr}$  is kept constant. Active power and reactive power from a

DFIG is controlled by  $I_{qr}$  and  $I_{dr}$  separately. With the power electronic devices, DFIGs do not participate in power system oscillation.

The voltage drop disturbance does not affect the wind turbine mechanical torque in Figure 7.16. The rotor speed and turbine speed experience small oscillations as the electromagnetic torque is affected as shown in Figure 7.20. The voltage drop brings oscillations to active and reactive power. However, they stabilize at the same values as the values before the voltage drop. This is accomplished by the adjustments of currents injected into the rotor as shown in Figure 7.23 and 7.24. The rotor currents have a dramatic change after the voltage drop as the rotor currents are very sensitive to the terminal voltage change.  $I_{dr}$  increases from 1.2 pu to 2.3 pu. In this model, no limitation is implemented on the rotor currents. However, the rotor currents are limited by the power electronic converter capacity in an actual DFIG system. Thus, the low voltage ride through (LVRT) is a critical problem for DFIG based wind generators. Due to the limitations of power electronic converter capacity, the reactive power supplied from DFIGs is restricted and its effects on power systems are discussed in Chapter 3.

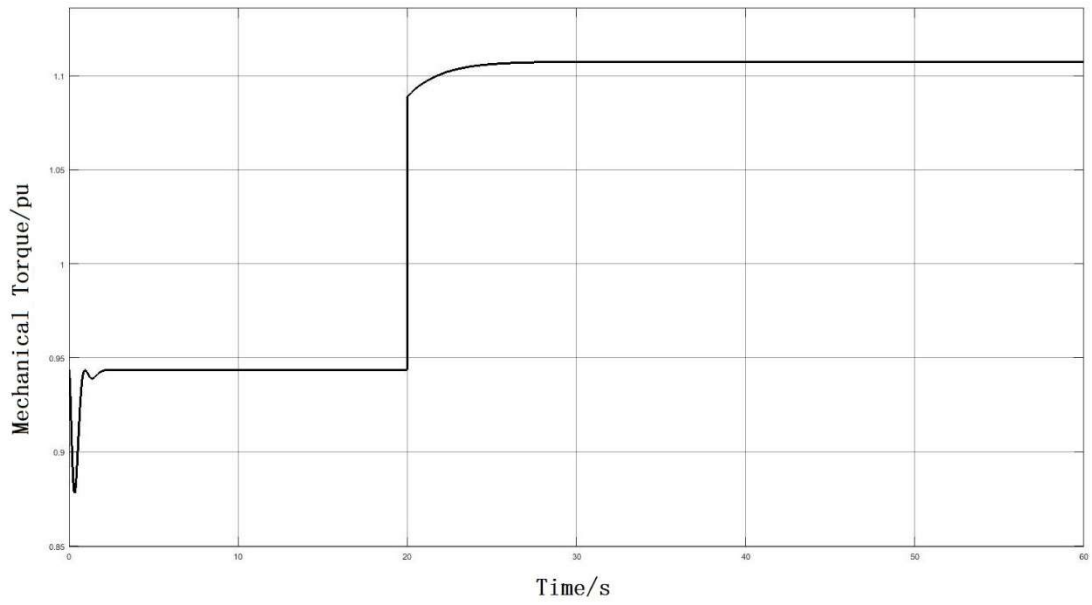


*Figure 7.16 Mechanical Torque Response of the DFIG System*

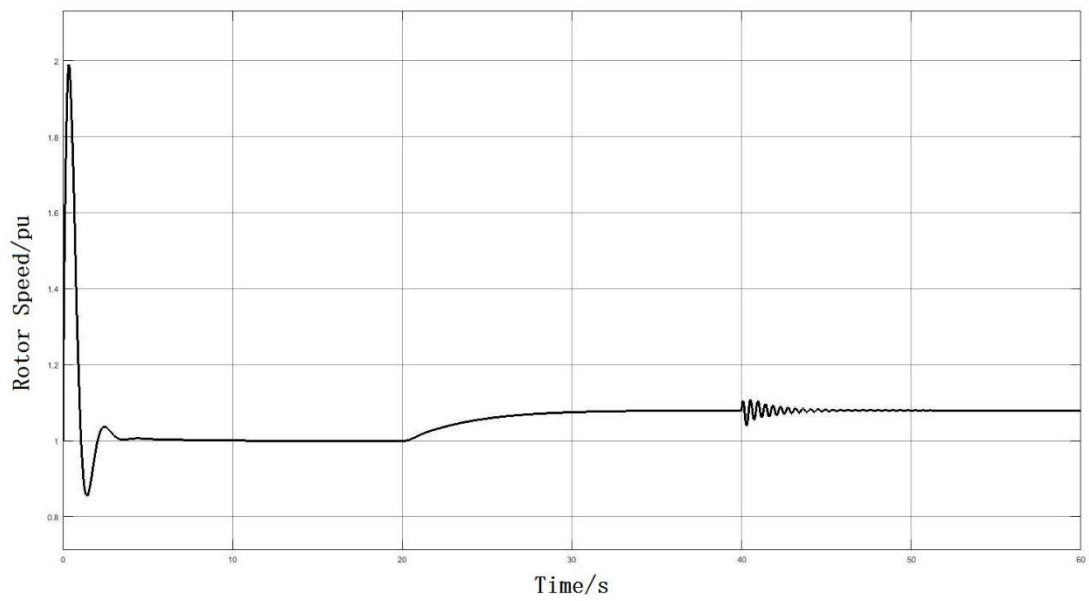


*Figure 7.17 Rotor Speed Response of the DFIG System*

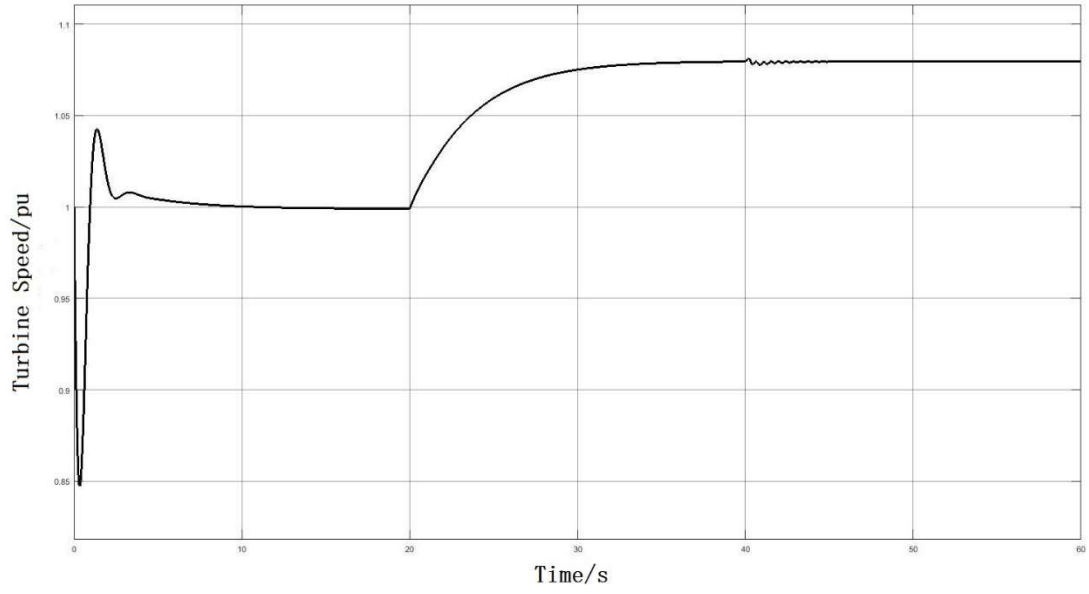


*Figure 7.18 Turbine Speed Response of the DFIG System*

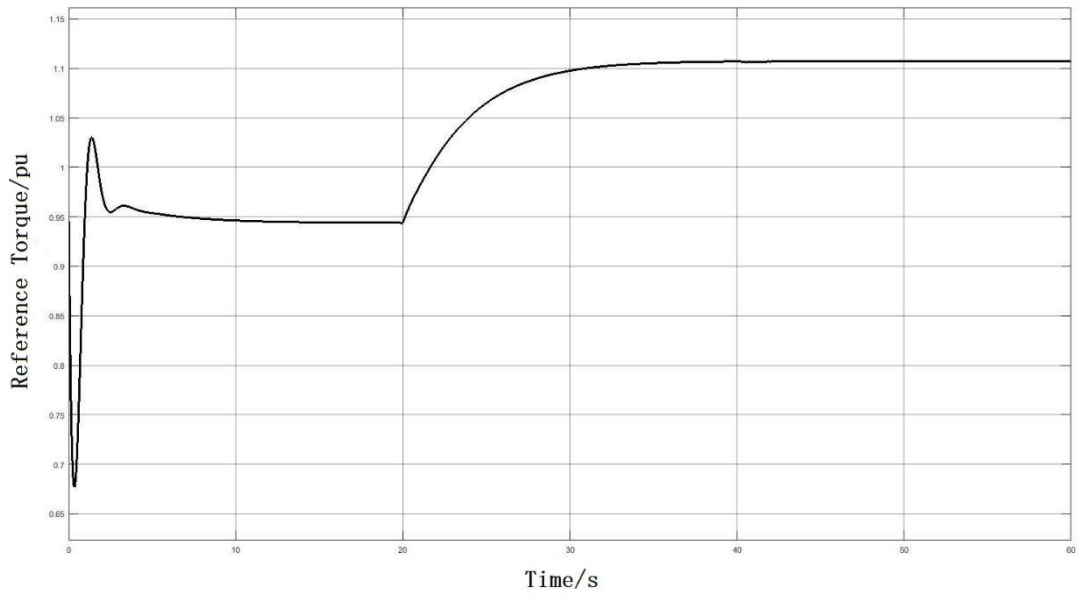


*Figure 7.19 Reference Torque Response of the DFIG System*

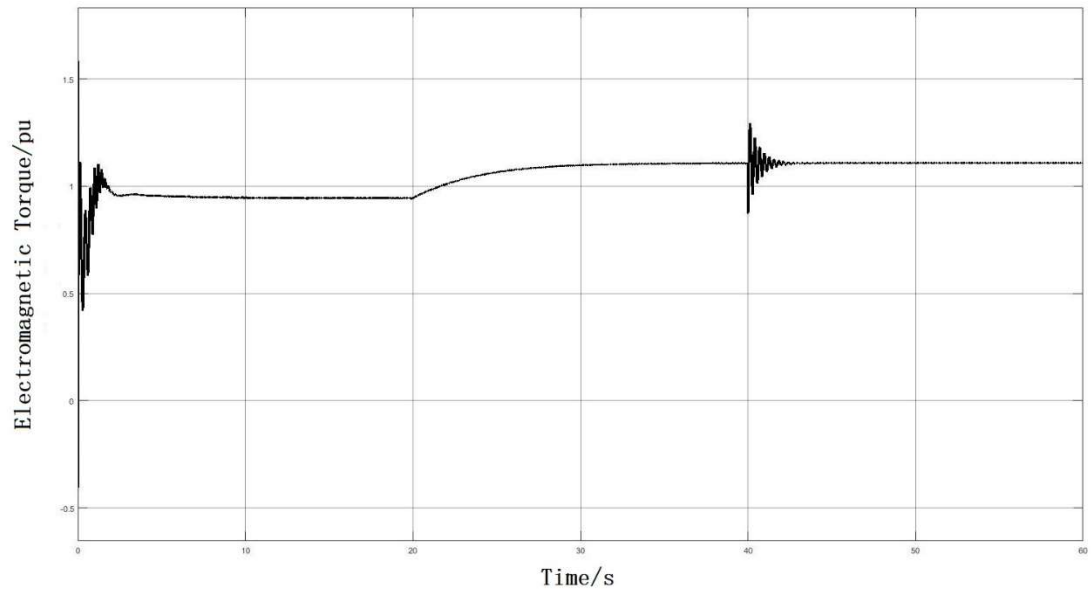


*Figure 7.20 Electromagnetic Torque Response of the DFIG System*

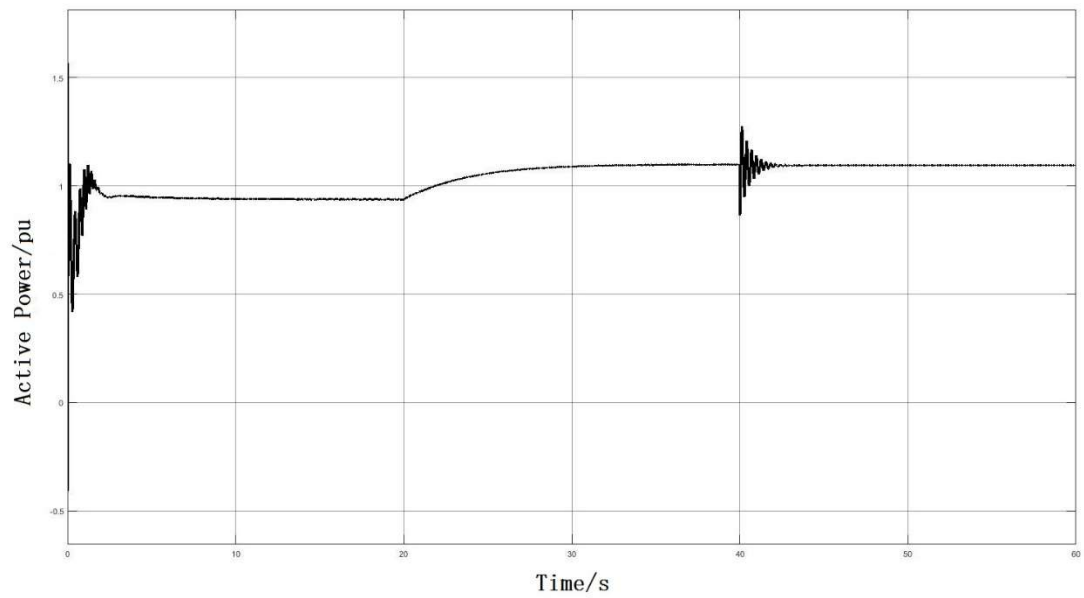


*Figure 7.21 Active Power Response of the DFIG System*

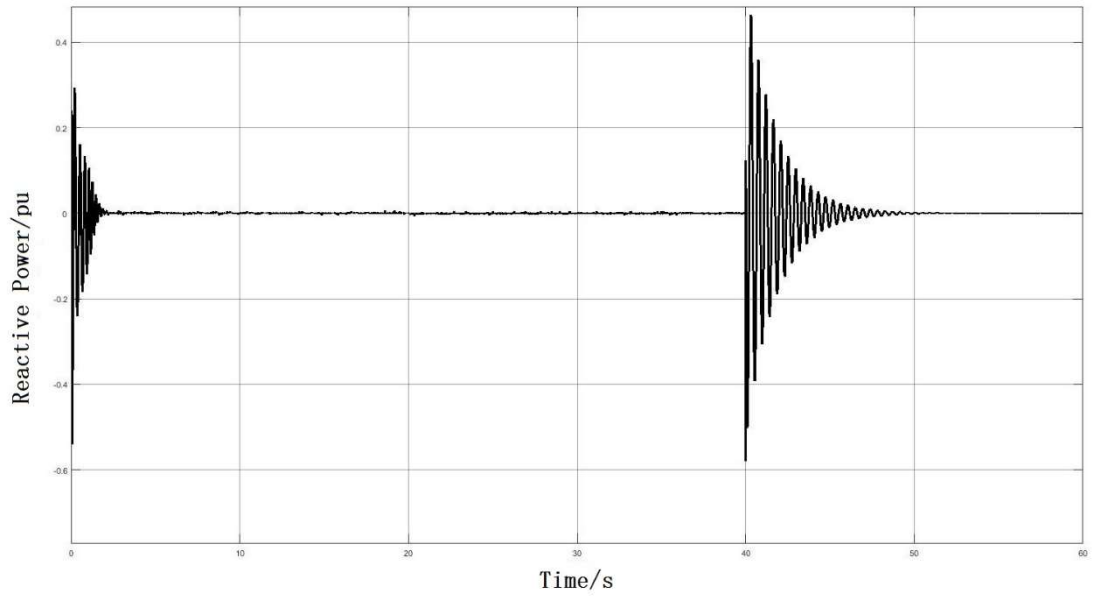


*Figure 7.22 Reactive Power Response of the DFIG System*

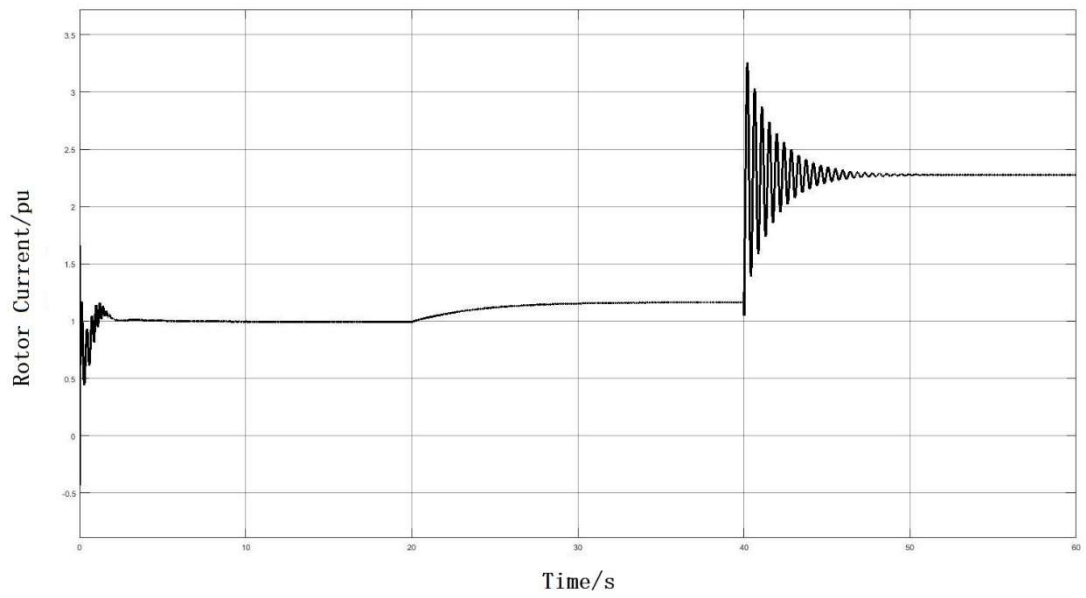


*Figure 7.23  $I_{dr}$  Response of the DFIG System*

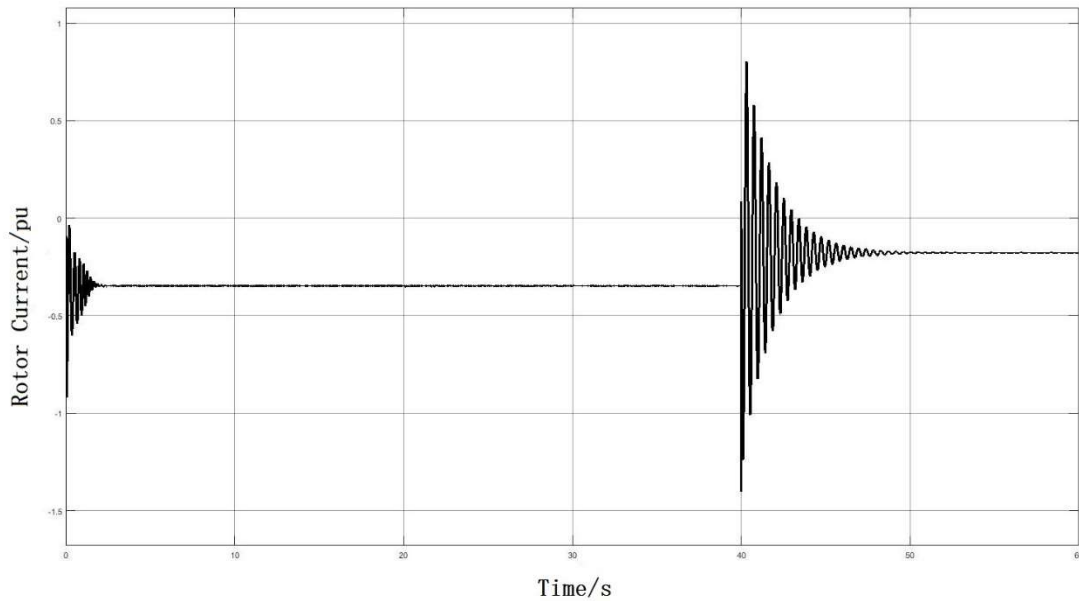


*Figure 7.24  $I_{qr}$  Response of the DFIG System*

The 5<sup>th</sup> and 3<sup>rd</sup> order models of DFIGs are compared and it is shown that the higher order model includes a high frequency oscillation. A comprehensive DFIG based wind generator is implemented in Simulink with the decoupled control method. The transient behaviors of a DFIG during different disturbances are shown. The critical problem of LVRT is discussed. This section gives an investigation on the transient behaviors of a single DFIG based generation system.

#### **7.4 Transient Stability Analysis with Wind Energy Integrations using PowerWorld**

For analyzing the transient stability of larger power systems, PowerWorld simulator is used. The generic GE dynamic model of wind generators included in PowerWorld is

used. For wind generators in PowerWorld, wind electrical machine model is represented by machine model, wind generator controller model is represented by exciter model and wind turbine mechanical model is represented by governor model.

The impacts of wind generators on power system transient stability have been explored by several papers [8, 32- 36]. Two simple systems are used in [32] and [33] for analyzing the impacts of DFIGs integration, which demonstrate certain beneficial effects. Analysis on a large system is presented in [8], which shows both beneficial and detrimental effect on power system dynamics under different scenarios. Besides on simulations, different transient stability indices are used for quantifying the effect of DFIGs integration [34]. More insights into the mechanisms that cause the influences are given [35] and [36]. This section aims to combine transient stability index and time domain simulation to analyze a simple and a complex system to obtain general conclusions.

#### **7.4.1 Transient Stability Evaluation Index**

Time domain simulation gives the system responses for a specific disturbance. Other general ways of expressing the system transient stability are needed. Two transient stability evaluation indices are introduced here, which are used for giving a general assessment of the overall system transient stability.

Critical fault clearing time is an important transient stability evaluation index. It gives the system tolerance for a specific large disturbance. Critical fault clearing times from

systems with and without wind energy integration of the same fault are used to reveal the impact that wind energy has on the power system transient stability.

Another transient stability evaluation index is transient stability index (TSI), defined in (7.39) [8].

$$TSI = \frac{360 - \delta_{max}}{360 + \delta_{max}} \quad (7.39)$$

$\delta_{max}$  is the largest rotor angle separation between two generators in the system during the fault. When TSI is larger than zero, the system is stable. When TSI is smaller than zero, the system is unstable. Its value indicates the stability level of the system. TSI will also be used in this research to give additional index for assessing transient stability of power systems.

#### **7.4.2 Case Study: Transient Stability Analysis of 9 Bus Power System with Wind Energy Integrations**

This section uses a 9 Bus power system with three generators to discuss how the integration of a DFIG based wind farm can influence the system transient stability. The one line diagram of the 9 Bus power system is shown in Figure 7.25 [14]. The system data is given in Appendix L. In the base case system, all three generators are synchronous generators with machine, exciter and governor models. To see how the wind energy integration affects the system transient stability, the synchronous generator at Bus 3 is replaced by a DFIG based wind farm with the same capacity.

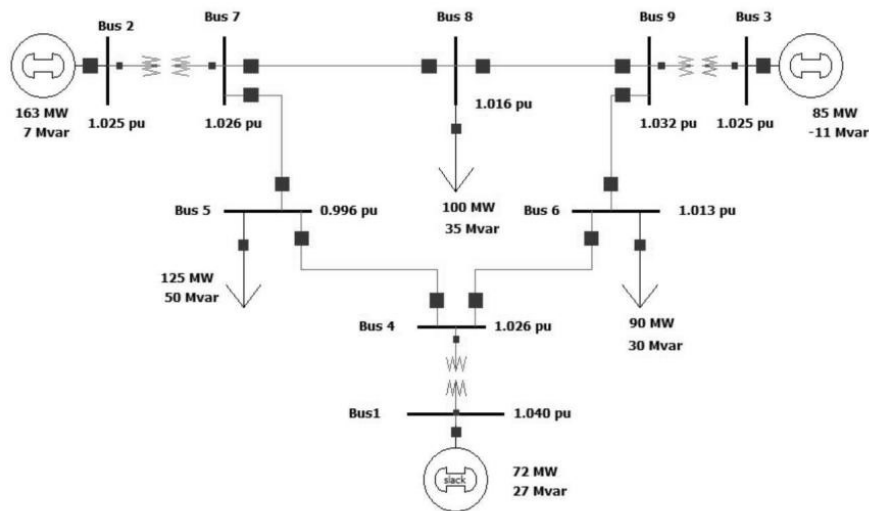


Figure 7.25 One Line Diagram of the 9 Bus Power System

The models used for generators at Bus 3 in PowerWorld are given in Table 7.1.

Table 7.1 Models Used in PowerWorld for Generator at Bus 3

Model	DFIG	Synchronous
Machine	GEWTG	GENROU
Exciter/Electrical	EXWTGE	IEEET1
Governor/Mechanical	WNDTGE	TGOV1

A three-phase fault is applied to Bus 4- 9 and the critical fault clearing times of base case and wind energy case are recorded in Table 7.2. It is shown that replacing the synchronous generator with a DFIG based wind farm increases the critical fault clearing time for faults at Bus 4- 6 while it decreases the critical fault clearing time for faults at Bus 7- 9. For different disturbances, DFIGs replacement has either positive or negative impact on the system transient stability.

*Table 7.2 Critical Fault Clearing Time Comparison*

Critical Fault Clearing Time	Base Case	Wind Energy
Bus 4	0.25625	0.29
Bus 5	0.30625	0.3175
Bus 6	0.34125	0.47
Bus 7	0.18125	0.174
Bus 8	0.2475	0.2
Bus 9	0.20625	0.2

In Table 7.2, the largest increase in critical fault clearing time is when a three-phase fault is applied to Bus 6. The critical fault clearing time increases by 0.12875 seconds. The rotor angle responses of generators at Bus 1 and Bus 2 for the base case and wind energy case are shown in Figure 7.26 and 7.27 respectively when the fault clearing time is 0.1 seconds. It is shown that the magnitudes of the oscillations of generators at Bus 1 and Bus 2 are all reduced when a DFIG based wind farm replaces the synchronous generator at Bus 3. For the base case, the largest rotor angle separation between generators at Bus 1 and 2 is  $74.0473^\circ$  and the TSI equals to 65.8805%. For the wind energy case, the largest rotor angle separation is  $67.2995^\circ$  and the TSI equals to 68.5001%. With the DFIG base wind farm replacing the synchronous generator at Bus 3, the largest rotor angle separation between generators at Bus 1 and 2 decreases by  $6.7478^\circ$  and the TSI increases by 2.6196%. It indicates that DFIGs replacement enhances the system rotor angle transient stability for three-phase fault at Bus 6.

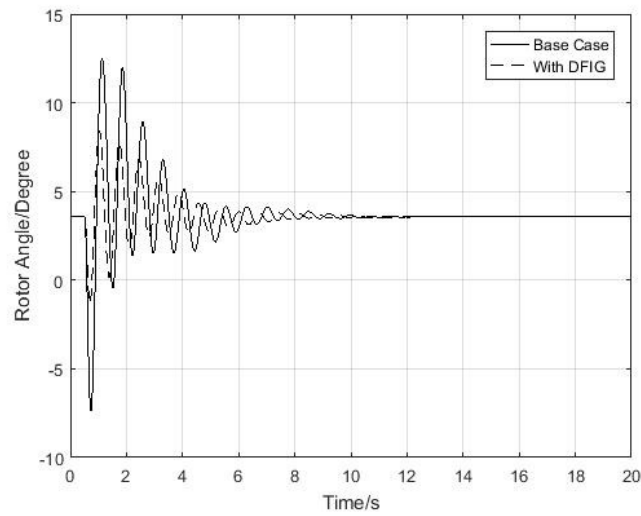


*Figure 7.26 Rotor Angle Responses of Generator at Bus 1 (Fault at Bus 6)*

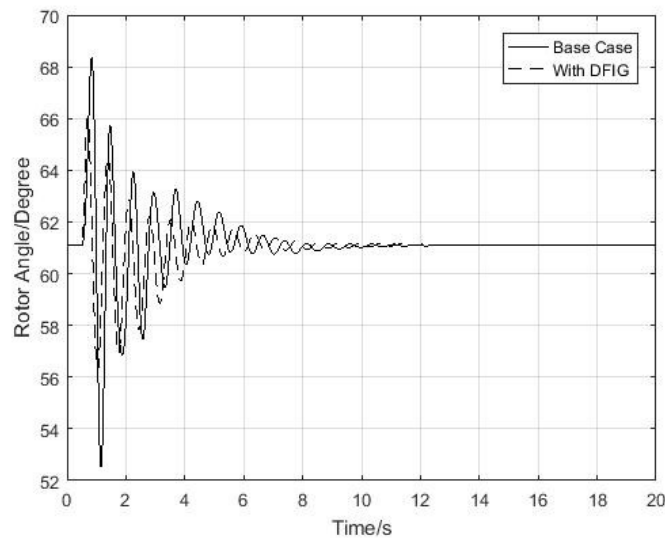


*Figure 7.27 Rotor Angle Responses of Generator at Bus 2 (Fault at Bus 6)*

The comparison of voltages at Bus 3 is shown in Figure 7.28 when a fault occurs at Bus 6 and cleared after 0.1 second. During the fault, the bus voltage drops to a lower value when a DFIG based wind farm replaces the synchronous generator at Bus 3. The reactive power output from the synchronous generator and the DFIG based wind farm are compared in Figure 7.29. It is shown that the synchronous generator can

provide more reactive power to support the bus voltage during the fault. The capability of DFIG voltage control cannot match that of a synchronous generator since its power converters have a limited capacity [35]. Due to this difficulty, many research efforts have been devoted to better control the DFIG for supporting the system during the fault [35, 37].

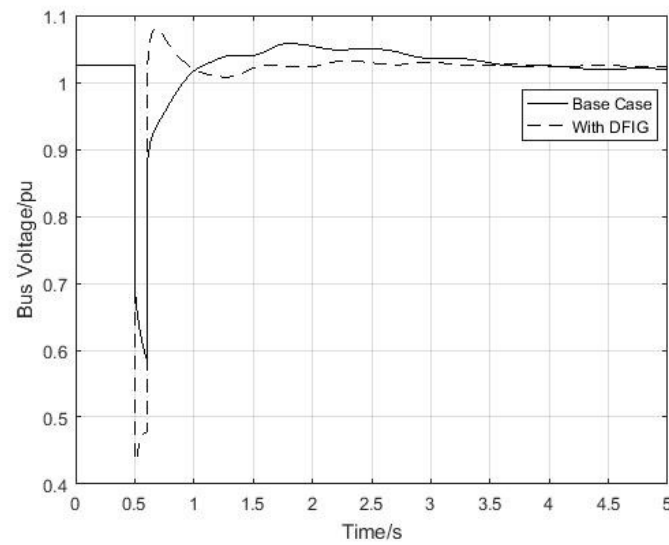


Figure 7.28 Comparison of Bus 3 Voltage (Fault at Bus 6)

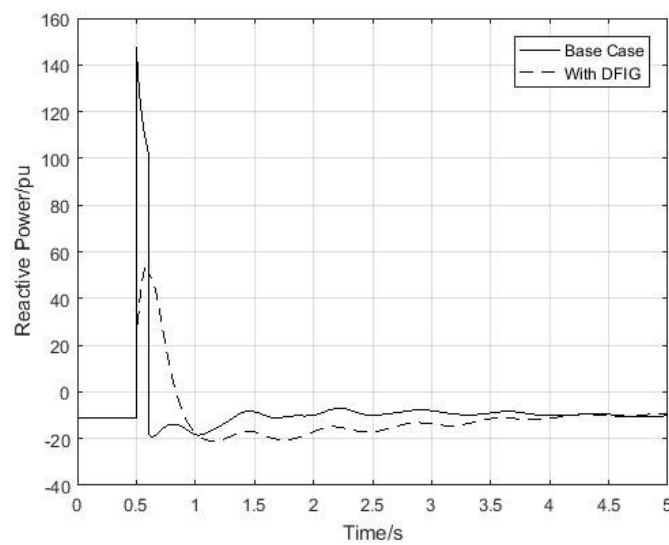
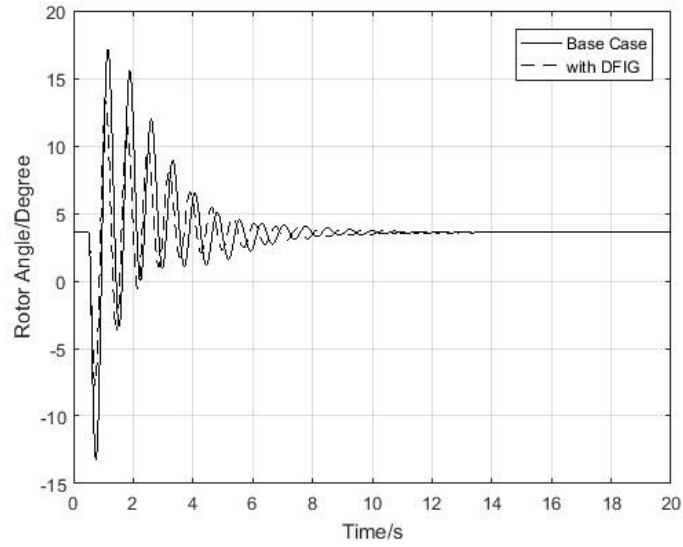
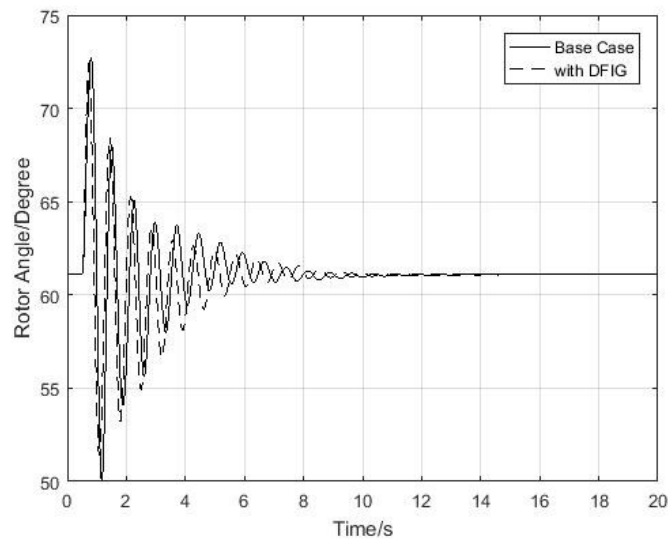


Figure 7.29 Comparison of Reactive Power Output (Fault at Bus 6)

In Table 7.2, the largest decrease in critical fault clearing time is when a three-phase fault is applied to Bus 8. The critical fault clearing time decreases by 0.0475 seconds. The rotor angle responses are shown in Figure 7.30 and 7.31 respectively when the fault clearing time is 0.1 second. It is shown in Figure 7.30 that even though the critical fault clearing time increases in the wind energy case, it still has certain damping effects on the generators rotor angle oscillation at Bus 1. This is because wind turbines of DFIGs do not participate in electromechanical oscillations which reduce the number of synchronous generators engaged in power system oscillation. However, the beneficial effect on the rotor angle oscillation is reduced when compared to the fault at Bus 6. The rotor angle oscillations of generator at Bus 2 are basically the same as shown in Figure 7.31. In the base case, the largest rotor angle separation between generators at Bus 1 and 2 is  $85.4257^\circ$  and the TSI is 61.64% when a three-phase fault occurs at Bus 8. The largest rotor angle separation is  $80.1102^\circ$  and the TSI is 63.60% in the wind energy case. Comparing these quantities with those obtained from previous fault at Bus 6, the beneficial effect is reduced.



*Figure 7.30 Rotor Angle Responses of Generator at Bus 1 (Fault at Bus 8)*



*Figure 7.31 Rotor Angle Responses of Generator at Bus 2 (Fault at Bus 8)*

When applying a fault at Bus 8 and cleared after 0.2475 second. The rotor angles of the base case are shown in Figure 7.32 and the rotor angles of the wind energy case are shown in Figure 7.33. Under this fault, the system is stable for the base case while unstable for the wind energy case. Considering this, the system transient stability is reduced with the wind energy integration.

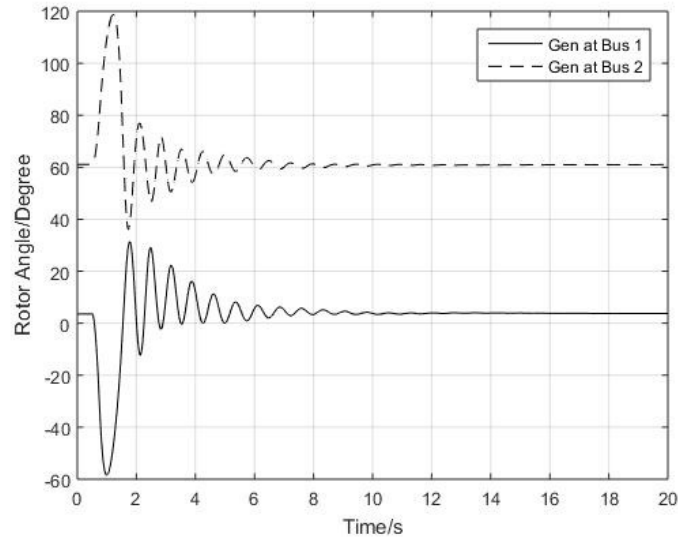


*Figure 7.32 Rotor Angle Responses of Base Case System*

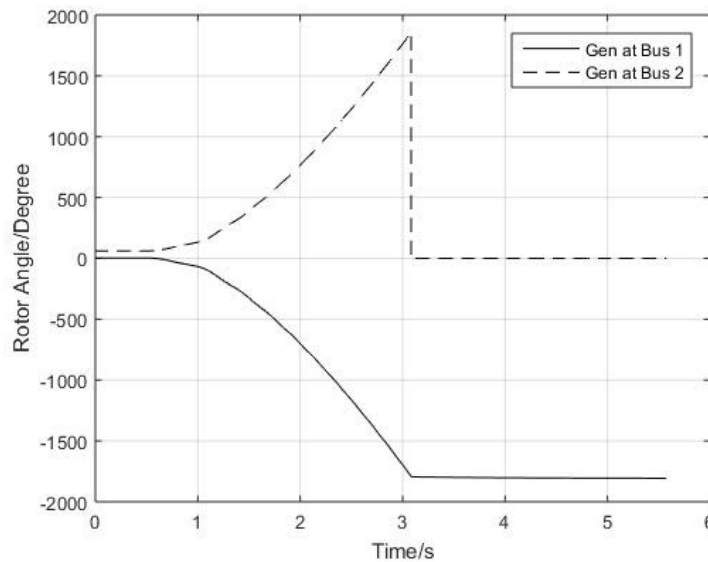


*Figure 7.33 Rotor Responses of Wind Energy Case*

This case study presents the impacts that DFIGs have on the power system transient stability using a small power system with 9 buses and 3 generators. It is hard to give a definitive conclusion on the impacts of large scale wind energy integrations. The impact of wind energy integrations on power system transient stability is a complicated problem and it can have either positive or positive impact under different

considerations. The power electronic devices decouple the mechanical parts of the DFIGs from the electrical parts connecting to the grid. It reduces the number of synchronous generators participating in the oscillations which could reduce rotor angle oscillations of synchronous generators in some cases. However, with the limitation of the capacity of the power electronic converters, the reactive power supplied from the DFIGs are providing insufficient support to terminal bus voltage. Advanced technique should be developed to diminish the negative impacts of large scale wind energy integrations.

#### **7.4.3 Case Study: Transient Stability Analysis of New England Power System**

The New England power system with 39 buses and 10 machines is used in this second case study. The one line diagram of the New England power system is shown in Figure 4.9 and the system data are given in Appendix D. Three cases are considered here. The first case is the base case New England power system while the other two cases are generator at Bus 32 and Bus 36 replaced by a DFIG based wind farm respectively. A three-phase fault is applied to Bus 16 at 0.5 s and cleared after 0.05 seconds. All generators used in this case study only contain the machine models and excitation models.

There are totally 39 buses within the New England power system and two buses are picked for analysis. The comparisons of the rotor angles at Bus 30 and 34 are given in Figure 7.34 and 7.35 respectively. It can be observed that the impact from the wind

farm replacement on rotor angle responses is smaller as the system is larger. The relative wind energy penetration is lower in a large system.

From Figure 7.34 and 7.35, it is shown that DFIGs replacement at Bus 32 has a negative effect on damping the rotor angle oscillation, while the DFIGs replacement at Bus 36 offers improvement to the rotor angle stability. As the wind generators do not participate in oscillations and cannot provide damping torques, if they replace synchronous generators with significant damping effects in the system, they will produce detrimental effects on the power system transient stability. It shows that many factors are included in wind energy integrations and it is hard to get a universal conclusion. The results come from the balancing between the positive and negative factors.

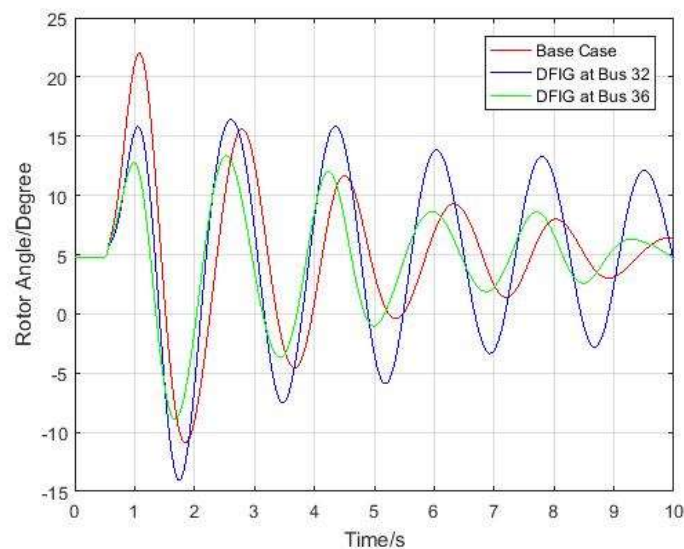


*Figure 7.34 Generator 30 Rotor Angle Responses of the New England Power System*

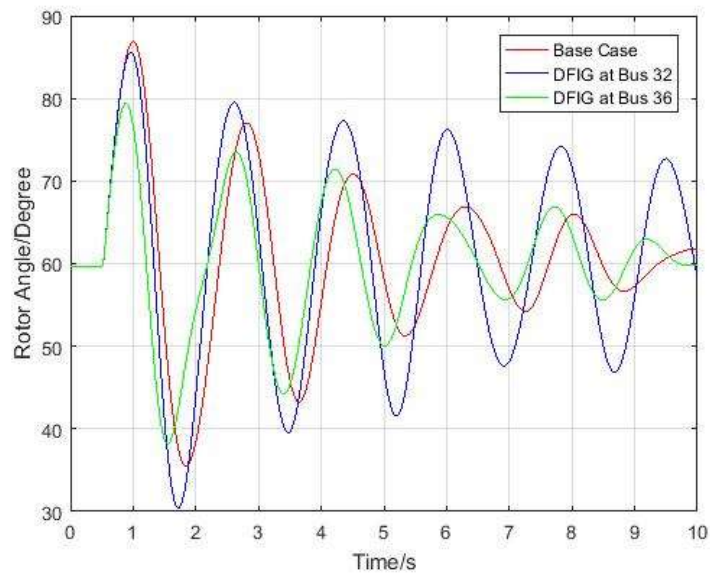


*Figure 7.35 Generator 34 Rotor Angle Responses of the New England Power System*

The comparisons of reactive power and bus voltage of Bus 32 from the base case and the case with DFIGs at Bus 32 are shown in Figure 7.36 and 7.37. It shows the similar features as in the previous 9 Bus power system case study. The reactive power from the DFIG based wind farm is limited and cannot provide sufficient support for the bus voltage, which drops to a lower value during the fault.

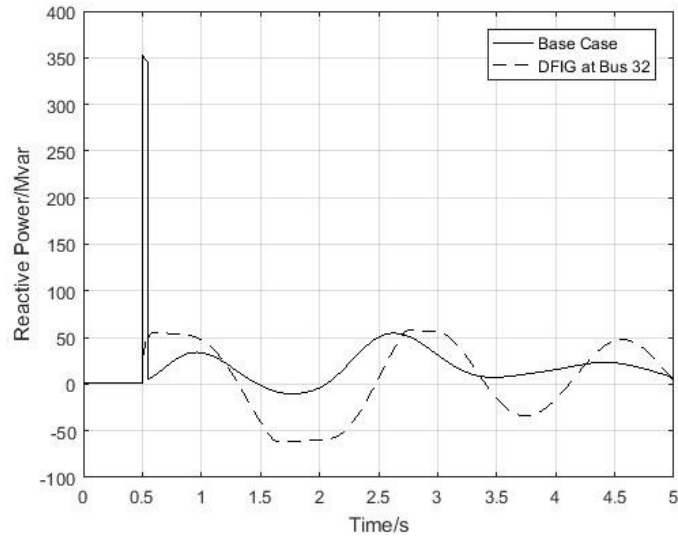


*Figure 7.36 Reactive Power Output Comparison at Bus 32 of the New England Power System*

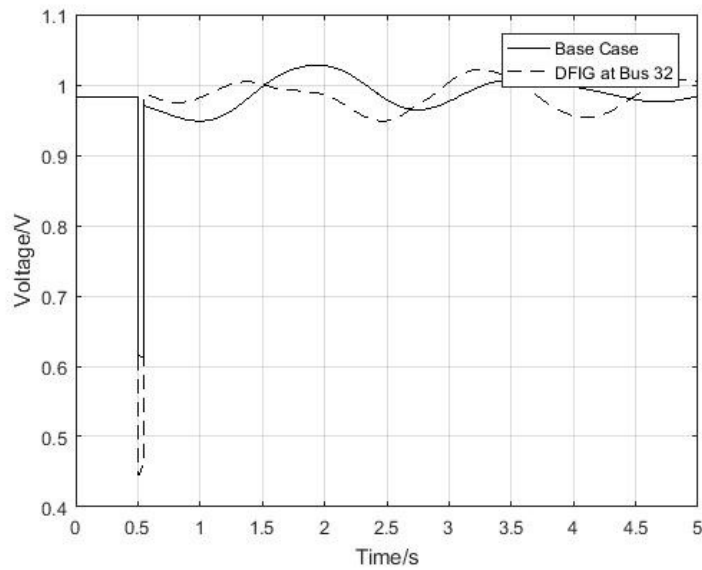


*Figure 7.37 Bus Voltage Comparison at Bus 32 of the New England Power System*

The New England power system is used in this case study. The effects of the DFIGs integration become smaller as the system gets larger and the penetration of wind energy decrease relatively. Replacing a synchronous generator at different buses will

either decrease or increase the transient stability, depending on the damping effect of the replaced synchronous generator provided to the system and the damping effect of the DFIG base wind farm.

It should be noted that the output variations of the wind farms are not considered in the above two case studies in section 7.4 and 7.5. The impact of wind farms unpredictable outputs on power system operations are discussed in Chapter 3. This chapter focuses on the effects that DFIGs have on the power system transient stability. If the unpredictable feature of the wind farms power outputs is considered, it might have further negative effects on the transient stability.

## **7.5 Summary**

This chapter focuses on the power system transient stability analysis with wind energy integrations.

- Time domain simulation is first applied to a SMIB system with a synchronous generator. Two models of the synchronous generator are considered. The formed DAEs are solved in Matlab and verified by PowerWorld. It gives the basic understanding of conducting time domain simulation.
- 5<sup>th</sup> and 3<sup>rd</sup> order models of DFIGs are compared using time domain simulation. It is found that the 5<sup>th</sup> order model includes the high frequency oscillation with the inclusion of the stator flux transients. The 3<sup>rd</sup> order model reveals only the

low frequency oscillation, which can reduce the computational burden in power system analysis.

- A mathematical model of DFIG based wind generator with decoupled control is implemented in Simulink. The wind speed increase and terminal voltage drop disturbances are applied to the system. It is shown that the DFIG generation system generates more power when wind speed increases and the rotor currents are largely affected by low terminal voltage variations. With the power electronic devices, DFIGs do not participate in the power system oscillation and the reactive power supplied from a DFIG is limited by the capacity of power electronic converter.
- In the 9 Bus system, it is found that the DFIGs replacement increases and decreases critical fault clearing time for different faults. The integration of the DFIG based wind farm improves the rotor angle stability while it decreases the voltage profiles.
- From the New England power system, the DFIGs replacement shows different effects as it depends on whether the damping effect provided by DFIG can be higher than the replaced synchronous generator. Careful consideration is required when replacing a synchronous generator with dedicated controllers and significant damping on the system.
- Many factors are influencing the power system transient stability with wind energy integrations. It is difficult to give an overall definitive conclusion. The effects of wind energy integration in power systems are better determined on a

case by case basis.

# Chapter 8

## Conclusions and Future Work

### 8.1 Conclusions

The desire for integrating more wind farms into power systems to reduce the environmental pollutions from fossil fuel and tackle the energy crisis is on the increase. However, the integrations of large scale wind energy have presented great challenges to power system operation. These challenges should be understood in order to maintain the reliable and secure operation of a power system. Doubly Fed Induction Generator (DFIG), the most popular type of wind generators, and its effects on power system operation are discussed in this thesis. The effects of the DFIG integration on power system steady state, small signal stability and transient stability are the focus of this thesis.

The wind energy developments and technologies were introduced and the details of DFIGs are discussed. Power system steady state operation with wind energy integrations is presented. Both power system small signal stability and transient stability analysis with DFIGs are discussed in detail. Case studies are given for each

of the analysis.

The following conclusions are made from the studies presented in this thesis.

- A DFIG based wind farm is represented by a PV bus generator with fixed real power and limited reactive power capability in steady state operation while a DFIG is basically an induction machine with rotor voltage not equal to zero in dynamic simulations.
- Wind generators with power electronic devices have a better performance in power system steady state operation. The location and connection scheme of a wind farm should be carefully planned to optimize the overall system performances. The intermittency of the wind farm power output is its largest drawback, which causes system voltage drops and insecurity.
- The integration of DFIGs has certain positive effects on damping the low frequency oscillations when a synchronous generator without controller is replaced by a wind farm as shown in Chapter 5. However, the negative impacts are shown when a synchronous generator with appropriate controllers is replaced. In modern power systems, synchronous generators are normally equipped with suitable controllers. The DFIGs replacement will cause a reduction on the small signal stability. Some factors can be optimized, such as connecting to a strong grid and different connection locations to minimize the negative effect.
- The DFIGs improve the rotor angle stability in some cases because the

mechanical and electrical components are decoupled by the power electronic converters. DFIGs decrease the voltage profiles during the fault as the reactive power supplied from the DFIGs is limited. It has detrimental effects on the system transient stability when a synchronous generator with significant damping effects is replaced by a DFIG based wind farm.

- From the steady state and dynamic analysis, the practical energy storage technologies and advanced dynamic controllers are required to further enlarge the sharing of wind energy in electricity generation market.
- There are no clear conclusions for the effects brought by wind energy integrations. It should be determined case by case using appropriate analysis methods. It depends on the balancing of beneficial effects of the integrated DFIGs and the replaced synchronous generators in the studies system.

## **8.2 Future Work**

Some suggestions are listed below for future work as an extension of this thesis.

- Besides DFIGs, other types of wind generators can be used to investigate their effects on power system operation and compare the performances with each other.
- For steady state analysis, the contingency analysis may be extended to N-2. The optimization of the system with wind energy integrations may be included

depending on local government policies.

- For the dynamic analysis, more complex wind generator models may be used and the control of the DFIGs may be investigated to minimize the negative effects.
- In this thesis, the largest system used is the New England system with 39 buses and 10 machines. A larger and complex system can be used for further analysis.

## References

- [1] Gwec.net, “*GLOBAL STATUS OVERVIEW - GWEC*”, [Online]. Available: <http://www.gwec.net/global-figures/wind-energy-global-status/>.
- [2] C. Abbey, F. Katiraei, C. Brothers, L. Dignard-Bailey and G. Joos, “*Integration of distributed generation and wind energy in Canada*”, in IEEE Power Engineering Society General Meeting, 2006.
- [3] Canadian Wind Energy Association, “*Installed Capacity - Canadian Wind Energy Association*”, [Online]. Available: <http://canwea.ca/wind-energy/installed-capacity/>.
- [4] Nrcan.gc.ca, “*Ramea Island | Natural Resources Canada*”, 2015. [Online]. Available: <http://www.nrcan.gc.ca/energy/renewable-electricity/wind/7319>. [Accessed: 02- Feb- 2016].
- [5] T. Ackermann, “*Wind power in power systems*”, Chichester, West Sussex, England: John Wiley, 2005.
- [6] H. Mendoza, “*Researchers on Schedule to 3D Print First Induction Motor by The End of 2015*”, *3DPrint.com*, 2014, [Online]. Available: <http://3dprint.com/18176/induction-motor-3d-printed/>. [Accessed: 08- Feb- 2016].
- [7] B. Wu, Y. Lang, N. Zargari and S. Kouro, “*Power conversion and control of wind energy systems*”, Hoboken, N.J.: Wiley, 2011.
- [8] D. Gautam, V. Vittal and T. Harbour, “*Impact of Increased Penetration of DFIG-Based Wind Turbine Generators on Transient and Small Signal Stability of*

*Power Systems*”, IEEE Trans. Power System, Vol. 24, No. 3, 2009, pp. 1426-1434.

[9] V. Vittal and R. Ayyanar, “*Grid integration and dynamic impact of wind energy*”, New York, NY: Springer, 2013.

[10] J. G. Slootweg, “*Wind power: Modelling and impact on power system dynamics*”, TU Delft, Delft University of Technology, 2003.

[11] J.G. Slootweg, H. Polinder and W.L. Kling, “*Dynamic modelling of a wind turbine with doubly fed induction generator*”, 2001 Power Engineering Society Summer Meeting, 15-19 July 2001, pp.644-649.

[12] Siegfried Heier, “*Grid Integration of Wind Energy Conversion Systems*”, John Wiley & Sons Ltd, 1998.

[13] P. Kundur, “*Power system stability and control*”, New York: McGraw-Hill, 1994.

[14] M. Yamamoto and O. Motoyoshi, “*Active and reactive power control for doubly-fed wound rotor induction generator*”, IEEE Transactions on Power Electronics, Vol. 6, No. 4, 1991, pp. 624-629.

[14] PowerWorld Simulator, Version 19, PowerWorld Corporation, Champaign, IL, USA, February, 2016.

[15] S. Grijalva, A. M. Visnesky Jr., “*The effect of generation on network security: spatial representation, metrics and policy*”, IEEE Transactions on Power Systems, Vol. 21, No. 3, August 2006, pp. 1388-1395.

[16] J. Glover, T. Overbye and M. Sarma, “*Power system analysis and design*”, 5th ed,

CENGAGE Learning, 2012.

[17] M. Albadi and E. El-Saadany, “*Overview of wind power intermittency impacts on power systems*”, *Electric Power Systems Research*, Vol. 80, No. 6, 2010, pp. 627-632.

[18] Ieso.ca, “*IESO Power Data*”, 2016. [Online]. Available: <http://www.ieso.ca/pages/power-data/default.aspx#>. [Accessed: 19- Feb- 2016].

[19] P. Kundur, J. Paserba, V. Ajarapu, G. Andersson, A. Bose, C. Canizares, N. Hatziargyriou, D. Hill, A. Stankovic, C. Taylor, T. Cutsem and V. Vittal, “*Definition and classification of power system stability IEEE/CIGRE joint task force on stability terms and definitions*”, *IEEE Transactions on Power Systems*, Vol.19, No.3, Aug. 2004, pp.1387-1401.

[20] L. Grigsby, “*The electric power engineering handbook*”, Boca Raton, FL: CRC Press, 2012.

[21] B. Pal and B. Chaudhuri, “*Robust control in power systems*”, New York: Springer, 2005.

[22] Milano Federico, Power system analysis toolbox, PSAT version 2.1.9, 2015.

[23] D. Mondal, A. Chakrabarti and A. Sengupta, “*Power system small signal stability analysis and control*”, London: Academic Press, 2014.

[24] I. Hiskens, “*Report of the IEEE PES Task Force on Benchmark Systems for Stability Controls*”, 2013. [Online]. Available: <http://www.sel.eesc.usp.br/ieee/>

- [25] K. Padiyar, "*Power system dynamics*", Hyderabad [India]: BS Publications, 2008.
- [26] J. Machowski, J. Bialek and J. Bumby, "*Power system dynamics*", Chichester, U.K.: Wiley, 2008.
- [27] F. Mei and B. Pal, "*Modal Analysis of Grid-Connected Doubly Fed Induction Generators*", IEEE Transactions on Energy Conversion, Vol.22, No.3, 2007, pp.728-736.
- [28] M. Moechtar, T. Cheng and L. Hu, "*Transient stability of power system-a survey*", WESCON/'95. Conference record. 'Microelectronics Communications Technology Producing Quality Products Mobile and Portable Power Emerging Technologies', Nov. 1995, pp.166-, 7-9.
- [29] MATLAB and Statistics Toolbox Release 2012b, The MathWorks, Inc., Natick, Massachusetts, United States.
- [30] V. Akhmatov, "*Induction generators for wind power*", 1st ed. Brentwood, Essex, U.K.: Multi-Science Pub., 2005.
- [31] O. Anaya-Lara, "*Wind energy generation*", 1st ed. Hoboken, NJ: John Wiley & Sons, 2009.
- [32] L. Shi, S. Dai, Y. Ni, L. Yao and M. Bazargan, "*Transient stability of power systems with high penetration of DFIG based wind farms*", 2009 IEEE Power & Energy Society General Meeting, Calgary, AB, 2009, pp. 1-6.

- [33] E. Muljadi, C. Butterfield, B. Parsons and A. Ellis, “*Effect of Variable Speed Wind Turbine Generator on Stability of a Weak Grid*”, IEEE Transactions on Energy Conversion, Vol. 22, No. 1, 2007, pp. 29-36.
- [34] S. Liu, G. Li and M. Zhou, “*Power system transient stability analysis with integration of DFIGs based on center of inertia*”, CSEE Journal of Power and Energy Systems, vol. 2, no. 2, 2016, pp. 20-29.
- [35] M. Edrah, K. Lo and O. Anaya-Lara, “*Impacts of High Penetration of DFIG Wind Turbines on Rotor Angle Stability of Power Systems*”, IEEE Transactions on Sustainable Energy, Vol. 6, No. 3, 2015, pp. 759-766.
- [36] E. Vittal, M. O'Malley and A. Keane, “*Rotor Angle Stability With High Penetrations of Wind Generation*”, IEEE Transactions on Power Systems, Vol. 27, No. 1, 2012, pp. 353-362.
- [37] F. Hughes, O. Anaya-Lara, N. Jenkins and G. Strbac, “*Control of DFIG-Based Wind Generation for Power Network Support*”, IEEE Transactions on Power Systems, Vol. 20, No. 4, 2005, pp. 1958-1966.

## Appendix A: 7 Bus Power System

Appendix A contains the data of 7 Bus power system [16] discussed in the thesis. The generation schedule and load demand are presented in Table A.1 and A.2 respectively

*Table A.1 Generation Schedule and Generator Limits of 7 Bus Power System*

Bus	Real Power Generation (MW)	Maximum Real Power Generation (MW)	Minimum Real Power Generation (MW)
1	103.1	400	0
2	164.37	500	100
4	100 (wind)	N/A	N/A
6	200.17	500	150
7	200.11	600	0

*Table A.2 Load Demand of 7 Bus Power System*

Bus	Real Power Load (MW)	Reactive Power Load (Mvar)
2	40	20
3	110	40
4	80	30
5	130	40
6	200	0
7	200	0

## Appendix B: IEC Power System

Appendix B contains the data of IEC power system [16] discussed in the thesis. The generation schedule and load demand are presented in Table B.1 and B.2 respectively.

*Table B.1 Generation Schedule and Generator Limits of IEC Power System*

Bus	Real Power Generation (MW)	Maximum Real Power Generation (MW)	Minimum Real Power Generation (MW)
1-Piper345	495.09	1350	0
2-Condor345	1120	1300	300
23-Eagle345	505	700	0
31-Pheasant161	300	450	0
35-Hen345	800	800	300
42-Cardinal161	350	350	0

*Table B.2 Load Demand of IEC Power System*

Bus	Real Power Load (MW)	Reactive Power Load (Mvar)
5-Ostrich161	60	15
6-Crow161	55	15
10-Bluebird345	268	128
11-Dove161	130	30
12-Sparrow161	175	30
13-Oriole161	140	32
14-Hawk161	176.25	15
16-Mallard161	165	29.8

17-Owl161	132	15
19-Eagle161	110	20
24-Bluebird161	115	25
25-Robin161	160	35
29-Parrot161	112	40
30-Rook161	200	60
31-Pheasant161	95	23
32-Woodpecker161	75	15
33-Flamingo161	198	35
34-Canary161	87	19
36-Heron161	160.57	21
37-Lark161	135	10
38-Peacock161	88.35	11
39-Kiwi161	130	45
40-Hen161	140	20
41-Finch161	128.38	27.57
42-Cardinal161	150	50
43-Turkey161	150	39

## Appendix C: Two Area Power System

Appendix C contains the data of Two Area power system [13] discussed in the thesis.

The steady state and dynamic data are presented in Table C.1 and C.2 respectively.

*Table C.1 Steady State Data of Two Area Power System*

Bus	Type	Voltage (pu)	Gen MW	Load MW	Load Mvar
1	Slack	1.03	700	0	0
2	PV	1.01	700	0	0
3	PV	1.03	719	0	0
4	PV	1.01	700	0	0
7	PQ	-	-	967	-100
9	PQ	-	-	1767	-250

*Table C.2 Dynamic Data of Two Area Power System*

Bus	H	$R_a$	$X_d$	$X'_d$	$X''_d$	$X_q$	$X'_q$	$X''_q$	$X_l$	$T'_{d0}$	$T''_{d0}$	$T'_{q0}$	$T''_{q0}$
1	6.5	0.0025	1.8	0.3	0.25	1.7	0.55	0.25	0.2	8	0.03	0.4	0.05
2	6.5	0.0025	1.8	0.3	0.25	1.7	0.55	0.25	0.2	8	0.03	0.4	0.05
3	6.175	0.0025	1.8	0.3	0.25	1.7	0.55	0.25	0.2	8	0.03	0.4	0.05
4	6.175	0.0025	1.8	0.3	0.25	1.7	0.55	0.25	0.2	8	0.03	0.4	0.05

## Appendix D: New England Power System

Appendix D contains data of New England power system [24] discussed in this thesis.

The steady state and dynamic data are presented in Table D.1 and D.2 respectively.

*Table D.1 Steady State Data of New England Power System*

Bus #	Type	Voltage (PU)	Gen MW	Load MW	Load Mvar
1	PQ	-	0	0	0
2	PQ	-	0	0	0
3	PQ	-	0	322	2.4
4	PQ	-	0	500	184
5	PQ	-	0	0	0
6	PQ	-	0	0	0
7	PQ	-	0	233.8	84
8	PQ	-	0	522	176
9	PQ	-	0	0	0
10	PQ	-	0	0	0
11	PQ	-	0	0	0
12	PQ	-	0	7.5	88
13	PQ	-	0	0	0
14	PQ	-	0	0	0
15	PQ	-	0	320	153
16	PQ	-	0	329	32.3
17	PQ	-	0	0	0
18	PQ	-	0	158	30
19	PQ	-	0	0	0
20	PQ	-	0	628	103

21	PQ	-	0	274	115
22	PQ	-	0	0	0
23	PQ	-	0	274.5	84.6
24	PQ	-	0	308.6	-92
25	PQ	-	0	224	47.2
26	PQ	-	0	139	17
27	PQ	-	0	281	75.5
28	PQ	-	0	206	27.6
29	PQ	-	0	283.5	26.9
30	PV	1.0475	250	0	0
31	Slack	0.982	-	9.2	4.6
32	PV	0.9831	650	0	0
33	PV	0.9972	632	0	0
34	PV	1.0123	508	0	0
35	PV	1.0493	650	0	0
36	PV	1.0635	560	0	0
37	PV	1.0278	540	0	0
38	PV	1.0265	830	0	0
39	PV	1.03	1000	1104	250

*Table D.2 Dynamic Data of New England Power System*

Unit #	H	$R_a$	$X_d$	$X'_d$	$X_q$	$X'_q$	$T'_{d0}$	$T'_{q0}$	$X_l$
1	500	0	0.02	0.006	0.019	0.008	7	0.7	0.003
2	30.3	0	0.295	0.0697	0.282	0.17	6.56	1.5	0.035
3	35.8	0	0.2495	0.0531	0.237	0.0876	5.7	1.5	0.0304
4	28.6	0	0.262	0.0436	0.258	0.166	5.69	1.5	0.0295
5	26	0	0.67	0.132	0.62	0.166	5.4	0.44	0.054
6	34.8	0	0.254	0.05	0.241	0.0814	7.3	0.4	0.0224
7	26.4	0	0.295	0.049	0.292	0.186	5.66	1.5	0.0322
8	24.3	0	0.29	0.057	0.28	0.0911	6.7	0.41	0.028
9	34.5	0	0.2106	0.057	0.205	0.0587	4.79	1.96	0.0298
10	42	0	0.1	0.031	0.069	0.008	10.2	0	0.0125

## **Appendix E: Single Machine Infinite Bus System with A Synchronous Generator**

Appendix E contains the data of single machine infinite bus system with A Synchronous Generator discussed in this thesis.

The system parameters are given below [16] and all in per units.

$$E_b=1, X_d=2.2, X_q=1.76, X'_d=0.2, X'_q=0.2, T'_{d0}=8, T'_{q0}=1, H=10.$$

## Appendix F: Single Machine Infinite Bus System with A DFIG

Appendix F contains data of single machine infinite bus system with A DFIG discussed in this thesis.

The system parameters are given below.

$$E_b = 1, R_s = 0.00706, R_r = 0.005, L_{ss} = 3.071, L_{rr} = 3.056, L_m = 2.9, X_s = 3.071,$$

$$X'_s = 0.319, T'_0 = \frac{L_{rr}}{R_r}.$$

## Appendix G: Eigenvalues Comparison of Two Area Power System

Appendix G presents the complex eigenvalues of Two Area Power System without and with AVRs and PSSs.

*Table G.1 Eigenvalues of Two Area Power System without AVRs and PSSs*

Base Case	Bus 1	Bus 2	Bus 3	Bus 4
-0.5716±j6.5632	-0.5939±j6.6688	-0.5971±j6.643	-0.5620±j6.5951	-0.5784±j6.5645
-0.5815±j6.7099	-0.2156±j4.8401	-0.2815±j3.7406	-0.6455±j3.7161	-0.3814±j3.9234
-0.2622±j3.3208	-2.1752±j0.1588	-2.3725±j1.3906	-2.1355±j1.2251	-1.7663±j1.5299
0.5034	-0.1570±j1.0853	-0.1240±j1.2264	-0.0173±j1.5528	-0.0907±j1.4618
0.0198	0.70175	0.80269	0.56715	0.55288

*Table G.2 Eigenvalues of Two Area Power System with AVRs and PSSs*

Base Case	Bus 1	Bus 2	Bus 3	Bus 4
-6.7026±j26.6642	-6.3183±j27.535	-5.8017±j27.4323	-4.6607±j28.785	-3.9911±j30.5263
-9.81±j20.5769	-10.0934±j19.5166	-9.892±j19.1872	-9.6461±j20.4889	-9.9722±j20.0022
-30.2395±j0.0967	-9.6118±j13.3514	-30.4622±j0.1604	-9.881±j13.238	-9.9045±j13.2554
-9.8255±j13.3165	-3.3375±j6.0841	-24.2731±j0.6577	-3.165±j5.9773	-3.1353±j5.9787
-9.676±j13.2867	-0.7298±j4.7914	-9.6376±j13.3734	-0.4579±j4.2877	-0.4365±j4.2651
-3.1115±j5.983	0.0981±j1.7097	-3.3033±j6.0846	-0.0385±j1.5714	-0.0584±j1.4321
-3.3777±j6.0761	-4.8454±j0.1494	-0.5020±j4.4807		-0.7308±j0.0041
-0.2865±j3.6675		0.0311±j1.7373		
-4.6326±j0.0679		-4.7441±j0.1581		

## Appendix H: Five-Bus Two-Machine Power System

Appendix H contains the data of Five-Bus Two-Machine power system [16] in the thesis. The steady state data are presented in Table H.1.

*Table H.1 Steady State Data of Five-Bus Two-Machine System*

Bus	Type	Voltage (pu)	Real Power Generation (MW)	Load (MVA)
1	Slack	1.00	-	0
2	PQ	-	0	800
3	PV	1.05	520	80
4	PQ	-	0	0
5	PQ	-	0	0

## Appendix L: 9 Bus Power System

Appendix L contains the data of 9 Bus power system [14] in the thesis. The generations and loads are presented in Table L.1 and L.2 respectively.

*Table L.1 Generation Schedule and Generator Limits of 9 Bus Power System*

Bus	Real Power Generation (MW)	Maximum Real Power Generation (MW)	Minimum Real Power Generation (MW)
1	72	450	0
2	163	240	0
3	85	90	0

*Table L.2 Load Demand of 9 Bus Power System*

Bus	Real Power Load (MW)	Reactive Power Load (Mvar)
5	125	50
6	90	30
8	100	35